Physicochemical characterisation of atmospheric particles in the vicinity of iron and steel industries in Australia

by

Kazi Abu Bakar Mohammad Mohiuddin

Bachelor of Science (Honors) in Civil Engineering &
Master of Science in Civil Engineering

A thesis submitted in fulfillment of the requirements for the degree of

Doctor of Philosophy

Graduate School of the Environment

Department of Environment & Geography

Faculty of Science

Macquarie University, Sydney

Australia

August 2014

Abstract

Atmospheric particulate matter is one of the major air pollutants which is complex in behavior, heterogeneous in mixture, variety in size, unknown in dose-response and mounted to the priority in air quality research. Emission of particles to the atmosphere from iron and steel processing industries is an increasing concern due to deleterious effects on process efficiency, human health, and environment. The negative impacts of atmospheric particles on human health and environment are dependent on their physical (particle size, morphology) and chemical properties (concentration, chemistry and speciation of metals and other elements of concern). The comprehensive understanding of the characteristics of these air particles is essential to ensure the healthier air quality, safe human health and environment. This PhD study provides a detailed physicochemical assessment of atmospheric particles collected in the vicinity of three iron and steelmaking plants and to indicate the importance of trace metal content and their distribution, bonding structure, mineral content and speciation of the particles, in addition to the assessment of the particle size and concentrations. In this study, atmospheric sampling sites were selected downstream of three iron and steel processing operations in Australia and one background site in an urban area with little industrial activity. An eight staged Micro Orifice Uniform Deposit Impactor (MOUDI) sampler with Teflon substrate was deployed to the study areas to collect the air particles. The collected particles were analysed using a series of non-destructive cutting-edge analytical techniques such as Proton Induced X-Ray emission (PIXE) for elemental content and distribution, Fourier Transform Infra-Red (FTIR) for bonding structure, X-Ray Diffraction (XRD) for mineral content, Scanning Electron Microscopy (SEM) for surface morphology, and synchrotron-based X-Ray Emission near Edge Structure (XANES) for speciation of air particles.

This study revealed significantly higher metal concentrations in the atmospheric particles collected in the industrial sites, comparing to the background urban site, demonstrating local influence of the industrial activities to the air quality. The $PM_{2.5}$ fractions in the PM_{10} particles at all sampling sites are found ranged from 35 to 62% indicating fine particles made a significant contribution to this size fraction at these sampling sites. Similarly, PM_1 to the total PM_{10} at all sites varied from 20 to 46% and contributed significantly to the PM_{10} mass loading. When compared to the background sampling site, all detected metals in the particles collected near the iron and steelmaking operations had 3.4 to 14 times higher

concentrations of PM_{10}, $PM_{2.5}$ and PM_1. The modality types of the particles were found variable between the mass and elements, and among elements in the urban and industrial areas indicating the elemental modal distribution are as important as particle mass for particle pollution modelling.

Iron (Fe) was found to be the dominant metal in the particles collected in vicinity of the iron and steel processing industries contributing up to 12% of the total particle mass loading. The industrial Fe fraction in the submicron and ultrafine size particles was estimated at up to 95% which may be released from high temperature industrial activities with the iron and steelmaking industries being one of the major contributors. The iron in the particles collected near the steelmaking site equipped with electric arc furnace indicated dominant Fe(III) oxide iron phases in all particle size fractions. The atmospheric particles collected near the integrated iron and steelmaking facilities operated by the blast furnace route, had similar iron phase speciation with presence of both Fe(II) and Fe(III) iron phases in the coarse and fine particle size ranges, while for the ultrafine size range of particles, Fe(III) was the dominant form of iron.

This study suggests that the metal composition of size resolved air particles varies significantly between sites and the associated metal exposure value is considerably higher in the vicinity of iron and steel processing industries than in the urban area for the same particle concentration level. Hence, these industrial elemental loadings can highly influence the atmospheric pollution at local urban and regional levels and are required to consider in the atmospheric particles monitoring, modelling, risk assessment, and PM standards settings.

List of publications

The publication lists are provided below which was derived from this thesis. The authors (candidate's) contribution in these publications is also explained in respective appendices.

Journal articles

J1. **Mohiuddin, K.**, Strezov, V., Nelson, P. & Stelcer, E. 2014. Characterisation of trace metals in atmospheric particles in the vicinity of iron and steelmaking industries in Australia. *Atmospheric Environment,* 83**,** 72-79.

J2. **Mohiuddin, K.,** Strezov, V., Nelson, P. F., Stelcer, E. & Evans, T. 2014. Mass and elemental distributions of atmospheric particles nearby blast furnace and electric arc furnace operated industrial areas in Australia. *Science of The Total Environment,* 487**,** 323-334.

'Prepared for publication' articles

P1. **Mohiuddin, K.**, Strezov, V., Nelson, P. & Evans, T. 2014. Bonding structure and mineral analysis of size resolved atmospheric particles near Australian steelmaking sites. *Journal of Aerosol Science (to be submitted)*.

P2. **Mohiuddin, K.**, Strezov, V., Nelson, P. & Evans, T. 2014. Speciation of size resolved iron containing particles in proximity of Australian steelmaking industries. *Aerosol Science and Technology (to be submitted)*.

Edited book chapter

B1. **K Mohiuddin**, V Strezov and P Nelson 2010, "Industrial and Environmental Sustainability of Ironmaking Technologies", Book Chapter 5, Advances in Environmental Research, Volume 12, Nova Science Publishers Inc, ISBN 978-1-61122-540-2.

Peer-reviewed conference papers

C1. **K Mohiuddin**, V Strezov, T Evans and P Nelson (2010), "Assessment of CO_2, PM_{10} and heavy metal emissions from iron and steel industries in Australia", Chemeca 2010: The 40th Australasian Chemical Engineering Conference, paper # 443 (10 pages). ISBN: 978-085-825-9713.

C2. **Mohiuddin, K.,** Strezov, V., Stelcer, E. & Nelson, P. F. 2013, "Chemistry of air particles collected near Australian Industrial sites", 21st International Clean Air & Environment Conference: CASANZ 2013 Conference, paper# 179 (5 pages). ISBN: 978-0-9874553-2-1.

Poster presentations

C3. **K. Mohiuddin**, V Strezov, E Stelcer, A Morrison and P Nelson (2012) "Characterization of size resolved air particulates in the vicinity of electric arc furnace steelmaking facility", Poster presentation in the sixth international conference on environmental science and technology held on June 25-29, 2012 at Houston, Texas, USA.

C4. **K Mohiuddin**, V Strezov, E Stelcer, A Morrison and P Nelson (2011) "Iron containing aerosol in Sydney airshed", poster presentation in the 17th AINSE conference of nuclear and complimentary techniques of analysis held on 5-7 December 2011 at Canberra, Australia.

Declaration

I certify that this PhD research work entitled as "Physicochemical characterisation of atmospheric particles in the vicinity of iron and steel industries in Australia" has been carried out by me and any part of this research work has not been submitted anywhere for the award of any degree other than Macquarie University.

I also certify that this is an original research work and the thesis is written by me. Any assistance I received in the process of my research work and thesis preparation has been properly acknowledged.

In addition, I certify that all information and data from sources other than this primary research is appropriately referenced.

_____

Kazi Abu Bakar Mohammad Mohiuddin

Dated: August 30, 2014

Acknowledgments

I would like to start recalling the Almighty, the One who set the breathing air free for us, and provided me the life, health, intellect, and opportunity to perform this research. My principal supervisor Associate Professor Vladimir Strezov possesses unique personality and strength, who taught me the passion and trying hard dealing with research. I am truly impressed, and feeling worthy having his imminence, who trained me how to shape my skills and abilities to be the best of myself in the research and academia. Without his attributes this thesis would never been existed. I also have high admiration on my associate supervisor Professor Peter Nelson having many rare qualities. Discussing for ten minutes with him is worth like ten hours trying hard. He provided me the pin point directions when I was distracted, and it is very easy to be distracted in the research world.

I sincerely acknowledge the support received from Tim Evans from Rio Tinto for industrial support and preparation of research method, Tony Morrison from MQ Uni for sampling atmospheric particles, Rob Mitchell and Pushan Shah from EPA SA for sampling at Whyalla, Darco for sampling at Cringila, Swathi Gowda for sampling at Rooty Hill, Eduard Stelcer from ANSTO for PIXE analysis, Damian Gore and Russell Field from MQ Uni for XRD analysis, Debra Birch and Nicole at MQ Uni for SEM-EDS analysis, and Chris Glover from Australian Synchrotron for XANES analysis.

Many thanks to my officemates named Kamal Hossain, Rabiul Islam, Scott, Fabiola, Suraj, Ria, Aale Ali, Teerapat, Patrick and others especially for their time, discussion, coffee and foods, caring and sharing, emotional attachments and so on. Only thanks would not be justified for Rabiul Bro as he practically implemented his research on disaster recovery by providing me emotional support, cash support, and especially continuous food support for short and long term during my disastrous phase of research.

Countless thanks to N SK Md Shahed Ul Kalam, Nilufar Easmin, Tarannum Naz, Ahsanul Kabir, Ashraful Alam, John, Marco Amati, Tris, Pushan, Tiffany Hong, Ye Wu, Tao Kan, Xiaofeng Li, Yaoyao Ji, Rebecca Wilson, Chuanping Meng, Yuna Kim, Faraj, Upma, Donrita, Gunnella, Emma, Farhana, and all others for their invaluable time and friendship.

I am struggling finding appropriate words to be grateful for my wife, and two kids Mariam 8yrs of age and Muhammad 3yrs of age. Simply 'Thank you'. You travelled many lands and oceans to be with me. Then you sacrificed day-after-day and night-after-night so that I can be attached more with my research. The pure heart of my wife, patience of Mariam, and tears and sounds of Muhammad was my ultimate strength to elevate my research potential. I didn't return yours favors, and I owe you my life.

I am thankful for the families of Shahed Bro, Shamim Uncle, Robiul Bro, Shahjahan Bro, Abdur Raoufe Bro, Israfil Bro, Mukul Bro, Ali Bro, Bashir Bro, Sohel Bro, Arif Bro, Mamun Bro, and others living in Sydney who supported my family in many ways during my candidature and family health crisis. I am also offering a very special debt of deep gratitude to families living overseas, among them my parents, parents-in-law, brothers, brothers-in-law, sisters, uncles, uncles-in-law and others for their unceasing prayers, love and encouragement, and emotional supports during every crisis I faced to balance between research and life. Among them parents were the sincerest according to their capacity.

Finally I would like to acknowledge the financial support from the Australian Research Council (grant no: LP110200638), the AINSE award (grant no: ALNGRA11102), the MQ University HDR support (grant no: HDR40940155), and the MQRES scholarship from the MQ University. I am also highly grateful for laboratory supports from the ANSTO, Sydney to perform PIXE analysis, the Australian Synchrotron, Victoria, Australia to perform XANES experiment on the XAS beamline, the Microscopy lab at MQ University to perform SEM-EDS analysis, the XRD lab at MQ University for XRD analysis, and the ARL online laboratory for back trajectories and dispersion modelling.

Dedication

To

my parents who taught me morality

&

my beloved wife, and kids who shared my burden

&

those who will continue to take the burden to ensure the healthier air quality

Table of Contents

Abstract iii
List of publications v
Journal articles v
'Prepared for publication' articles v
Edited book chapter v
Peer-reviewed conference papers v
Poster presentations vi
Declaration vii
Acknowledgments ix
Dedication xi
List of Tables xvii
List of Figures xix
Acronyms xxiii
Chapter 1 25
Introduction 25
1.1 Problem Statement 25
1.2 Objectives and scope of the study 27
1.3 Structure of the thesis 28
1.4 References 31
Chapter 2 35
Industrial and Environmental Sustainability of Ironmaking Technologies 35
2.1 Introduction 35
2.2 Iron Ore Types and Deposits 36
2.3 Iron Ore Production 39
2.4 Trade of Iron Ore 42
2.5 Supply, Demand and Price of Iron Ore 43
2.6 Ironmaking Processes 44
2.6.1 Raw Materials Preparation 45
2.6.2 Blast Furnace (BF) 46
2.6.3 Blast furnace productivity 49
2.6.4 Direct Reduced Iron (DRI) 50
2.6.4 Direct Iron Smelting 51
2.7 Australian Ironmaking Perspective 52
2.8 Conclusions 56
2.9 References 57

Chapter 3 61
Assessment of CO_2, PM_{10} and Heavy metal emissions from iron and steel industries in Australia 61
3.1 Introduction 61
3.2 Methods 62
3.3 Energy consumption and steel production in Australia 62
3.4 CO_2 emissions 64
3.5 PM_{10} emissions 65
3.6 Heavy metal emissions 66
3.7 Atmospheric emission reduction 67
3.7.1 Improving process efficiency 67
3.7.2 Process switching 68
3.7.3 Other processes 69
3.8 Conclusions 70
3.9 References 70
Chapter 4 73
Characterisation of trace metals in atmospheric particles in the vicinity of iron and steelmaking industries in Australia 73
4.1 Introduction 73
4.2 Methods 75
4.2.1 Sampling sites 75
4.2.2 Sampling equipment 76
4.2.3 Sample analysis 77
4.3 Results and Discussion 78
4.3.1 Mass analysis 78
4.3.2 Elemental concentrations 80
4.3.3 Particle fraction of trace elements 82
4.3.4 Inter-elemental correlation 83
4.3.5 Percent metal fraction and metal enrichment factor 87
4.4 Conclusions 89
4.5 References 90
Chapter 5 93
Mass and elemental distribution of atmospheric particles nearby blast furnace and electric arc furnace operated industrial areas in Australia 93
5.1 Introduction 93
5.2 Materials and methods 94
5.3 Results and Discussion 96
5.3.1 Particle size distribution 96
5.3.2 Particle mass concentration 100
5.3.3 Elemental distribution 102

5.3.4 Elemental MMAD and GSD....106
5.3.5 Elemental mass fraction of atmospheric particles....107
5.3.6 Relative particle number and surface area distribution....109
5.3.7 Relative industrial contribution....112
5.4 Conclusions....114
5.5 References....114
Chapter 6....119
Bonding structure and mineral analysis of size resolved atmospheric particles near steelmaking industrial sites....119
6.1 Introduction....119
6.2 Materials and methods....121
6.2.1 Sampling details....121
6.3.2 FTIR analysis....122
6.3.3 XRD analysis....122
6.4 Results and discussion....123
6.4.1 FTIR analysis....123
6.4.2 Functional group distribution....127
6.4.3 Functional groups fraction....128
6.5 XRD analysis....129
6.5.1 Mineral identification and composition....129
6.6 Conclusions....134
6.7 References....135
Chapter 7....139
Speciation of size resolved iron containing particles in proximity of Australian steelmaking industries....139
7.1 Introduction....139
7.2 Materials and methods....140
7.2.1 Sampling locations....140
7.2.2 Sampling equipment....141
7.2.3 Windrose and back trajectory analysis....142
7.2.4 PIXE analysis....142
7.2.5 SEM-EDS analysis....142
7.2.6 XANES analysis....143
7.2.7 Particle dispersion analysis....143
7.3 Results and Discussion....144
7.3.1 Wind direction and back-trajectories analysis....144
7.3.2 Mass and iron concentration in atmospheric particles....146
7.3.3 Morphology of iron containing particles....147
7.3.4 Iron speciation....148

7.3.5 Dispersion of particles from steelmaking industries 153
7.4 Conclusions 154
7.5 References 155
Chapter 8 159
Conclusions and Recommendations 159
8.1 Summary of the conclusions 159
8.2 Recommendations for future studies 162
Appendix A: Declaration of authorship contribution 165
Appendix B: Supplementary data for dispersion model 169

List of Tables

Table 2.1 Physical and optical properties of iron ores (Downs and Hall-Wallace, 2003) 37

Table 2.2 Typical chemistry of iron ores (GMD, 2010; MII, 2010) 39

Table 2.3 Hematite ore grading for both lump and fines (IRCGD, 2007).....39

Table 2.4 Worldwide estimated iron ore reserve (USGS, 2010).....41

Table 2.5 Worldwide import and export of iron ore from 2005 to 2008 (ABARE, 2009).....43

Table 2.6 Typical composition of blast furnace slag (OMNR, 1992) 49

Table 2.7 Emissions of atmospheric pollutants per million tonne of iron ore production from iron ore mining industries in Australia (NPI, 2009; USGS, 2010) 55

Table 3.1 Energy use by BF-BOF & Scrap-EAF route in different countries (RITE, 2008) ……..69

Table 4.1 PM_{10}, $PM_{2.5}$ and PM_1 mass concentrations, $\mu g/m^3$ ……78

Table 4.2 Average elemental concentrations of selected elements in PM_{10}, $PM_{2.5}$ and PM_1 from the four sampling sites [range of values determined in (brackets)], ng/m^3.....81

Table 4.3 Inter-elemental correlations of coarse particles (10<Dp<2.5 μm).....84

Table 4.4 Inter-elemental correlations of intermodal particles (2.5<Dp<1 μm) 85

Table 4.5 Inter-elemental correlations of submicron particles (Dp<1.0μm).....86

Table 4.6 Percent Metal Fraction for PM_{10}, $PM_{2.5}$ and PM_1 at CR, WH, RT and MQ sites....87

Table 4.7 Metal enrichment factor (MEF) for PM_{10}, $PM_{2.5}$ and PM_1 at CR, WH, RT sites.....88

Table 5.1 Cumulative mass distribution calculation ……98

Table 5.2 MMAD and GSD values for all PM samples; Mean (Min – Max) 100

Table 5.3 Total mass concentration (in $\mu g/m^3$) and variability (dimensionless) of PM.....101

Table 5.4 MMAD [in μm] and GSD [dimensionless] values at all sampling sites 106

Table 6.1 Absorbance observed in FTIR spectra of air particles ……...123

Table 6.2 Mineral content (%) as a function of total crystalline materials in size resolved atmospheric particles at CR, RT, WH, and MQ sites 132

Table 7.1 Operational parameters of the MOUDI sampler (Marple et al., 1991) ……141

Table 7.2 Qualitative speciation of XANES data 151

List of Figures

Figure 2.1 Global iron ore production from the year 2000 to 2008 (USGS, 2010).....41

Figure 2.2 Trend of iron ore production in different countries from 1994 to 2008 (USGS, 2010) 42

Figure 2.3 Global iron ore price from 1994 to 2010 (World Bank, 2010).....44

Figure 2.4 Global Blast Furnace hot metal production from 1980 to 2009 (WSA, 2010) 48

Figure 2.5 Global DRI production from the year 1990 to 2008 (Midrex, 2009) 51

Figure 2.6 Global DRI production by process types from 1990 to 2008 (Midrex, 2009).....52

Figure 2.7 Iron ore production in Australia from 2000 to 2008 (USGS, 2010).....53

Figure 2.8 Blast furnace iron ore production in Australia from 1980 to 2009 (WSA, 2010). 55

Figure 2.9 DRI production in Australia from 2000 to 2004 (WSA, 2010).....56

Figure 3.1 Energy consumption from iron and steel industries in Australia from 1980 to 2008 (ABARE, 2009) 63

Figure 3.2 Crude steel production in Australia from 1980 to 2008 (WSI, 2009) 63

Figure 3.3 CO_2 emissions from iron and steel industries in Australia (DCCEE, 2009) 64

Figure 3.4 CO_2 emissions (t CO_2/t crude steel) from iron and steel industries in Australia 65

Figure 3.5 PM_{10} emission from iron and steel industries in Australia (NPI, 2009) 66

Figure 3.6 Emission of priority air toxins from iron and steel industries in Australia (NPI, 2009) 67

Figure 3.7 Energy consumption in the Australian iron and steel industries (ABARE 2009, & WSI, 2009).....68

Figure 4.1 Windrose plots at CR, RT, WH and MQ sites. These windroses were constructed during the PM sampling campaign using 96 hours meteorological data starting from May 22, June 27, August 03 and November 04, 2011 at MQ, RT, CR and WH sites respectively……...76

Figure 4.2 Mass concentration of PM_{10}, $PM_{2.5}$ and PM_1 for all sampling sites.....79

Figure 4.3 Coarse, Intermodal and Submicron PM fractions to PM_{10} mass.....80

Figure 4.4 Correlation between $PM_{2.5}$ and PM_1 at sampling sites.....80

Figure 4.5 Coarse, Intermodal and Submicron fractions of trace elements; Cr was below detection limits at the MQ site 83

Figure 5.1 Map of sampling locations in Australia 96

Figure 5.2 Average particle size distribution at CR, RT, WH and MQ sites; vertical line shows the lowest and highest concentration values 97

Figure 5.3 Average cumulative mass distribution of atmospheric particles; vertical line shows the lowest and highest percentage values 99

Figure 5.4 PM mass concentration for different PM size distributions 101

Figure 5.5 Mean elemental modal distribution of atmospheric particles 103

Figure 5.6 Cumulative frequency of selected elements 104

Figure 5.7 Elemental mass fraction (in percentage) of air particles at all MOUDI stages . 108

Figure 5.8 Elemental number distribution of atmospheric particles 110

Figure 5.9 Elemental surface area distribution of atmospheric particles 111

Figure 5.10 Industrial Fe contribution in percentage at CR, RT and WH site 113

Figure 6.1 FTIR scans for size resolved aerosol samples at CR and RT sites 125

Figure 6.2 Functional group distribution as a function of particle size at CR, RT, WH and MQ sites 127

Figure 6.3 Coarse, intermodal and submicron PM functional group fractions 129

Figure 6.4 Typical XRD diffraction pattern of size resolved atmospheric particles at WH site 131

Figure 7.1(a-d) Windrose plots during sampling campaign at site CR site (03 Aug 11, ending after 48 hrs), RT site (18 Jul 11, ending after 24 hrs), WH site (04 Nov 11, ending after 46 hrs), and MQ site (23 Jun 11, ending after 78 hrs); these samples were subjected to iron speciation study 145

Figure 7.2(a-d) Backward air-mass trajectories ending at level height of 200 m (red-colored line), 500 m (blue-colored line), and 1000 m (green-colored line) during sampling campaign at site CR site (03 Aug 11, ending after 48 hrs), RT site (18 Jul 11, ending after 24 hrs), WH site (04 Nov 11, ending after 46 hrs), and MQ site (23 Jun 11, ending after 75 hrs), including the variation in relative humidity and relative distances of trajectories 146

Figure 7.3(a-d) Mass and Iron concentration at each MOUDI stage in all sampling sites 147

Figure 7.4(a-i) Morphology of iron containing particles identified by SEM-EDS at industrial CR, RT, and WH sites 148

Figure 7.5 Fe K-edge XANES spectra for the set of calibration standards applied in this study 149

Figure 7.6 Fe K-edge XANES spectra for samples located at sites: (a) Macquarie Park (MQ); (b) Rooty Hill (RT); (c).Cringila (CR); (d) Whyalla (WH). 151

Figure 7.7 Dispersion and concentration of iron containing particles releasing from Whyalla steelworks during sampling campaign starting on 4 Nov 11, considering single point source and 1 unit mass of iron containing particles.....153

Acronyms

PM	Particulate matter
AQI	Air quality index
NEPM	National environment protection measure
MOUDI	Micro orifice uniform deposit impactor
PTFE	Polytetrafluoroethylene
PIXE	Proton induced x-ray emission
SEM	Scanning electron microscope
EDS	Energy dispersive spectrometer
FTIR	Fourier Transform Infra-red X-ray
XRD	X-ray diffraction
XAS	X-ray absorbance spectrometry
XANES	X-ray emission near Edge structure
PD	Powder diffraction
EPA	Environmental protection authority
NSW	New South Wales
SA	South Australia
OEH	Office of environment and heritage
ABS	Australian bureau of statistics
BF	Blast furnace
BOF	Basic oxygen furnace
EAF	Electric arc furnace
AISI	American iron and steel institute
WSA	World steel association
ABARE	Australian bureau of agricultural and resource economics
MQ	Macquarie
CR	Cringila
RT	Rooty Hill
WH	Whyalla

Chapter 1

Introduction

Preface

This chapter describes the problem statement, aims and scope, and thesis structure related to the atmospheric particles nearby iron and steelmaking industries. The thesis structure provides the thesis objectives [A1 to A6] linked with thesis chapters [Ch1 to Ch8] and corresponding publications [J1, J2, B1, C1, P1, P2]. This chapter also presents the overview of the whole thesis.

1.1 Problem Statement

Atmospheric particulate matter (PM) has become one of the major air quality issues in Australia to maintain the standard quality of life. Air particles originated from industrial sectors have been considerably influencing the surrounding atmospheric quality, human health and environment. Iron and steel industry is one of the major energy intensive sectors which emits significant amount of particles to the atmosphere and hence affects the surrounding air quality. Emission of atmospheric particles depends on complex interactions of raw materials, processing techniques and pollution control measures which all contribute to the productivity, process efficiency, and environmental sustainability of iron and steelmaking industries. Improved understanding of iron ore properties and ironmaking processes is essential to reduce the atmospheric particle emission and hence ensure the environmental sustainability, especially for the iron and steel production. Historical atmospheric emission data from iron and steelmaking industries in Australia is also required to assess the emission trend and process efficiency which will lead to improved understanding of industrial point emission sources for atmospheric particles.

The impact of these atmospheric particles to the human health and environment depends on their size and chemistry. When particles are released to the atmosphere, they can stay and travel in the air for long time, adsorb gaseous molecules onto their surface, colloid

with each other, change their size, and be removed from the atmosphere by deposition processes. Elevated atmospheric particle levels can pose increasing health risks, especially for vulnerable groups, including the very young and the elderly. Epidemiological investigations indicate that human mortality and morbidity is increased due to higher concentration of inhalable particles (Pope III, 2000; Dominici et al., 2005; Ning and Sioutas, 2010). Respirable particles in the size range of $PM_{2.5}$ and PM_1 are particularly hazardous, as they can be transported deep in the alveolar region of the lungs and the bloodstream (Park and Wexler, 2008; Valiulis et al., 2008).

Apart from the PM size and mass distribution, the chemical composition of particles is particularly important when atmospheric particles are generated from industrial activities. For example, inhalation of iron dust has been linked to reduce lung function (Banks et al., 1999), and can lead to chronic obstructive pulmonary disease (COPD) (Driscoll et al., 2005). Atmospheric particles generated from iron and steel industries have high concentrations of Cd, Cr, Fe, Mn, Ni and Zn compared to other trace metals (Machemer, 2004; Querol et al., 2007). Pope (1996 & 1992) described that the closure of a Utah Valley steel mill resulted in an overall decrease in PM_{10} concentration and associated iron, copper and zinc content of the particulates in the local airshed. Therefore, the chemical characterisation of atmospheric particles in addition to the particle size and mass concentration is essential to ensure the safe and healthier environment.

Standards for particulate matter (PM) concentrations in air are primarily set to protect the public from adverse health effects by limiting their short and long term exposure. The mandated Australian 24 hour average National Environmental Protection Measure (NEPM) concentration for PM in Australia is $50\mu g/m^3$ for PM_{10} and there exists an advisory standard concentration of $25\mu g/m^3$ for $PM_{2.5.}$ While concentration levels of PM in Australia are defined by the NEPM, the elemental chemical composition of particles, with the exception of lead (Pb), are not standardised. In NSW PM is monitored and reported by the NSW Environment Protection Authority (EPA). An air quality index using atmospheric particle concentration is then calculated based on the measured PM_{10} and $PM_{2.5}$ as a proportion of the NEPM maximum concentrations. Depending on particle concentration levels, the air quality index (AQI) is assigned linearly to different categories starting from very good to hazardous levels. However, the index assigned accounts only for the PM concentration levels, without consideration of the chemical composition and speciation of the particles. Improved

understanding of chemical characteristics of particles is essential to evaluate the potential impacts of atmospheric particles on air quality.

There are few studies that dealt with elemental concentration of atmospheric particles in Australia, mostly related to mineral dust (Radhi, 2010), and motor vehicles dust (Lim, 2007; Gramotnev, 2007), biomass burning (Keywood et al., 2013; Reisen et al., 2013), secondary organic aerosol (Keywood et al., 2011), and source apportionment (Chan, 1997; Cohen et al., 2014; Cohen, 1998; Keywood et al., 2000). However, some fundamental questions remain unresolved related to the high temperature iron and steel processing industries in Australia. Such as, what is the dominant size and trace metal in atmospheric particles nearby industrial sites? What are the distribution, enrichment factor and speciation of trace metals in atmospheric particles? What are the spectral variation, bonding structure and mineral distribution in atmospheric particles? This study is the first attempt so far in response to these research questions by in-depth characterisation of size resolved atmospheric particles in the vicinity of iron and steel industries in Australia. The study was performed by sampling nearby two integrated blast furnace-basic oxygen furnace (BF-BOF) and one electric arc furnace (EAF) iron and steelmaking industries in Australia in addition to one urban background site with little or no industrial activity. The outcome of this study aims to improve the understanding of air quality and provide input at improving air quality management performance at proximity of industrial operations.

1.2 Objectives and scope of the study

This study aims to manifest the role of atmospheric particles on air quality and environment nearby the major steelmaking industries in Australia. The ultimate goal of the study is to assess the atmospheric particles and their comprehensive characteristics so that this information can be applied to ensure healthier air quality, safe human health and environment especially in the industrial airshed in Australia.

The major objectives of this study are:

A1. To review the iron ore properties, their production and processes of ironmaking technologies;

A2. To compile the historical emission data of atmospheric particles generated from iron and steelmaking industries in Australia;

A3. To determine the mass and trace metal content of PM_{10}, $PM_{2.5}$ and PM_1;

A4. To evaluate the mass and elemental distribution of size resolved atmospheric particles;

A5. To assess the bonding structure and mineral content of atmospheric particles, and

A6. To investigate the speciation of size resolved iron containing particles.

At present the state governments are mainly responsible for the air quality management in Australia. It includes the monitoring, modelling, and risk assessment of atmospheric particles. The scope of this study is to collect and compile the existing information related to iron ore properties, production, ironmaking processes, and historical emission data from Australian iron and steelmaking industries. In addition, the atmospheric particles were collected from three industrial sites and one urban background site in Australia using Micro Orifice Uniform Deposit Impactor (MOUDI) sampler. The sampled particles were analysed by Proton Induced X-Ray emission (PIXE) for elemental content and distribution, Fourier Transform Infra-Red (FTIR) for bonding structure, X-Ray Diffraction (XRD) for mineral content, Scanning Electron Microscopy (SEM) for surface morphology, and synchrotron-based X-Ray Emission near Edge Structure (XANES) for speciation of atmospheric particles. Experimental data was analysed to acquire the comprehensive understanding of physicochemical characteristics of atmospheric particles. Therefore, this study will enhance the particle monitoring, modelling and risk assessment processes by considering the trace metal content and their distribution, mineral content and speciation of atmospheric particles in addition to the particle size and mass concentration.

1.3 Structure of the thesis

The thesis is structured as thesis by publication. It includes two published journal papers, one edited book chapter, two peer-reviewed conference papers, and two papers prepared for publication which are interlinked in eight chapters, as stated below. In addition, all bibliography of cited publications has been incorporated in the relevant chapters.

Chapter 1 : This chapter includes problem statement, objectives and scope, and thesis structure which links all the chapters and publications together with study objectives.

Chapter 2 : Literature assessment of ironmaking technologies was performed in this chapter. This chapter refers to the published edited book chapter [B1] and responds to the thesis objective [A1], and named as "Industrial and environmental sustainability of ironmaking technologies". It focuses on the review of iron ore properties, their production and processes of ironmaking technologies. This chapter provides the understanding of basic sustainability parameters to minimise the atmospheric particle emissions from iron and steelmaking industrial point sources.

Chapter 3 : The atmospheric emission data from iron and steelmaking industries in Australia was compiled in this chapter. This chapter refers to the published peer-reviewed conference paper [C1], response to the thesis objective [A2], and titled as "Assessment of CO_2, PM_{10} and heavy metal emissions from iron and steel industries in Australia". It provides the historical emission trend from iron and steelmaking industries in Australia and possible options to reduce those emissions.

Chapter 4 : This chapter includes the sampling protocol of atmospheric particles by Micro Orifice Uniform Deposit Impactor (MOUDI) sampler, Laboratory analysis method using Proton Induced X-Ray Emission (PIXE) technique, and finally analysis of PIXE data for PM_{10}, $PM_{2.5}$ and PM_1 to evaluate the elemental concentration, inter-elemental correlation, percent metal fraction and metal enrichment factor. This chapter refers to the published journal article [J1], responds to the thesis objective [A3], and titled as "Characterisation of trace metals in atmospheric particles in the vicinity of iron and steelmaking industries in Australia". It provides the in-depth understanding of the leading metal contributors and average metal enrichment of atmospheric particles, and hence the importance of chemical

composition of atmospheric particles which is currently not regulated to provide the comprehensive risk assessment.

Chapter 5 : This chapter presents analysis of size resolved atmospheric particles to evaluate the size, mass and elemental distribution, relative particle number, surface area distribution, and relative industrial contribution of leading metal contributors to particle formation. This chapter refers to the published journal article [J2], responds to the thesis objective [A4], and is named as "Mass and elemental distribution of atmospheric particles nearby blast furnace and electric arc furnace operated industrial areas in Australia". The chapter provides the improved understanding of mass and elemental distribution, including modality of atmospheric particles, and the industrial iron fraction, which is a leading metal contributor in atmospheric particles in the vicinity of iron and steelmaking industries.

Chapter 6 : The laboratory testing protocols of Fourier Transform Infra-Red (FTIR) and X-Ray Diffraction (XRD) techniques, analysis of FTIR and XRD testing results are shown in this chapter. This chapter refers to the paper prepared for journal publication [P1], responds to the thesis objective [A5] and is entitled as "Bonding structure and mineral content of size resolved air particles in the vicinity of iron and steelmaking industries in Australia". It includes data and analysis on relative content and distribution of iron minerals in addition to the spectral variation and functional group distribution of size resolved atmospheric particles.

Chapter 7 : This chapter includes the sampling method and testing protocol using Scanning Electron Microscopy (SEM) and synchrotron-based X-Ray Emission Near Edge Structure (XANES) techniques, analysis of SEM and XANES data. This chapter refers to the article prepared for journal publication [P2], responds to the thesis objective [A6], and is named as "Speciation of size resolved iron containing particles in the vicinity of iron and steel processing industries in Australia". It shows the surface texture, structure, and oxidation states of iron containing

particles which will provide the fingerprint technique to identify the source and fate of size resolved atmospheric particles in the vicinity of iron and steelmaking industries.

Chapter 8 : This chapter includes the conclusions of the findings of this study including their implications, and provides recommendations for future research.

Appendices : This section provides the lists of appendices used in this thesis.

It is required to inform the reader that thesis by publication is the preferred Macquarie University's thesis model. This format was selected to contribute to the physicochemical characterisation of particles in the air quality management practices and the relevant publications can have faster and greater impact than a traditional dissertation. However, this style has some disadvantages over the traditional thesis as there are variety of writing styles related to publishing guidelines and repetitions of materials, especially with sampling protocols on which the research depends. It is also noted that the published articles have been systematically subjected to the review process by two or more reviewers in the relevant field. For this, the chapters were retained and largely preserved the integrity of the respective published formats. The overall intent was to reveal the comprehensive understanding of physicochemical characteristics of size resolved atmospheric particles in the vicinity of iron and steel processing industries in Australia based on a series of cutting-edge analytical techniques, their rigorous analysis followed by a logical process to reach the final conclusions with their implications to provide and protect the safe and healthier environment.

1.4 References

Banks, D. E., Shah, A. A., Lopez, M. & Wang, M.-L. 1999. Chest illnesses and the decline of FEV1 in steelworkers. *Journal of occupational and environmental medicine,* 41**,** 1085-1090.

Bollati, V., Marinelli, B., Apostoli, P., Bonzini, M., Nordio, F., Hoxha, M., Pegoraro, V., Motta, V., Tarantini, L. & Cantone, L. 2010. Exposure to metal-rich particulate matter modifies the expression of candidate microRNAs in peripheral blood leukocytes. *Environmental health perspectives,* 118**,** 763.

Chan, Y.-C. 1997. *Identification of sources of PM2.5 and PM10 aerosols in Brisbane.* PhD thesis, Griffith University.

Cohen, D., Stelcer, E., Atanacio, A. & Crawford, J. 2014. The application of IBA techniques to air pollution source fingerprinting and source apportionment. *Nuclear Instruments and Methods in Physics Research Section B: Beam Interactions with Materials and Atoms,* 318**,** 113-118.

Cohen, D. D. 1998. Characterisation of atmospheric fine particles using IBA techniques. *Nuclear Instruments and Methods in Physics Research Section B: Beam Interactions with Materials and Atoms,* 136**,** 14-22.

Dominici, F., Mcdermott, A., Daniels, M., Zeger, S. L. & Samet, J. M. 2005. Revised analyses of the National Morbidity, Mortality, and Air Pollution Study: mortality among residents of 90 cities. *Journal of Toxicology and Environmental Health, Part A,* 68**,** 1071-1092.

Driscoll, T., Nelson, D. I., Steenland, K., Leigh, J., Concha-Barrientos, M., Fingerhut, M. & Prüss-Üstün, A. 2005. The global burden of disease due to occupational carcinogens. *American journal of industrial medicine,* 48**,** 419-431.

Gramotnev, G. 2007. *Analysis of dispersion and propagation of fine and ultrafine particle aerosols from a busy road.* PhD thesis, Queensland University of Technology.

Keywood, M., Guyes, H., Selleck, P. & Gillett, R. 2011. Quantification of secondary organic aerosol in an Australian urban location. *Environmental Chemistry,* 8**,** 115-126.

Keywood, M., Kanakidou, M., Stohl, A., Dentener, F., Grassi, G., Meyer, C., Torseth, K., Edwards, D., Thompson, A. M. & Lohmann, U. 2013. Fire in the Air: Biomass burning impacts in a changing climate. *Critical Reviews in Environmental Science and Technology,* 43**,** 40-83.

Keywood, M. D., Ayers, G. P., Gras, J. L., Gillett, R. W. & Cohen, D. D. 2000. Size distribution and sources of aerosol in Launceston, Australia, during winter 1997. *Journal of the Air & Waste Management Association,* 50**,** 418-427.

Krombach, F., Münzing, S., Allmeling, A.-M., Gerlach, J. T., Behr, J. & Dörger, M. 1997. Cell size of alveolar macrophages: an interspecies comparison. *Environmental health perspectives,* 105**,** 1261.

Lim, M. C. H. 2007. *Chemical and physical characterisation of aerosols from the exhaust emissions from motor vehicles.* PhD thesis, Queensland University of Technology.

Machemer, S. D. 2004. Characterization of airborne and bulk particulate from iron and steel manufacturing facilities. *Environmental science & technology,* 38**,** 381-389.

Ning, Z. & Sioutas, C. 2010. Atmospheric processes influencing aerosols generated by combustion and the inference of their impact on public exposure: a review. *Aerosol and Air Quality Resarch,* 10**,** 43-58.

Park, S. & Wexler, A. 2008. Size-dependent deposition of particles in the human lung at steady-state breathing. *Journal of Aerosol Science,* 39**,** 266-276.

Pope Iii, C. 1996. Particulate pollution and health: a review of the Utah valley experience. *Journal of exposure analysis and environmental epidemiology,* 6**,** 23.

Pope Iii, C. A. 2000. Review: Epidemiological basis for particulate air pollution health standards. *Aerosol Science & Technology,* 32**,** 4-14.

Pope Iii, C. A., Schwartz, J. & Ransom, M. R. 1992. Daily mortality and PM10 pollution in Utah Valley. *Archives of Environmental Health: An International Journal,* 47**,** 211-217.

Querol, X., Viana, M., Alastuey, A., Amato, F., Moreno, T., Castillo, S., Pey, J., De La Rosa, J., Sánchez De La Campa, A. & Artinano, B. 2007. Source origin of trace elements in PM from regional background, urban and industrial sites of Spain. *Atmospheric environment,* 41**,** 7219-7231.

Radhi, M. 2010. *Physical and chemical properties of Australian continental aerosols.* PhD thesis, University of New South Wales.

Reisen, F., Meyer, C. & Keywood, M. D. 2013. Impact of biomass burning sources on seasonal aerosol air quality. *Atmospheric Environment,* 67**,** 437-447.

Valiulis, D., Šakalys, J. & Plauškaitė, K. 2008. Heavy metal penetration into the human respiratory tract in Vilnius. *Lithuanian Journal of Physics,* 48.

Chapter 2

Industrial and Environmental Sustainability of Ironmaking Technologies

Preface

This literature assessment chapter describes the properties and production of iron ore in addition to the ironmaking process so that the industrial and environmental sustainability can be ensured in the ironmaking sectors. This chapter refers to the edited book chapter [B1] and the thesis objective [A1]. It also provides the particle emission and the productivity scenario of Australian Ironmaking industries.

2.1 Introduction

During ironmaking, iron is extracted from iron ore by chemical reduction. Ironmaking is an important step for steelmaking and is one of the largest capital and energy intensive processes. The conventional and dominant route for ironmaking is the blast furnace in which metallurgical coke is used as reductant. The production capacity of modern blast furnace processes has improved about threefold compared to the original blast furnaces. However, alternative ironmaking processes are now considered due to the requirement to maintain and further improve energy efficiency, productivity and reduce pollutant emissions of blast furnace operations. Feed materials in blast furnaces, coke and sinter, require separate cokemaking and sintering operations, which are also energy intensive with negative environmental impacts. The direct reduced iron (DRI) processes utilise non-coking coals or gas for reduction thereby decreasing pollutant emissions aiming to improve environmental sustainability. For this, DRI processes are expected to play a significant role in the future by eliminating the coking, sintering or pelletising process and their associated expenditures and emissions.

Ironmaking processes consume fossil fuels for their energy source and limestone to assist with impurity removal, with both being a source of greenhouse gas (GHG) emissions. About 2 tonnes of CO_2 per tonne steel is emitted during ironmaking and steelmaking which contributes approximately 6-7% of the total anthropogenic CO_2 emissions (Kim and

Worrell, 2002). Iron and steelmaking industries are now facing increasing pressure to minimise GHG emissions in order to address global climate change concerns.

The quality of iron ore is also important parameter to achieve product quality. Iron ore is produced via extraction from deposits within the crust that are located in different parts of the world and processed according to their types and grades. Global supply and demand of iron ore, shipping cost and global economic situations are also affecting the iron ore mining and processing industry. Thus, reduction of raw materials consumption per unit production is a priority to enhance the industrial productivity. This chapter discusses the ironmaking processes, including their raw materials production and consumption globally, required to ensure their industrial and environmental sustainability.

2.2 Iron Ore Types and Deposits

Earth's crust comprises of oxygen (46.6%), silicon (27.7%), aluminum (8.1%), iron (5.0%) and other elements, such as magnesium, calcium, sodium, potassium etc. (John, 1987). Iron ore is a naturally occurring rock and the mineral deposits primarily consist of iron oxides, such as, hematite, magnetite, goethite or siderite. About 98% of the iron ore is used either directly or converted to briquettes, concentrates, pellets and sinter to produce metallic iron and steel. Iron ores also have limited applications for production of medical, biochemical, electrical and other metallurgical products. According to the Mineral Information Institute (2010), the formation of iron ore is not fully understood but is believed that most was formed about 1.6 to 1.8 billion years ago by chemical precipitation of iron from shallow oceans. Banded Iron Formations (BIFs) are treated as highly debatable chemical precipitates which are explained by the alternating layers of iron-rich and amorphous silica-rich layers (Harnmeijer, 2003). There were attempts to classify BIFs on different basis, such as mineralogical composition (James, 1954; James, 1966), proposed tectonic setting (Gross, 1965) and depositional environment (Kimberley, 1978; Simonson, 1985).

Table 2.1 shows the physical and optical properties while Table 2.2 shows the elemental information and chemistry of different iron ores. Hematite is an important iron ore mineral with blood colour when in a powdered form. Depending on appearance and crystal arrangement hematite ores can be found in different varieties, such as hematite rose, tiger iron, kidney ore, ooalitic hematite or specularite. For example, ooalitic hematite

is a sedimentary formation composed of small grains with reddish brown colour. Hematite ore is mainly deposited in Australia, Brazil, England, Mexico and the Lake Superior region in USA. The typical ore grading of India is shown in Table 2.3 including their size and chemistry.

Magnetite is a common accessory mineral in igneous and metamorphic rocks. Magnetite ores are of lower grade metal oxide deposits. These can be easily refined into ore concentrate due to their magnetic properties. According to Gindalbie Metals (2010) about 50% of the Gindalbie's iron ore pellets are produced from magnetite ore and used for steel manufacturing. The appearance of magnetite ores are black and have opaque octahedral crystals.

Goethite is a hard, brownish iron oxy-hydroxide mineral formed by the weathering of other iron rich minerals. It is deposited in Australia, England, United States, India, Brazil, Africa etc. Some impurities such as Si, Al, P, Mn and H_2O can be found with goethite ores. Goethite is also traditionally used as a colorant amongst aboriginal tribes in Australia in prehistoric times (Onoratini and Perinet, 1985).

Siderite is a valuable iron mineral composed of iron carbonate (FeCO3) and can be found in hydrothermal layers and sedimentary rocks in a variety of crystalline structure forms. Siderite can be found in Australia, Brazil, England, Germany, Peru, USA and Canada. These types of ore can have some magnesium and calcium, zinc or cobalt as impurities.

Table 2.1 Physical and optical properties of iron ores (Downs and Hall-Wallace, 2003)

	Hematite	Magnetite	Goethite	Siderite
Physical properties				
Cleavage	Parting due to twinning	Very good in one direction	Perfect in one direction	Perfect in one direction
Fracture	Uneven to subconchoidal	Uneven	Uneven	Uneven, Conchoidal
Hardness	5 – 6	5.5 – 6.5	5 – 5.5	3.5 – 4.5
Sp Gravity (gm/cc)	5.26 (meas.) 5.255 (calc.)	5.175 (meas.) 5.20 (calc.)	4.28 (meas.) 4.18 (calc.)	3.96 (meas.) 3.392 (calc.)
VHN[1] (100 g load)	1000 – 1100	681 – 792	667	--
Optical properties				
Color	Steel-gray, dull to bright red, white to gray white	Black	Yellow, brown, brownish red to Black	Yellowish-brown to greyish-brown
	Hematite	Magnetite	Goethite	Siderite
Streak	Cherry red or reddish brown	Black	Blackish brown, yellowish to radish brown	White
Luster	Metallic or submetallic to dull	Metallic to submetallic	Metallic to dull Earthy	Vitreous, Silky, Pearly
Optical class	Uniaxial	Isotropic	Biaxial, uniaxial for red light	Uniaxial

[1]Vickers hardness number

Table 2.2 Typical chemistry of iron ores (GMD, 2010; MII, 2010)

Ore type	Typical chemistry
Hematite	Fe_2O_3 (98.14%), FeO (1.54), Mn_2O_3 (0.54%), MnO (0.38%)
Magnetite	i) Fe_2O_3 (68.85%), FeO (30.78%), SiO_2 (0.27%), Al_2O_3 (0.21%), TiO_2 (trace), MgO (trace), CaO (trace); ii) Fe_2O_3 (67.16%), FeO (31.21%), SiO_2 (0.11%), Al_2O_3 (0.44%), TiO_2 (0.29%), MnO (0.09%), MgO (0.02%), Cr_2O_3 (0.08%);
Goethite	Fe_2O_3 (89.65%), SiO_2 (0.36%), H_2O^* (10.19%)
Siderite	FeO (61.08%), CO_2 (38.19%), MnO (1.12%), MgO (0.13%), CaO (0.10%)

*Bound water not free water .

Table 2.3 Hematite ore grading for both lump and fines (IRCGD, 2007)

Grade	Size (mm)	Fe % (min)	SiO_2 % (max)	Al_2O_3 % (max)	P % (max)	Na_2O + K_2O (max) %
Lump:						
High	+10	+ 65	3	3	0.10	0.15
Medium	10 to 100	62 – 65	2.5	4.5	0.10	0.15
Low	10 to 100	56 – 62	SiO_2 + Al_2O_3: 8 – 10		0.10	0.15
Fines:						
High	< 10	65		4.5	0.10	0.15
Medium	< 10	62 – 65	4	4.5	0.10	0.15
Low	< 10	<62	SiO_2 + Al_2O_3: 8 – 10		0.10	0.15

2.3 Iron Ore Production

The global iron ore production has significantly increased in the last 15 years due to the increasing demand for steel products, namely due to the economic growth of China. Table 2.4 indicates the estimated reserves of crude ore with the iron ore content in different countries. Figures (2.1 & 2.2) show the global iron ore production and trends in different countries. According to the statistics of US Geological Survey (USGS, 2010), the amount of worldwide iron ore production for 2008 was over 2 billion tonnes, which has doubled in

gross weight from the year 2000. About 50 countries produce iron ore but more than two-thirds of the global production is located in only 5 countries, China, Brazil, Australia, India and Russia. Australia is ranked second for iron ore production with 350 Mt produced in 2008, behind China (366 Mt) and well ahead of India (214 Mt), Russia (99 Mt), Ukraine (72 Mt) and United States (54 Mt). The mine production estimates for China by USGS shown in Figure 2.2 are based on crude ore, rather than usable ore, which are reported for the other countries. The largest iron ore producing company is the Brazilian mining corporation Vale, followed by the Anglo-Australian companies BHP Billiton and Rio Tinto Group.

The global reserves of iron ore are estimated at 150 Bt with an iron content of 73 Bt. Ukraine has the largest amount (30 Bt) of reserve crude ore compared to other countries, such as Russia (25 Bt), China (21 Bt) and Australia (20 Bt) (USGS, 2010). However, according to the iron ore grading, Russia has the largest amount of iron reserve at 14 Bt, compared to Australia (13 Bt), Ukraine (9 Bt), Brazil (8.9 Bt) and China (7.2 Bt). The estimated amount of geological deposits of iron ore gives an indication of the global iron ore source and distribution. About 70% of geological deposition of iron ore is distributed in only five countries, Ukraine, Russia, China, Australia and Brazil. According to USGS (2010), more than 800 billion tonnes of global crude ore resources are estimated containing more than 230 billion tonnes of iron. At the time of economic recession, steel product consumption decreased in developing countries while in Asian countries and Latin America it increased. This led to slowdown of the international iron ore trade. New iron ore production projects are currently initiated in Australia, South America, South Africa and West Africa.

Table 2.4 Worldwide estimated iron ore reserve (USGS, 2010)

Country	Iron ore reserve, Mt	
	Crude ore	Iron content
Australia	20,000	13,000
Brazil	16,000	8,900
Canada	1,700	1,100
China	22,000	7,200
India	7,000	4,500
Iran	2,500	1,400
Kazakhstan	8,300	3,300
Mauritanian	700	400
Mexico	700	400
Russia	25,000	14,000
South Africa	1,000	650
Sweden	3,500	2,200
Ukraine	30,000	9,000
United states	6,900	2,100
Venezuela	4,000	2,400
Other countries	11,000	6,200
World total (rounded)	160,000	77,000

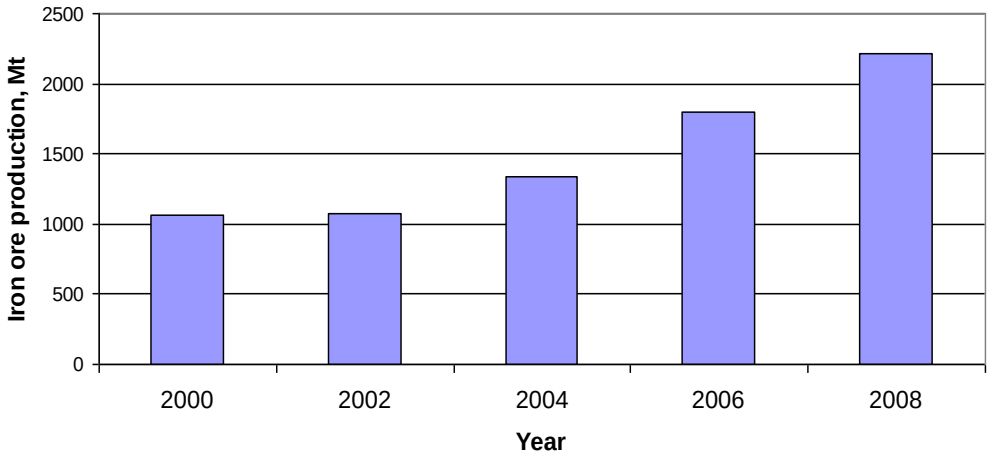

Figure 2.1 Global iron ore production from the year 2000 to 2008 (USGS, 2010)

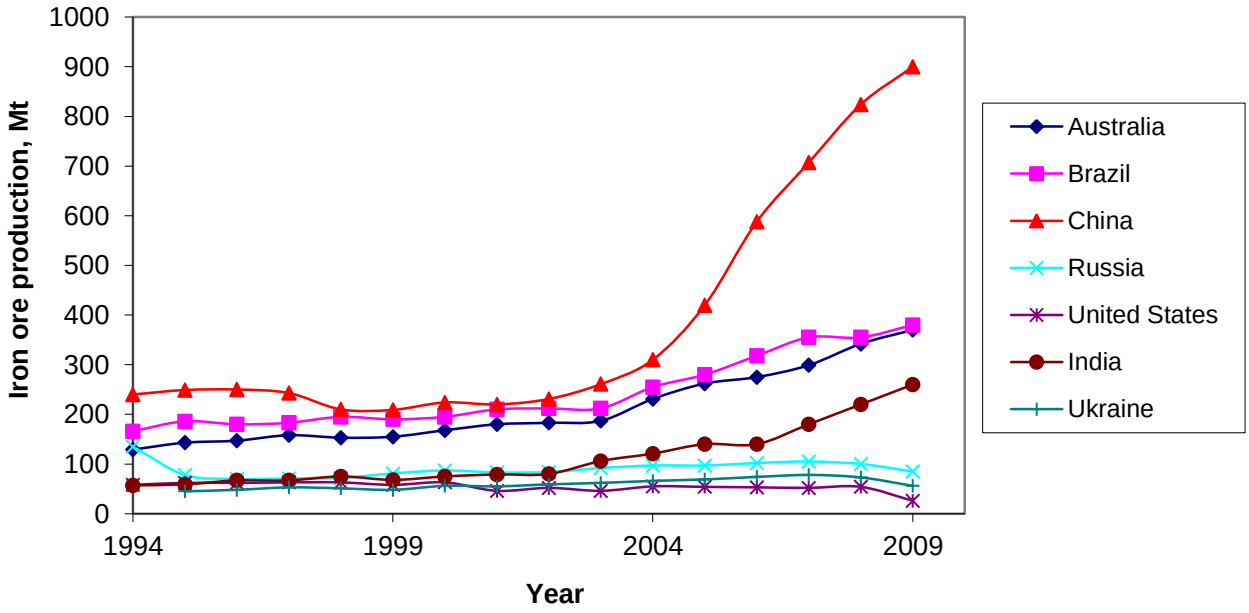

Figure 2.2 Trend of iron ore production in different countries from 1994 to 2008 (USGS, 2010)

2.4 Trade of Iron Ore

Iron ore production and consumption determine the global trade of iron ore and is shown in Table 2.5. Iron ore trade has been increasing and reached 913 Mt in 2008 which is 22% more than the trade in 2005. China is the top ranked country importing iron ore at about 50% of the world's total export. Chinese imported iron ore level has increased by 60% from 2005 to 2008. Japan also increased the iron ore import by 1.4% in 2008 compared to 2007. Australian iron ore exports have increased by 14% to 281 Mt in 2007 and 9.2% in 2008 showing growth in production capacity of iron ore. Iron ore exports in Brazil increased by 15% to 310 Mt in 2008 becoming the largest iron ore export country in the world. Brazil's export was boosted due to the increased production and strong demand from China. India has the fastest growing iron ore export industry and is the third exporting iron ore country with about one third of the Australian export amounts. South Africa, Canada and Sweden are also significant iron ore export countries contributing to meet the global consumption needs.

Table 2.5 Worldwide import and export of iron ore from 2005 to 2008 (ABARE, 2009)

	Import and Export of iron ore (Mt)			
	2005	2006	2007	2008
Iron ore Imports:				
EU 27	160	172	175	182
Japan	132	134	139	141
China	275	326	392	442
Korea	43	44	44	46
Chinese Taipei	15	15	16	16
World Total	744	781	842	913
Iron ore Exports:				
Australia	239	247	281	307
Brazil	223	252	269	310
India	81	95	97	99
Canada	28	28	26	27
South Africa	27	26	30	33
Sweden	18	19	20	22
World Total	744	781	842	913

2.5 Supply, Demand and Price of Iron Ore

The price of iron ore directly affects the cost of steel products, such as steel bars, cars, and steel machines. Chinese iron ore production cost is generally higher than in other countries due to the low iron content in the Chinese iron ore and the requirement to increasingly import iron ore from other countries, such as Australia. China also continues their mining profitably by increasing the use of low grade iron ore depending on the global iron ore price. Figure 2.3 shows the iron ore price that followed the annual benchmark pricing system with the price below 40 US$ per tonne iron ore before 2004 (World Bank, 2010). From 2004, the price increased by two to three times within four years and reached the record value of 140 US$/t in 2008. The price was about 100 US$ per tonne of iron ore in 2009. Due to the short term pricing contracts, in March 2010 the iron ore price was set at about 180 US$ per tonne which is 90% more than the price in the year 2009.

Iron ore market was affected recently by demand downturn due to the drop in steel demand during the global economic recession in 2008. Iron ore price can be fixed by benchmark system or by short term pricing contract, depending on the supply-demand balance and reduction in variation of the spot market price. For example, the two largest iron ore producers, Vale SA and BHP Billiton started short-term price contracts with the Asian steel mills in March 2010. The increasing demand of iron ore by the Asian mills in the last decade, especially in China, has driven the rise in price of iron ore.

2.6 Ironmaking Processes

Ironmaking is the most energy intensive part of the iron and steel making process. The fundamental nature of ironmaking process is to produce metallic iron from iron ore in a process termed smelting. Heat is required for generating high temperature to convert to metallic iron from iron ore. Oxygen is removed from iron ore by adding a chemical reductant. The blast Furnace (BF) is the main route to produce iron for steelmaking in which metallurgical coke is used as fuel and reductant. Alternative ironmaking processes, such as Direct Reduced Iron (DRI) by using non-coking coal as a reductant without the requirement to produce coke first, are also developed due to high cost of coking coal and negative environmental impacts of coking and sinter plants.

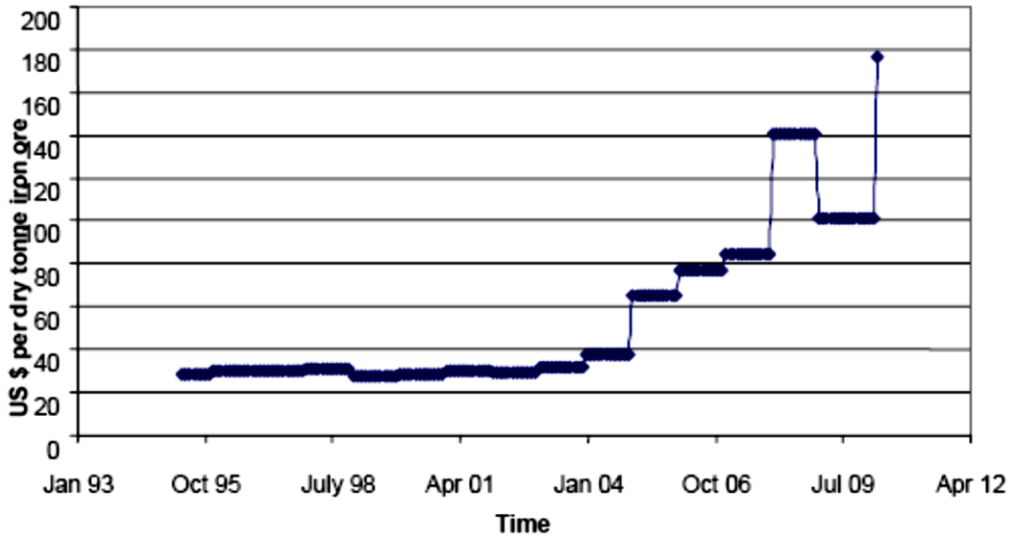

Figure 2.3 Global iron ore price from 1994 to 2010 (World Bank, 2010).

2.6.1 Raw Materials Preparation

2.6.1.1 Beneficiation

Beneficiation is a process during which iron content of low grade iron ores is increased through concentration. It also decreases the impurities of iron ore and increases the productivity of iron and steelmaking. Beneficiation of iron ores is performed by different techniques, such as washing, jigging, magnetic or gravity separation and flotation. The selection of suitable techniques depends on the nature and behavior of impurities within the ore structure, as iron ores have different characteristics depending on their geological location. Specific beneficiation and metallurgical treatment is required according to the iron ore types. For example, crushing, milling and heavy liquid separation are recommended beneficiation processes for iron ores containing high silica content, due to their higher density compared to the silicates. After crushing, fine particles pass through a bath of solution containing bentonite used to increase the density of the solution. After proper calibration of the density of solution, iron ore can be collected from the sink, while silicates are floated and removed.

2.6.1.2 Agglomeration

Blast Furnace (BF) use agglomerated iron ores, due to the charging requirements of the operation. Agglomeration is performed by igniting iron ores at lower temperature causing only interfacial fusion with or without additives, such as limestone and dolomite. Two types of agglomeration process, such as sintering for making sinter and pelletising for making pellets, are commonly used. Sinter is a uniform size clinker like aggregate used as feed material in the blast furnace which is produced from coarser fines of iron ore mixed with fine coke particles (coke breeze), limestone, dolomite fines and other metallurgical wastes from the processing plant. Sintering reduces coke consumption, increases productivity and improves overall BF performance. Sinter plants generate particulate matter originated from different compounds such as iron oxides, sulphur oxides, carbonaceous compounds, chlorides, fluorides, ammonia, and various metal composites (Steiner, 1976). Particles can be controlled by cyclones, electrostatic precipitators, scrubbers or fabric filters. The collected particles are generally recycled as feedstock to the sinter plant or can be dumped in landfills (Baker Environmental, 1992; EPA, 1995). Wastewater is generated from wet air pollution control devices and its composition may include suspended solids, oil and grease, ammonia-nitrogen, cyanide, phenolic compounds, and heavy metals, such as lead, zinc, arsenic, cadmium, copper, chromium and selenium (EPA, 2000).

A pellet is a spheroid mass typically 8 – 18 mm in diameter produced from fine moist iron ore followed by high temperature firing. Moist concentrates are rolled in a revolving drum to prepare small spheroid forms termed green pellet or ball. The green pellets are heated in a high temperature furnace to produce hard pellets containing 60 – 65% iron which are suitable for the blast furnace. The furnace used for pelletising requires about 240 MJ heat per tonne of produced pellets for natural magnetite and 1,500 MJ heat per tonne pellets for limonite (Metals Advisor, 2010).

2.6.2 Blast Furnace (BF)

The blast furnace is a tall shaft-type counter flow reactor used to produce hot metal by physically converting and chemically reducing iron oxides**.** This is the first step to produce steel products from iron oxides. A modern blast furnace is capable to produce liquid iron at about 13000 tonnes per day. In comparison, the original blast furnaces from the 14th century were with capacity of one tonne per day. The raw materials, such as iron ore (lump, pellet or sinter), coke, and limestone are fed from the top and preheated air is blown from the bottom of the blast furnace. The iron rich ore can charge directly into the blast furnace without further processing. Lower graded ore is processed and converted into sinter or pellet to increase the iron content before feeding the blast furnace. Several chemical reactions shown below are involved in the furnace to produce liquid iron and liquid slag. Coke plays important physical, chemical and thermal role in the blast furnace process. Coke in the blast furnace has physical role to maintain the furnace permeability. Its chemical role is to supply carbon in the high temperature zone of the furnace for production of reducing CO gas. Coke also acts as a direct reductant to reduce iron oxides. Coke supplies about 80% of the required heat of the blast furnace by its thermal process.

$C + O_2 \rightarrow CO_2 + \text{heat}$ (2.1)

$CO_2 + C \rightarrow 2CO$ (2.2)

$3Fe_2O_3 + CO \rightarrow CO_2 + 2\ Fe_3O_4$ (Begins at 450 ^{0}C) (2.3)

$Fe_3O_4 + CO \rightarrow CO_2 + 3\ FeO$ (Begins at 600 ^{0}C) (2.4)

$FeO + CO \rightarrow CO_2 + Fe$ [or $FeO + C \rightarrow CO + Fe$] (Begins at 700 ^{0}C) (2.5)

$CaCO_3 \rightarrow CaO + CO_2$ (2.6)

$FeS + CaO + C \rightarrow CaS + FeO + CO$ (2.7)

Coke is ignited with preheated air at the bottom of the blast furnace (Equation 2.1). Reducing gas is produced by coke carbon gasification reaction with oxygen. CO_2 is reduced to CO (Equation 2.2 – Boudard reaction) as the reaction occurs at high temperature with excess carbon. The reducing gas (CO) flows upward to reduce iron bearing materials and produce hot metal (Equations 2.3-2.5). The limestone in BF is converted into CaO at about 875 ^{0}C (Equation 2.6) and used to remove sulphur from the hot metal which is essential for steelmaking. CaS (generated by Equation 2.7) is removed as a liquid slag. The quality of hot metal depends on the quality of coke and ferrous burden materials, such as sinter and pellet. According to Ricketts (2010) the typical hot metal contains Fe (93 - 95%), Si (0.30 – 0.90%), S (0.025 – 0.050%), Mn (0.55 – 0.75 %), P (0.03 – 0.09%), Ti (0.02 – 0.06%) and C (4.1 – 4.4%). The impurities of coke, pellet and sinter are removed from the blast furnace as liquid slag, off-gases and particles.

2.6.2.1 Global production of hot metal

Hot metal production by blast furnace will remain the dominant route of ironmaking in the foreseeable future because of its production capacities and maturity of the technology providing better thermal balance in the furnace reactor. A slight decrease of blast furnace production by about 1% may be achieved by increasing production through electric arc furnace. Figure 2.4 shows the blast furnace hot metal production globally from 1980 to 2009. The global metal production in 2000 was 576 million tonnes which increased about 64% in 2007 and reached the production of 948 million tonnes. Then the production decreased by about 5.5% reaching 898 million tonnes in 2009 due to the economic recession and decreased demand for steel. The rapid production growth in China steel sector, as indicated in Fig 2.2 and Table 2.5, has contributed to the rapid increase of global hot metal production since 2004.

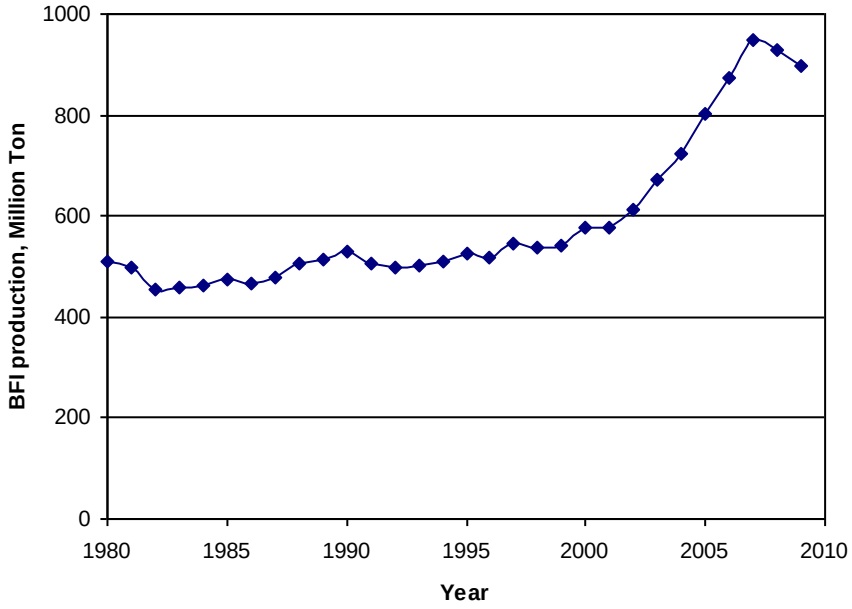

Figure 2.4 Global Blast Furnace hot metal production from 1980 to 2009 (WSA, 2010)

2.6.2.2 Pollutants production and emissions

The formation of liquid slag and its mineralogical composition influence the quality of hot metal. Typical compositions of slags are shown in Table 2.6. The melting characteristics and fluidity of slag has a significant role to determine the BF productivity as the cohesive zone of BF is predominantly influenced by the melting zone of slag. The liquid slag is formed from silica (SiO_2), alumina (Al_2O_3), magnesia (MgO) or calcia (CaO) originated from iron ore, pellet, sinter, flux or coke. These slags are removed from the bottom of the furnace by floatation as liquid iron is denser than the liquid slag. Slags can be granulated by using water jet and instantly cooled from 1500 ^{0}C to 100 ^{0}C. The granulated slag can be used as raw material for cement industry or as aggregate for roads.

Emissions of particulate matter and off-gases result from the furnace top gas and hot blast stove of the blast furnace. Top gas can be cleaned by a dust collector, cyclone gas cleaning and washing equipment. The heat from the off-gases can be recovered to preheat the air entering the BF and to generate steam to produce compressed air in the boiler house. Blast furnace off gas composes primarily of CO. The particulate emission areas are the taphole, main runner, skimmer, hot metal and slag runner and transfer points. The generated particles can be removed by cleaning the extracted flow through control technologies, such as fabric filters or electrostatic precipitators. The particulate matter may contain solid components containing Fe, C, SiO_2, Al_2O_3, CaO, and MgO (Steiner, 1976). Emission of particulate matter, SO_x, NO_x, CO can also be reduced by controlling the hot blast stoves. A

portion of particulate matter and off gases is still released to the atmosphere which may cause negative impacts on human health and environment. Improvement of blast furnace slag and off-gas management by recycling and recovery activities can enhance the process efficiency and reduce the pollution load.

Table 2.6 Typical composition of blast furnace slag (OMNR, 1992)

Constituent	Percent							
	1949[a]		1957[a]		1968[a]		1985[a]	
	Mean	Range	Mean	Range	Mean	Range	Mean	Range
Calcium Oxide (CaO)	41	34-48	41	31-47	39	32-44	39	34-43
Silicon Dioxide (SiO_2)	36	31-45	36	31-44	36	32-40	36	27-38
Aluminum Oxide (Al_2O_3)	13	10-17	13	8-18	12	8-20	10	7-12
Magnesium Oxide (MgO)	7	1-15	7	2-16	11	2-19	12	7-15
Iron (FeO or Fe_2O_3)	0.5	0.1-1.0	0.5	0.2-0.9	0.4	0.2-0.9	0.5	0.2-1.6
Manganese Oxide (MnO)	0.8	0.1-1.4	0.8	0.2-2.3	0.5	0.2-2.0	0.44	0.15-0.76
Sulfur (S)	1.5	0.9-2.3	1.6	0.7-2.3	1.4	0.6-2.3	1.4	1.0-1.9

[a] Data source is the National Slag Association data: 1949 (22 sources); 1957 (29 sources); 1968 (30 sources) and 1985 (18 sources).

2.6.3 Blast furnace productivity

The productivity of ironmaking by blast furnace can be increased and also further optimised to reduce the specific consumption of raw materials and pollutants emission. The productivity of blast furnace can be increased by improving reactor permeability and decreasing the consumption of reducing agents. The reactor permeability can be improved by maximising the total gas throughput per unit time and by decreasing the specific gas requirement which can result in reduction of the specific consumption of reducing agents. The overall blast furnace permeability can be further improved by improving the composition and quality of burden materials, improving behavior of burden materials during reduction, controlling the shape and position of cohesive zone,

improving liquid evacuation from the hearth such as quantity of slag, coke size and liquid flow conditions (Lacroix et al., 2001). These activities can also reduce the specific gas consumption. In addition, the significant way to decrease the specific gas volume is the enrichment of high levels of gas injection to the reactor and thus reducing coke consumption. The furnace design (size and shape) and process control are also important factors to optimise the blast furnace productivity and performance.

2.6.4 Direct Reduced Iron (DRI)

The direct reduced iron (DRI) is an alternative ironmaking process in which iron ores are reduced using reducing gas consisting of hydrogen (H_2) and/or carbon monoxide (CO) or coal at relatively low temperature of about 1000 ^{0}C. There is an increasing interest in DRI processes for several reasons: i) insufficient supply and growing demand of quality iron scrap feed for Electric Arc Furnace (EAF) for steelmaking; ii) conventional steelmaking BF – BOF route is high cost and energy intensive; iii) DRI processes alleviate the need for coke production from coking coal essential for BF; iv) integrated steel plants are with larger pollution potential than DRI processes. Several DRI processes are commercially available with reasonable degree of process optimisation, however, their productivity rates are still not competitive with BF.

About 85% of the global DRI processes are produced by the gas based shaft furnace process, such as Midrex and HyL. Hot Briquetted Iron (HBI) is DRI that has been compacted at a temperature greater than 650 °C to minimise the specific area, thereby reducing the risk of ignition and reoxidation resulting in better handling, transporting, storage, and melting characteristics. Fluidised bed gas based processes, such as Fior, FINMET and Circored reduce iron ores in fluidised beds and have higher productivity and lower energy consumption. Finmet plant operates in Venezuela and Circored is in Trinidad. Rotary Hearth Furnace (RHF) and Rotary Kiln Furnace (RKF) processes such as FASTMET, INMETCO, IDI, SL/RN and the Circofer are processes that utilise coal as a reductant and were introduced because of the increased price of natural gas. DRI processes are often installed upstream to the electric arc furnace to transport hot iron directly, called the Hot Direct Reduced Iron (HDRI), to save energy and increase productivity.

Figure 2.5 shows the global DRI production from the year 1990 to 2008. The DRI production increased four times and reached 68.5 million tonnes in 2008 from 17.7 million

tonnes in 1990. Due to the economic recession the DRI production in 2008 achieved only small increase by 1.8% compared to the previous year. The global production by different DRI processes is shown in Figure 2.6. Midrex, HyL and coal based Rotary Kiln processes are the major contributors of DRI production. Midrex increased about four times with a share of about 58% of the total DRI production and reached production of 40 million tonnes in 2008. Rotary Kiln started to increase the production rapidly from the year 2001 reaching 17.3 million tonnes in 2008 which exceeded the production of 9.92 million tonnes by the HyL process. In 2008, the gas based processes produced 50 million tonnes DRI contributing about 73% of the global DRI production, whereas the coal based processes produced 17.6 million tones of DRI. Improved understanding of flow kinetics and effect of operational variables on reduction rates are required to increase the productivity and energy efficiency of the DRI processes. Coal based Scrap-EAF process from US generates the lowest CO_2 emissions of 641 kg per tonne liquid steel which shows the recycling potential of steel products (Geiger, 1998). Smelting reduction process can reduce CO_2 emission but also produces significant amount of off-gases which could be recycled to increase the process efficiency (Emi and Seetharaman, 2000).

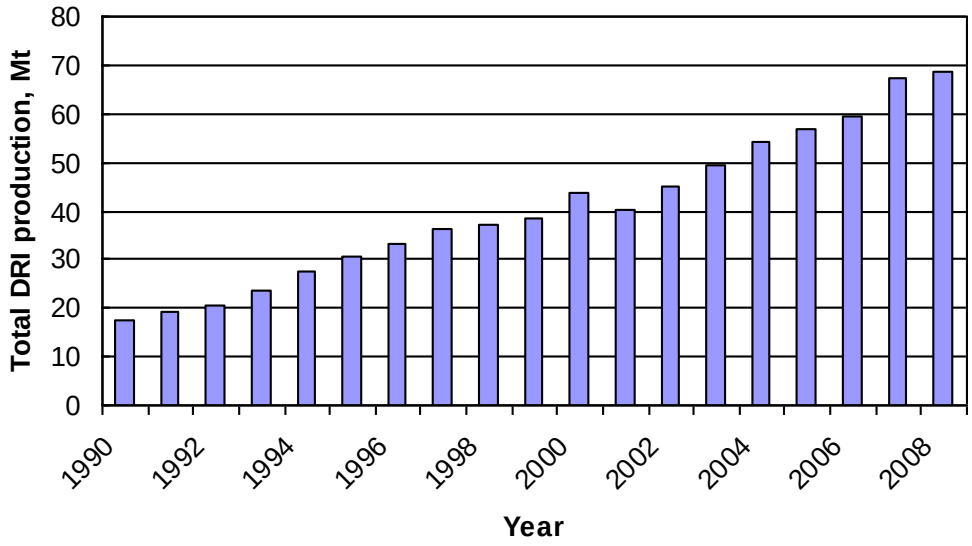

Figure 2.5 Global DRI production from the year 1990 to 2008 (Midrex, 2009) .

2.6.4 Direct Iron Smelting

Iron smelting process is developed to produce liquid iron directly from iron ore, coal and fines or concentrate. Coal is preferable reductant and energy source than natural gas because of its availability and lower cost. Agglomeration costs are also eliminated by directly using coal instead of blast furnace coke. There are several direct iron smelting

processes, such as commercially available COREX, AISI direct steelmaking, Japanese DIOS, Australian HIsmelt, Russian ROMELT, Hoogovens CCF, Italian CleanSmelt process and the Brazilian TECNORED, that were introduced with some success to increase the productivity and reduce the capital cost of iron production. The COREX process produces pig iron with reduced pollution and cost. The process is integrated with coal desulphurisation applying flexible coal types, while the generated excess electricity can be sold to the power grid (USEPA, 1995). Japanese Direct Iron Ore Smelting (DIOS) process replaces coke with coal in a powder or granular form which when directly fed to a smelting reduction furnace produces heat and melts ore, and reduces carbon dioxide emission by 4 to 5% compared to conventional BF process (Furukawa, 1994). The HIsmelt process in Australia is another coke-free iron smelting process. The Tecnored process utilises hot and cold blast and requires no additional oxygen resulting in much lower operating and investment costs compared to the traditional ironmaking processes. Iron smelting processes are still at their early phase and require better understanding to improve productivity and have major impact on the industry and environment.

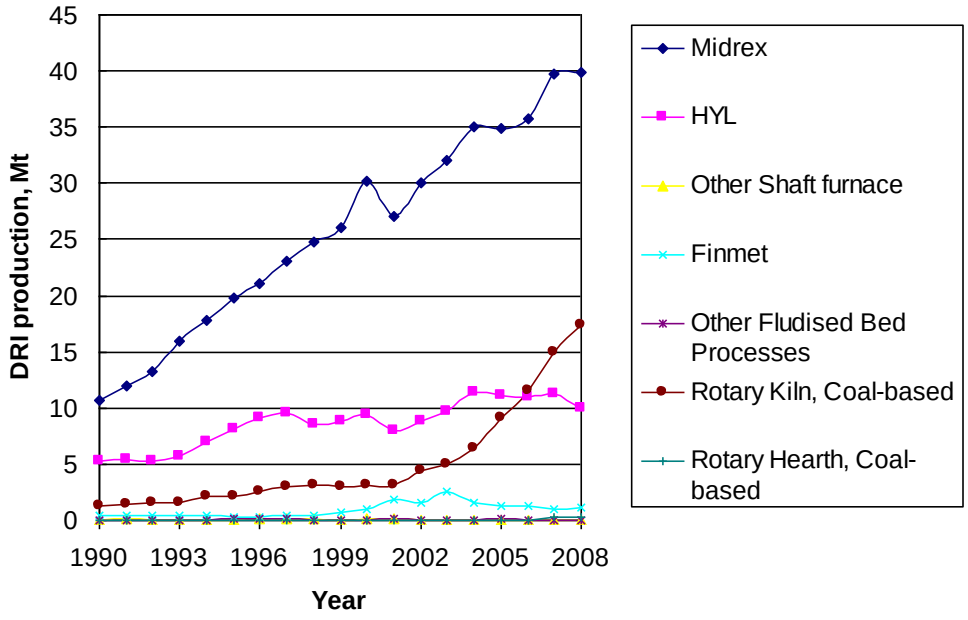

Figure 2.6 Global DRI production by process types from 1990 to 2008 (Midrex, 2009).

2.7 Australian Ironmaking Perspective

Iron ore is the fourth important mineral for the Australian economy with exports of approximately 90% of the total production designated to markets in Asia. The detailed

iron ore history of Australia is found from the works of Canavan (1965), Edmonds and Stenlake (1965), Raggatt (1968), Trendall (1979), Madigan (1980), Blockley et al. (1990), O'Leary (1993), Griffiths (1998) and Mudd (2009). Australia ranked third in 2007 by production, contributing about 16% of the global iron ore production, behind China and Brazil. Western Australia is the region dominating iron ore industry in Australia, contributing about 97% of the total iron ore production. About 24% of Australian iron ore constitutes of magnetite ore. The Pilbara region from Western Australia provides a significant iron ore resource. Iron ore mining is also performed in the Northern Territory, South Australia, Tasmania and New South Wales but in smaller scale. The production rates of iron ore in Australia are shown in Figure 2.7. Australian iron ore production rates increased by 8.9% in 2007 by addition of some deposit areas, such as Marillana, Mungada, Phils Creek and Red Hill-West Pilbara (Geoscience Australia, 2008). The iron ore resources in Australia are extensive and some of the highest in quality in the world. It is estimated that the resource life of the mining sites will exceed 65 years. The iron ore production forecast by ABARE (2009) suggests that production will be increased and will reach 522.8 Mt by 2012 and exports will also rise to 488.7 Mt over the same period. BHP Billiton and Rio Tinto are the two major companies for iron ore production which are also expanding their ore production and infrastructures. Iron ore industries in Australia achieve continuous profit increases from the increased iron ore operations which is one of the indicators of industrial sustainability.

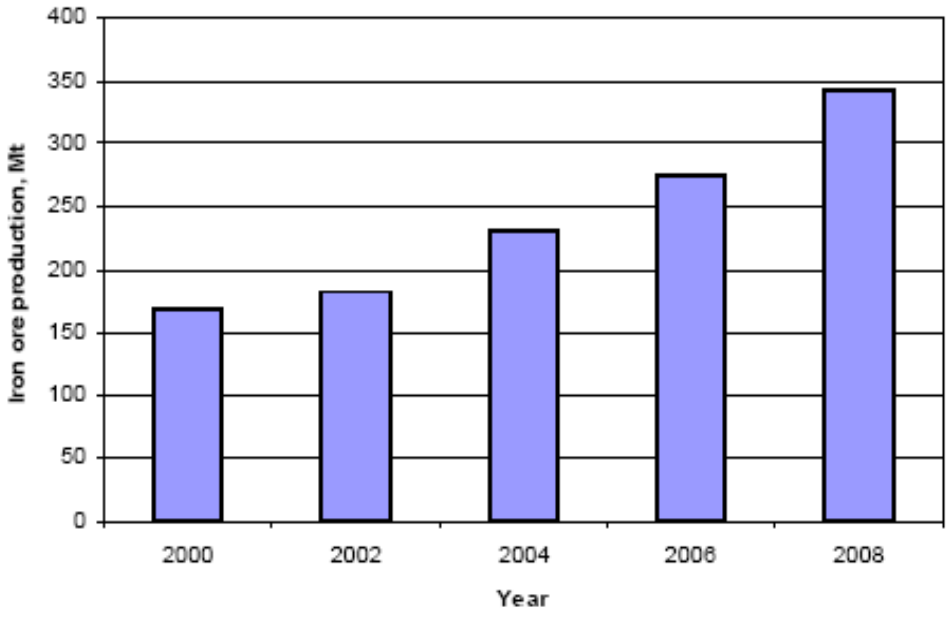

Figure 2.7 Iron ore production in Australia from 2000 to 2008 (USGS, 2010)

The iron ore industries are responsible and committed to operate in environmentally acceptable principles and to improve their environmental performance. Australian iron ore mines are required to maintain the environmental standards from planning to post operational site rehabilitation. Environmental requirements are also imposed to the mining industries to initiate or develop any projects by state and territory mining acts and related legislations. Reduction in pollutant emissions by the iron ore sector is an important target required to reduce air, water and land pollution. Other environmental aspects include visual landform, noise level, impacts on flora, fauna and historic sites, which are also important concerns to consider for minimising the negative environmental impacts.

Iron ore processing industries contribute to atmospheric pollutant emissions. Table 2.7 shows Australian atmospheric emissions of pollutants per million tonne of iron ore production from all mining facilities in Australia reported to the National Pollutants Inventory (NPI) from the year 2001 to 2008. The iron ore production doubled in the year 2008 compared to 2001 but the emissions of pollutants, such as PM_{10}, CO, NO_2, SO_2, As, Cr(VI), Cd, Ni, Pb and Hg decreased significantly in this period. The emission per million tonne iron production also decreased for PM_{10}, CO, NO_2, SO_2, As and Ni in 2008 compared to the previous year by improving the emission control processes and increasing the recycling and recovery activities of generated waste. But the emission of Hg, Cr(VI), Pb and Ni for the same period increased, which requires to be addressed to ensure environmental sustainability. Emissions can be further reduced by adopting energy efficient processes and reduction of raw materials consumption.

The iron ore impurities, such as presence of silica (SiO_2), phosphorous (P), alumina (Al_2O_3), sulphur, and smelting characteristics are the major concerns for the iron and steelmaking processes (Jack, 1922; Woodcock, 1980; Woodcock and Hamilton, 1993; Ferenczi, 2001). Majority iron ore processes include crushing, beneficiation to confirm with the quality requirements for smelting purposes by increasing iron grades and removing impurities (Madigan, 1980; Bensley *et al.*, 1993a; Bensley *et al.*, 1993b; Langenberg, 1993; Tan and Jackson, 1993).

Table 2.7 Emissions of atmospheric pollutants per million tonne of iron ore production from iron ore mining industries in Australia (NPI, 2009; USGS, 2010)

Pollutants	2001	2002	2003	2004	2005	2006	2007	2008
PM_{10} (t)	38.8	102.1	63.1	51.8	48.0	46.0	58.3	47.9
CO (t)	4.51	10.8	10.4	5.38	9.17	8.94	7.97	6.59
NO_2 (t)	8.26	32.1	20.9	9.52	10.2	9.4	8.81	6.44
SO_2 (t)	1.29	2.85	2.66	1.31	1.16	1.1	0.68	0.59
As (kg)	2.55	3.04	3.6	2.89	3.75	4.24	4.26	2.37
Cr(VI) (kg)	0.18	0.16	0.15	0.12	0.1	0.08	0.07	0.11
Ni (kg)	0.18	4.82	4.77	3.57	4.24	4.19	4.69	3.6
Pb (kg)	1.14	1.19	1.35	1.18	1.24	1.14	1.37	2.47
Cd (g)	75	41	46	28	24	23	35	57
Hg (g)	27	4	3	3	6	3	4	14

In 1850, the blast furnace was first introduced for iron ore processing in Mittagong, New South Wales in a small and eventually uneconomical project (Harper, 1928). The productivity of blast furnace improved significantly by the reduction of coke consumption and improving recycling facilities. Figure 2.8 shows the production of iron by blast furnace in Australia from 1980 to 2009. Supply and demand of export and local market, steel price and global economic recession are responsible for the significant fluctuations of blast furnace iron production in Australia.

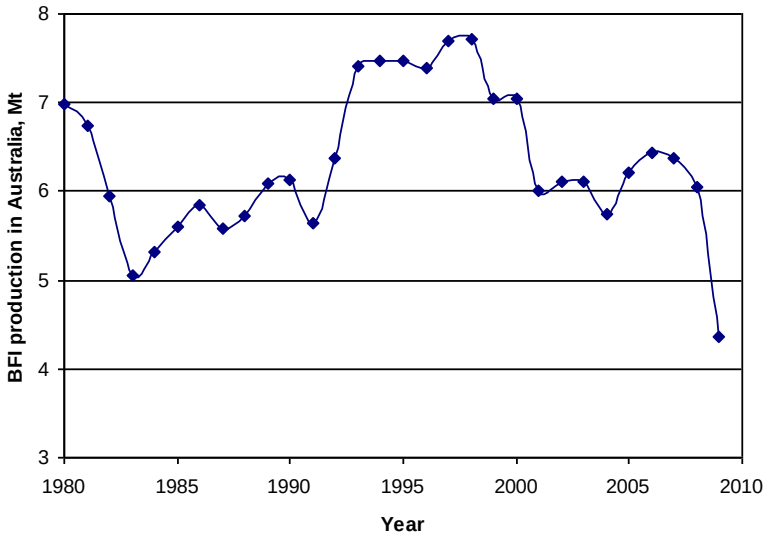

Figure 2.8 Blast furnace iron ore production in Australia from 1980 to 2009 (WSA, 2010).

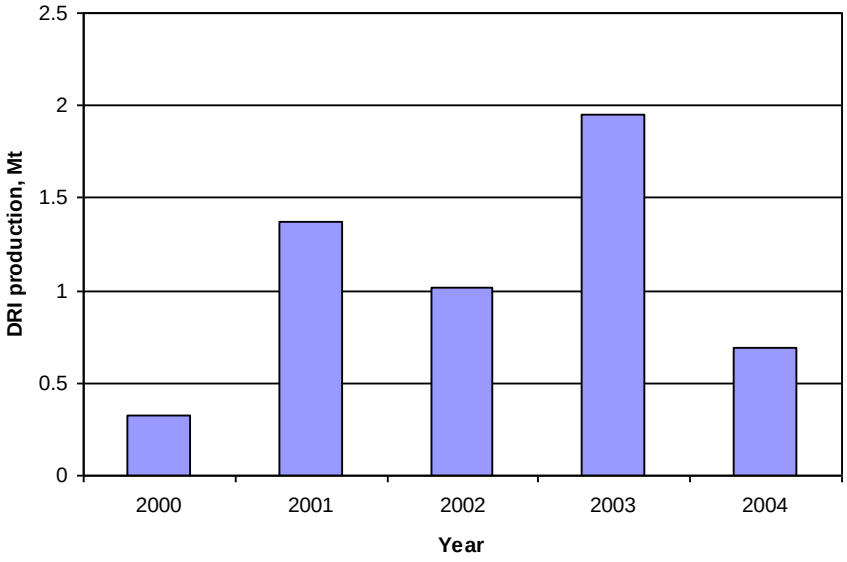

Figure 2.9 DRI production in Australia from 2000 to 2004 (WSA, 2010)

The emissions from blast furnace and associated material preparation for coke, sinter and pellet making are significant and need to be reduced to ensure the environmental sustainability. New direct iron ore reduction technologies have been introduced in Australia but with limited success. Figure 2.9 shows the DRI production in Australia from 2000 to 2004.

The HIsmelt process was installed to eliminate coke ovens, sinter plants and pellet plants which are potential source of emissions of greenhouse gas and toxic pollutants. This process accepts lower grade iron ore than blast furnace thus minimising waste and reducing cost. The HIsmelt process is with high energy efficiency and better emission performance, however, due to poor market conditions the HIsmelt process in Australia closed in 2004.

2.8 Conclusions

Iron ore is naturally occurring rock with mineral deposits primarily consisting of iron oxides, such as, hematite, magnetite, goethite or siderite. The global iron ore production has significantly increased in the last 15 years due to the increasing demand for steel products. To achieve industrial and environmental sustainability the industry aims to increase production rates while decreasing emissions of pollutants. The trend of pollutant emissions per tonne of iron from iron ore processing industries in Australia has significantly decreased over time. Productivity of blast furnace during ironmaking has

also increased and further attempts are being made to optimise the consumption of raw materials and pollutant emissions. Improvement of blast furnace slag and off-gas management by recycling and recovery activities enhances process efficiency and reduces pollution load. The DRI processes are in development in order to alleviate the need for coke ovens, sinter or pellet plants which are potential sources of pollutant emissions. Their contribution to global iron production increased four times since the year 1990. Improved understanding of flow kinetics and effect of operational variables on reduction rates are required to increase the productivity and energy efficiency of the DRI processes.

2.9 References

Australian Bureau of Agricultural and Resource Economics (ABARE) 2009, Data of global export and import of iron ore, Access on: 2010 May 15, Available From: http://www.abare.gov.au/publications_html/energy/energy_10/energy_10.html

American Iron and Steel Institute (AISI) 2001, Steel Industry Technology Roadmap - published by Strategic Planning for Research and Development committee of AISI.

Baker Environmental Inc. 1992, Report on Steel Industry Waste Generation, Disposal Practices, and Potential Environmental Impact, prepared for the American Iron and Steel Institute.

Bensley, C N, Fenton, K L and Turner, J. 1993a, Iron Ore Beneficiation by BHP Iron Ore in Western Australia. In "Australasian Mining and Metallurgy: The Sir Maurice Mawby Memorial Volume Second Edition", J T Woodcock and J K Hamilton (Ed's), Australasian Institute of Mining and Metallurgy (AusIMM), Parkville, VIC, Monograph 19, Vol. 1, pp 276-280.

Bensley, C N, Kyle, P and Watters, K N, 1993b, Iron Ore Crushing and Screening Practice at BHP Iron Ore Operations in Western Australia. In "Australasian Mining and Metallurgy: The Sir Maurice Mawby Memorial Volume Second Edition", J T Woodcock and J K Hamilton (Ed's), Australasian Institute of Mining and Metallurgy (AusIMM), Parkville, VIC, Monograph 19, Vol. 1, pp 263-270.

Blockley, J G, Reid, I W and Trendall, A F, 1990, Geological Aspects of Australian Iron Ore Discovery and Development. In "Geological Aspects of the Discovery of Some Important Mineral Deposits in Australia", K R Glasson and J H Rattigan (Ed's), Australasian Institute of Mining and Metallurgy (AusIMM), Parkville, VIC, Monograph 17, pp 263-285.

Canavan, F, 1965, Iron Ore Deposits of Australia. In "Eighth Commonwealth Mining and Metallurgical Congress", J McAndrew (Ed.), Australasian Institute of Mining and Metallurgy (AusIMM), Parkville, VIC, Vol. 1 Geology of Australian Ore Deposits, pp 13-23.

Downs, R.T. and Hall-Wallace, M. 2003, 'The American Mineralogist Crystal Structure Database'. American Mineralogist 88, 247-250.

Edmonds, W and Stenlake, R W, 1965, Iron and Steel. In "Eighth Commonwealth Mining and Metallurgical Congress", J T Woodcock (Ed.), Australasian Institute of Mining and Metallurgy (AusIMM), Parkville, VIC, Vol. 3 - The Australian Mining, Metallurgical and Mineral Industry, pp 21-65.

Emi, T and Seetharaman, S. 2000, Future steelmaking plant with minimized energy consumption and waste evolution, Scandinavian Journal of Metallurgy, Vol.29, pp.185–193.

Ferenczi, P A, 2001, Iron Ore, Manganese and Bauxite Deposits of the Northern Territory. Northern Territory Geological Survey (NTGS), NT Department of Mines and Energy (NTDME), Report 13, Darwin, NT, 121p.

Frukawa, T. 1994, 5000 Daily Tons of Direct Iron-Ore Smelting by 2000, *New Steel*. 10:11 (November, 1994), pp. 36-38.

Geiger GH. 1998, Proceedings of the International Symposium on global environment and the iron and steel industry, Beijing, China, CMS, pp. 191–196.

Geoscience Australia 2008, Australia's Identified Mineral Resources 2008. Geoscience Australia, Canberra.

Gindalbie Metals, 2010, Magnetite vs Hematite, Report published by Gindalbie Metals Limited, WA, Australia, Access: 2010 May 18, Available From: http://www.gindalbie.com.au/Our+Projects/Magnetite+vs.+Hematite/default.aspx

Goethite Mineral Data (GMD) 2010, "Data of Different Minerals extracted from American Mineralogist Database", USA, Access: 2010 May 17, Available From: <http://www.webmineral.com/data/Goethite.shtml>.

Griffiths, M, 1998, Of Mines and Men: Australia's 20TH Century Mining Miracle 1945-1985. Kangaroo Press, East Roseville, NSW, pp. 200.

Gross G.A., 1965, Geology of Iron Deposits in Canada, Volume 1. General Geology and Evaluation of Iron Deposits, Geological Survey of Canada Economic Report, 22.

Harnmeijer J.P 2003, Banded Iron-Formation: A Continuing Enigma of Geology, University of Washington, USA.

Information Research Centre for Geology Database (IRCGD) 2007, Classification of Iron ore, Rajasthan, India, Access: 2010 May 19, Available From: <http://www.geologydata.info/mettalic/ironore.htm>

Jack, R L, 1922, The Iron Ore Resources of South Australia. Geological Survey SA (GSSA), SA Department of Mines (SADM), Bulletin No 9, Adelaide, SA, pp. 71.

James H.L., 1954, Sedimentary facies of iron formation', Economic Geology, 49, pp. 235-293.

James H.L., 1966, Chemistry of the iron-rich sedimentary rocks, In: Fleischer M. (ed.), 'Data of Geochemistry', 6th edition, Paper 440-W, U.S. Govt. Printing Office, Washington D.C.

Kim Y, Worrell E, 2002, International comparison of CO_2 emission trends in the iron and steel industry. Energy Policy, Vol. 30(10): pp. 827–838.

Kimberley M.M., 1978, Palaeoenvironmental classification of iron formations, Economic Geology, Vol. 73, pp. 215-229.

Lacroix, P., Dauwels, G., Dufresne, P., Godijn, R., Perini, P.G., Stricker, K.P., Virtala, J. 2001, High blast furnaces productivity operations with low coke rates in the European Union, 4th European Coke and Ironmaking Congress Proceedings, Editions de La Revue de Métallurgie, Vol. 1, pp. Pp 259 – 268.

Langenberg, J T, 1993, Iron Ore Concentrator and Pipeline Operations of Savage River Mines, Savage River, Tasmania. In "Australasian Mining and Metallurgy : The Sir Maurice Mawby Memorial Volume Second Edition", J T Woodcock and J K Hamilton (Ed's), Australasian Institute of Mining and Metallurgy (AusIMM), Parkville, VIC, Monograph 19, Vol. 1, pp 284-286.

Madigan, R T, 1980, Developments in Iron Ore Mining and Treatment in Australia, 1960-1978. In "Australasian Mining and Metallurgy : The Sir Maurice Mawby Memorial Volume", J T Woodcock (Ed.), Australasian Institute of Mining and Metallurgy (AusIMM), Parkville, VIC, Monograph 10, pp 57-59.

Metals advisor, 2010. Agglomeration process of iron and steel industries, Access: 2010 April 30, Available From: <http://www.energysolutionscenter.org/heattreat/MetalsAdvisor/index.htm>

Midrex Technologies, 2009, 2008 World Direct Reduction Statistics, Published in first quarter 2009, Available From: <www.midrex.com>.

Mineral Information Institute (MII), 2010, Data of Different Minerals, CO, USA, Access: 2010 April 17, Available From: <http://www.mii.org/commonminerals.html>

Mudd, G M, 2009, The Sustainability of Mining in Australia: Key Production Trends and Their Environmental Implications for the Future. Research Report No RR5, Department of Civil Engineering, Monash University and Mineral Policy Institute, Revised - April 2009.

National Pollutant Inventory (NPI), 2009, Data of PM10 and heavy metals emission from iron ore mining facilities in Australia (ANZSIC class 0801), Department of the Environment, Water, Heritage and the Arts, Access: 2010 June 10-15, Available From: http://www.npi.gov.au/cgi-bin/npidownload.pl?proc=fac

O'Leary, M A, 1993, Overview of the Iron Ore Industry: Twenty-Five Years of Iron Ore Developments in Australia. In "Australasian Mining and Metallurgy : The Sir Maurice Mawby Memorial Volume Second Edition", J T Woodcock and J K Hamilton (Ed's), Australasian Institute of Mining and Metallurgy (AusIMM), Parkville, VIC, Monograph 19, Vol. 1, pp 231-237.

Onoratini, G., Perinet, G., 1985, Mineralogical data of prehistoric red colouring material of Provence: a proof that some of them were certainly obtained by goethite calcination. C. R. Acad. Science Ser. II (301/2), 119–124.

Ontario Ministry of Natural Resources (OMNR) 1992, Mineral Aggregate Conservation Reuse and Recycling, Report prepared by John Emery, Geotechnical Engineering Limited for Aggregate and Petroleum Resources Section, Ontario.

Raggatt, H G, 1968, Mountains of Ore: Mining and Minerals in Australia. Lansdowne Press, Melbourne, VIC, 416p.

Ricketts, J. A., 2010, An Introduction to Blast Furnace Technology". Published in American Iron and Steel Institute (AISI). Access: 2010 May 29, Available From: <http://www.steel.org/AM/Template.cfm?Section=Homeandtemplate=/CM/HTMLDisplay.cfmandContentID=5433>

Simonson B.M., 1985, Sedimentological constraints on the origins of Precambiran iron-formations, Geological Society of America Bulletin, 96, pp. 244-252.

Steiner, B.A. 1976, Air-pollution control in the iron and steel industry, International Metals Reviews (September).

Tan, L K and Jackson, A R, 1993, Iron Ore Crushing and Screening Practice by Hamersley Iron Pty Limited at Mount Tom Price and Paraburdoo, WA. In "Australasian Mining and Metallurgy : The Sir Maurice Mawby Memorial Volume Second Edition", J T Woodcock and J K Hamilton (Ed's), Australasian Institute of Mining and Metallurgy (AusIMM), Parkville, VIC, Monograph 19, Vol. 1, pp 270-273.

Trendall, A F, 1979, Mineral Deposits of Western Australia: Iron. In "Mining in Western Australia", R T Prider (Ed.), University of Western Australia Press, Perth, WA, pp 75-86.

U.S. EPA, 1995, Profile of the Iron and Steel Industry, EPA 310-R-95-005.

U.S. EPA, 2000, Development Document for the Proposed Effluent Limitations Guidelines and Standards for the Iron and Steel Manufacturing Point Source Category, EPA 821-B-00-011.

US Geological Survey (USGS), 2010 Iron Ore Statistics and Information, Published by US Geological Survey, Access: 2010 June 20, Available From: http://minerals.usgs.gov/minerals/pubs/commodity/iron_ore/

Woodcock, J T (Ed.) 1980, Australasian Mining and Metallurgy: The Sir Maurice Mawby Memorial Volume, Australasian Institute of Mining and Metallurgy (AusIMM), Monograph 10, Parkville, VIC.

Woodcock, J T and Hamilton, J K (Ed's), 1993, Australasian Mining and Metallurgy : The Sir Maurice Mawby Memorial Volume Second Edition, Australasian Institute of Mining and Metallurgy (AusIMM), Monograph 19, Parkville, VIC.

World Bank, 2010, 2009 World Development Indicator, Report published by World Bank Available From: <www.worldbank.org>.

World Steel Association (WSA), 2009, Data of crude steel production in Australia from 1980 to 2008, Access: 2010 March 15, Available From: http://www.worldsteel.org./?action=stats_search

Chapter 3

Assessment of CO_2, PM_{10} and Heavy metal emissions from iron and steel industries in Australia

Preface

This literature assessment chapter describes the energy consumption and steel production in Australian iron and steelmaking industries. The atmospheric emission of particles and heavy metals is presented here. The emission reduction alternatives are also discussed in this chapter. This chapter refers to the peer-reviewed conference paper [C1] and the thesis objective [A2].

3.1 Introduction

About half of commercial energy is consumed by the industrial sector and is responsible for approximately the same share of greenhouse gas emissions, particle emissions, and solid and liquid wastes that contaminate the environment. The iron and steel industry is one of the largest energy consumption sectors with approximately 10% of the total energy used for high-temperature processing (EG, 2008). Steel has a significant role in modern societies with continued demand due the versatile application of steel products, and its ability to be recycled with relatively low energy consumption. But atmospheric emission from steel industries is a worldwide problem that needs to be minimised. CO_2, PM_{10} and emissions of heavy metals, such as As, Cd, Cr, Ni, from the point sources of the iron and steel industry has significant local and global impacts on the environment and human health. The global steel industry sector contributes about 6-7% of the total anthropogenic emissions of CO_2 (Hu et al, 2006) due to the consumption of fossil fuels for energy and reduction, and limestone for purification of iron oxides. The industry also releases large amount of PM_{10} to the atmosphere with a potential adverse impact on human health by particle inhalation and respiration deposition (Seaton et al, 1995). Heavy metal emissions from the steel industry may also cause toxic effects on the earth's ecosystem by exceeding the threshold concentration limits (Berggren *et al,* 1990; DeVries and Bakker, 1996). This paper shows the trend of CO_2 and particulate matter emission associated with heavy

metals, like As, Cr(VI), Cd, Ni, Hg, to the atmosphere from iron and steel processing industries in Australia. Seventeen iron and steel industries from Australia have been selected and their emission data collected from the National Pollutant Inventory (NPI) database and analysed. Analysis of pollutants emission trends is necessary to improve the industry performance and reduce the negative impacts.

3.2 Methods

Iron and steel industry atmospheric emission data was collected from the National Pollutant Inventory database under the subclass of iron smelting and steel manufacturing facilities in Australia (ANZSIC class 2110) from the year 2001 to 2008. Seventeen iron and steel facilities were selected from different states in Australia out of which 7 were from New South Wales, three from Queensland, one from South Australia, two from Tasmania, two from Victoria and one from the Western Australia. Emission data was primarily estimated by the individual steel industry and reported to the NPI authority each year. The raw materials consumption data from the iron and steel industry were collected from the Australian Bureau of Agricultural and Resource Economics (ABARE). The crude steel production in Australia from 1980 to 2008 was collected from the World Steel Association database. Data analysis was undertaken to determine any trend in the emitted pollutants so that emission reduction possibilities can be identified and applied to improve the industries performance.

3.3 Energy consumption and steel production in Australia

Steel is produced in a high temperature technological process through reduction of iron ore by coke or some reducing gases like hydrogen and carbon monoxide. Figure 3.1 shows the raw material consumption of the iron and steel industry in Australia from 1980 to 2008 by descending order of coal, natural gas, electricity and other sources which include wood waste, LPG & fuel oils. Figure 3.2 shows the crude steel production in Australia from 1980 to 2008. Steel production data demonstrates considerable variation reaching a production level of 8.9 million tonnes in 1998 and then decreasing over the next five years by 21%. About 7.9 million tonnes of steel was produced in Australia in 2008. Metallurgical coal is the major fuel in this industrial process which requires prior transformation to coke in coke ovens. Energy use in coke ovens is not accounted for in the energy consumption of steel production as it is treated as a part of the fuel transformation sector. About 80% of the energy for iron and steelmaking was provided by coal in the year 1980. In response to

the growing steel production, coal consumption was reduced by 10 to 15% over the following 28 year period by substituting coal with natural gas. Natural gas is used in the Direct Reduction of Iron (DRI) process to provide reduction and heating, while electricity is the major input in the Electric Arc Furnace (EAF) process. Due to the increasing use of DRI and EAF processes, natural gas and electricity consumption has gradually increased by 10% and 5% respectively.

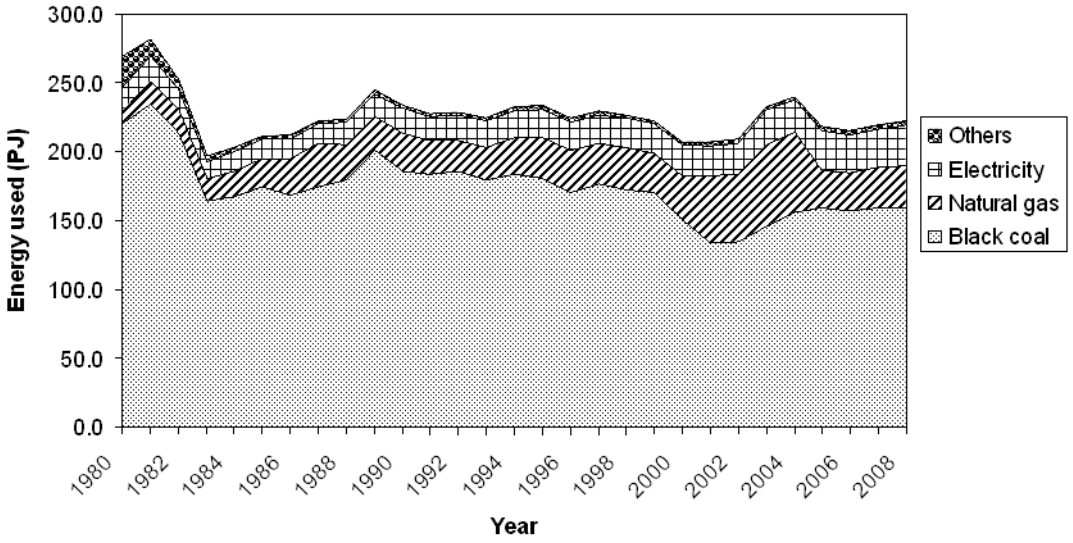

Figure 3.1 Energy consumption from iron and steel industries in Australia from 1980 to 2008 (ABARE, 2009)

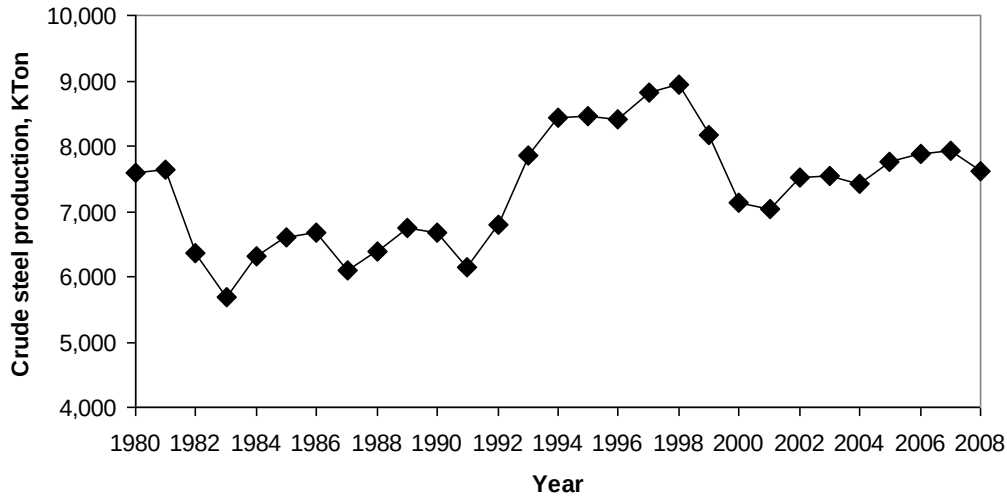

Figure 3.2 Crude steel production in Australia from 1980 to 2008 (WSI, 2009)

3.4 CO_2 emissions

Iron and steel industries are one of the major energy intensive sectors which generate large amount of carbon dioxide (CO_2) from various processes, such as coal combustion, ore reduction, electricity generation and limestone usage. Figure 3.3 shows the significant reduction in total CO_2 emissions from the Australian iron and steel industry from 1990 to 2008. In addition, CO_2 emission efficiency (tonne CO_2 per tonne steel production) has significantly reduced by approximately 40% in the 18 year period shown in Figure 3.4. The amount of total CO_2 production was more than twice the total steel production in the year 1990. Since 1991 CO_2 emissions have decreased, with minor fluctuations, to reach about 1.4 tonne CO_2 per tonne of crude steel in 2007 by reduced coke and increased recycling.

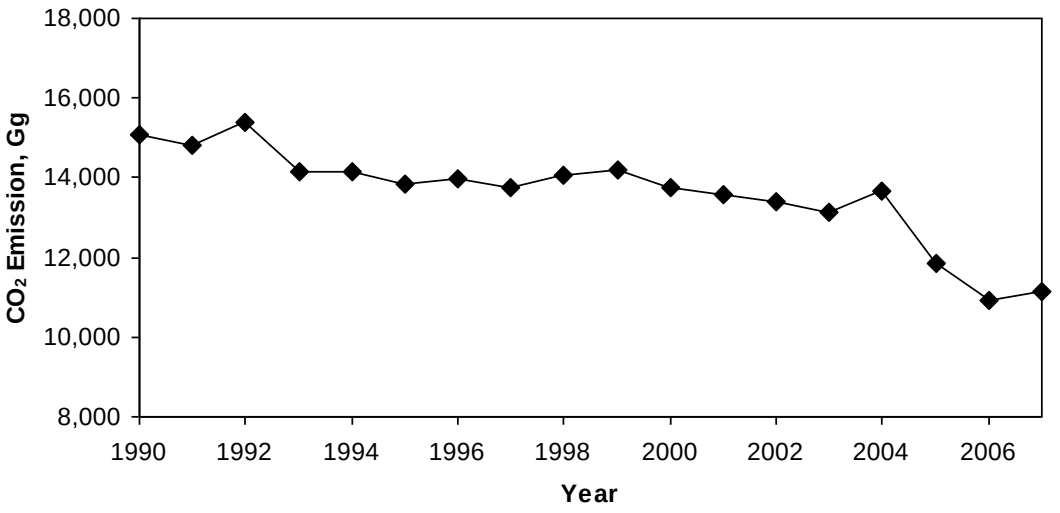

Figure 3.3 CO_2 emissions from iron and steel industries in Australia (DCCEE, 2009)

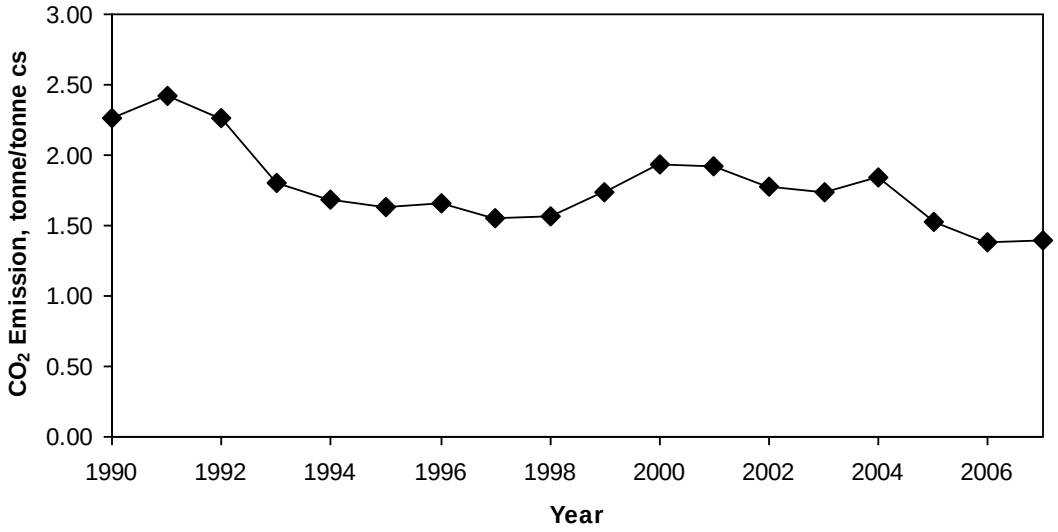

Figure 3.4 CO_2 emissions (t CO_2/t crude steel) from iron and steel industries in Australia

3.5 PM_{10} emissions

Iron and steel industries produce large amounts of particles which can enter the atmosphere and cause negative impacts to human health and the environment according to their physical and chemical properties. In the atmosphere, particles can change their size, adsorb gaseous molecules onto their surface, colloid with each other and be removed from the atmosphere by deposition processes. Epidemiological investigations strongly suggest that mortality and morbidity is increased due to higher concentration of inhalable particles (PM_{10}) (Pope, 2000, Parez et al 2002; Lin et al, 2004; Querol et al, 2004, Arditsoglou et al, 2005; Namdeo et al, 2005). Figure 3.5 shows the total PM_{10} emissions from iron and steel industries in Australia from 2001 to 2008. The figure shows step changes of PM_{10} emission performance data before the year 2004 and after 2006. The PM_{10} emission data exhibits a significant reducing trend from 2004 and reached 0.66 kg/tonne in 2006 but also uncertain increasing trends of about 4% are evident since 2006. Blue Scope steelmaking industry in Wollongong installed advanced emission reduction technology in 2004 (NPI, 2009). Due to the sharp decrease of CO_2 and PM_{10} emissions from BlueScope steel, which produced approximately 80% of total steel in Australia (NPI, 2009), the annual emissions from the Australian iron and steel industries resulted in a sharp decrease of national CO_2 and PM_{10} emissions for this industrial sector.

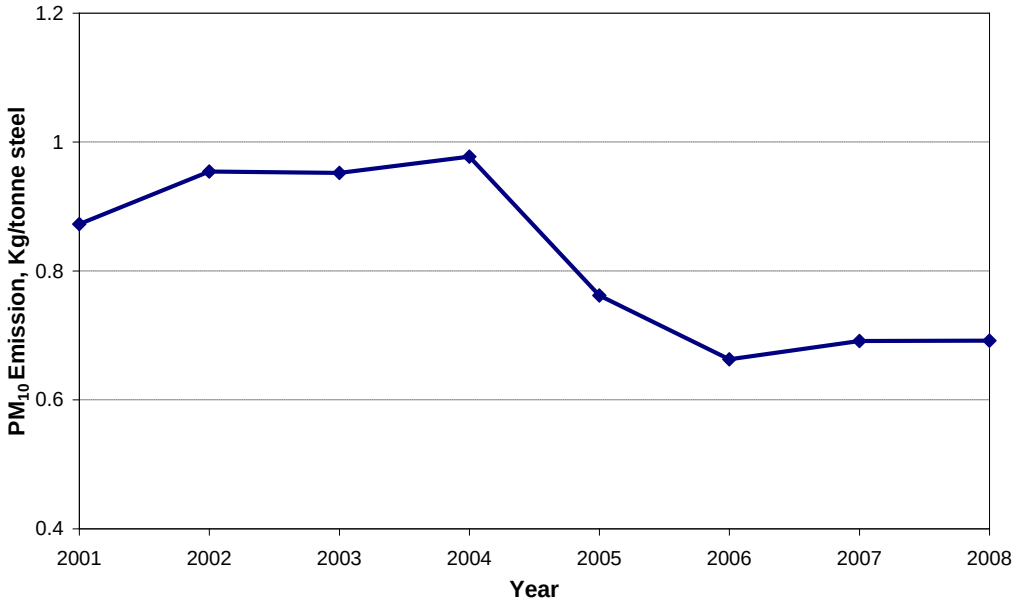

Figure 3.5 PM_{10} emission from iron and steel industries in Australia (NPI, 2009)

3.6 Heavy metal emissions

Some trace metals such as Chromium (Cr), Cadmium (Cd), Nickel (Ni), Lead (Pb), Manganese (Mn), Zinc (Zn), Molybdenum (Mo), Selenium (Se), Scandium (Sc) were found in high concentrations in PM_{10} collected from vicinity of iron and steel industry (Querol et al, 2007). Some of these metals like Cr(VI), Cd, Ni and Pb are acknowledged as priority toxic air pollutants by the Environmental Protection Agency. Figure 3.4 displays total emissions of priority air toxins from the iron and steel manufacturing industries in Australia for the period from 2001 to 2008. In 2003, Ni emissions were increased and reached about 160 mg/tonne steel and then decreased by about 55% in 2008. Cr(VI) and Hg also exhibited reducing trends whereas As and Cd emissions increased by about 4% and 30% in 2008 compared to the previous year which need to be addressed.

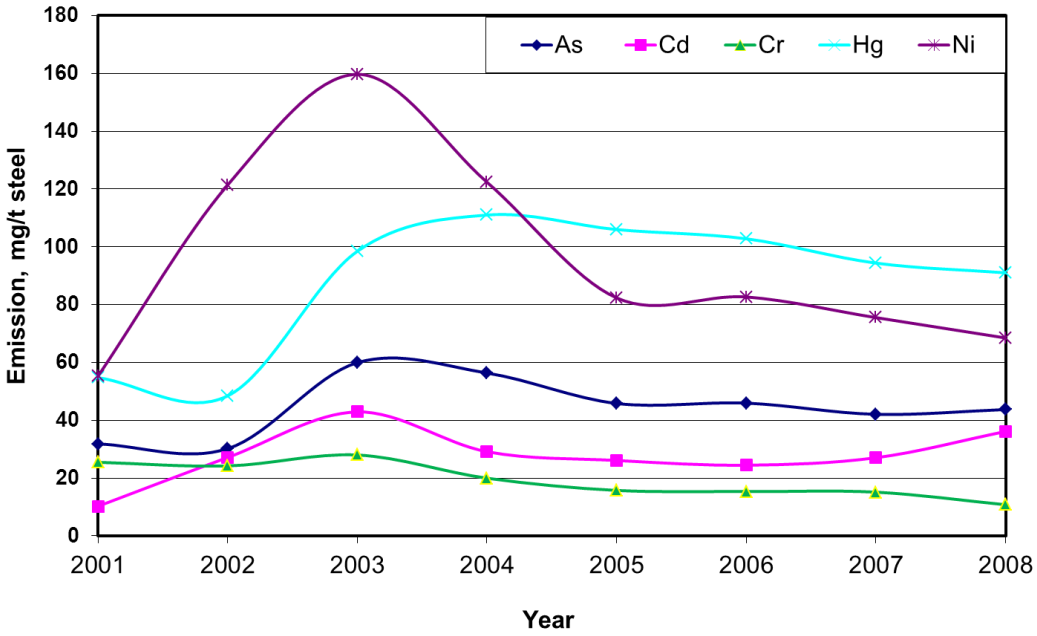

Figure 3.6 Emission of priority air toxins from iron and steel industries in Australia (NPI, 2009)

3.7 Atmospheric emission reduction

Atmospheric emissions from iron and steel industries can be reduced by improving energy efficiency, switching to low emission processes, and the installation of control technologies to minimise the negative impacts and to ensure the safe air quality.

3.7.1 Improving process efficiency

Improvements in iron and steelmaking process efficiency in terms of both energy and ore conversion results in a reduction in raw materials consumption and hence a reduction in CO_2, PM_{10} and heavy metals emissions. Significant pollutant reduction has been achieved by the Australian steel industry through improving energy efficiency. Figure 3.5 shows the trend of aggregated energy consumption per tonne steel production in Australia which has decreased over the period from 1980 to 2008. The energy efficiency has gradually reduced by 10% in the first 10 years from 1980. From 1990 energy efficiency significantly declined and reached the lowest energy consumption value (22 GJ/t) in the year 1998. The energy intensity slightly increased up to the year 2004 and then declined to 25 GJ/t in 2008, which may be due to the installation of energy efficient continuous casting process (NPI, 2009). The successive introduction of energy efficiency technologies, increasing recycling and fuel substitution from coal to natural gas into this sector has

influenced pollutant emissions. The steel production is influenced by the global steel market situation. Thus, it affects the process efficiency as the consumption of raw materials per ton steel may be increased by reducing the steel production from specific process type. In addition, the raw materials may be fed in the steel industry without producing any steel to overcome the faults in the process furnace.

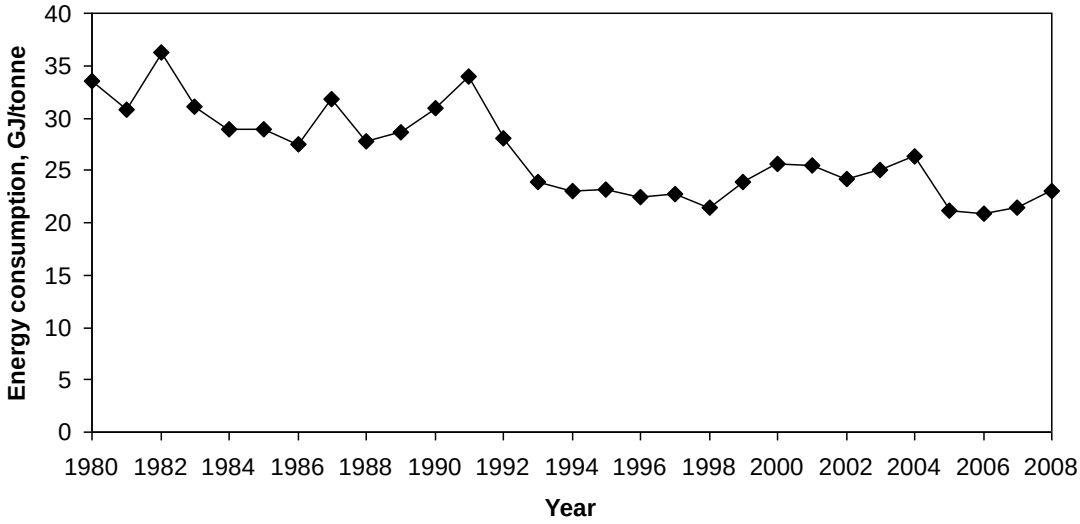

Figure 3.7 Energy consumption in the Australian iron and steel industries (ABARE 2009, & WSI, 2009)

3.7.2 Process switching

Process switching could be another option to reduce emissions by transferring from high energy to low energy consumption processes. Table 3.1 compares the energy efficiency of different countries by process-routes such as Blast Furnace – Basic Oxygen Furnace (BF-BOF) and Scrap-EAF. The Japanese BF-BOF process has the lowest energy consumption (24.7 GJ/t) which is 25% less than the energy used in Australia. The BF-BOF route of Russia consumes 1.2% more energy than Australia. In addition, Japan and Korea has the efficient Scrap-EAF process consuming the minimum energy of 8.4 GJ/t. The energy used by Scrap-EAF process in Australia is less than in Canada, UK, India and Russia.

Each country has a different share of steel production by BF-BOF and Scrap-EAF process routes. For this, changing the utilisation of process by increasing adoption of Scrap-EAF route can significantly reduce up to 60% of the overall energy consumption in each country. For example, if the steel production ratio in Australia by BF-BOF and Scrap-EAF route would be 1.5 with the existing techniques then the aggregated energy efficiency may be reduced to 20 GJ/t. Currently about 80% of total crude steel in Australia is

produced using BOF route. The replacement of open hearth furnace by BOF and EAF increases the process performance. Continuous casting techniques can decrease the energy consumption and increase the yield of steel and improve the product quality. Continuous casting can save about 0.5 – 0.8 GJ/t crude steel in energy compared to ingot casting (Mazur et al, 2003). Also for ironmaking, switching from blast furnace (BF) process to DRI can reduce significant the amount of atmospheric pollutants.

Table 3.1 Energy use by BF-BOF & Scrap-EAF route in different countries (RITE, 2008)

	BF-BOF	**Scrap-EAF**
Country	**Energy consumption GJ/t**	**Energy consumption GJ/t**
Australia	33.1	9.1
Canada	31.8	9.2
China	31.8	9.1
France	30.2	9.1
Germany	28.9	8.8
India	32.7	9.8
Japan	24.7	8.4
Korea	26.0	8.4
Russia	33.5	10.0
UK	30.6	9.4
USA	31.4	8.6

3.7.3 Other processes

A long term approach for additional reduction of pollutant emissions from iron and steel industries may be achieved by increasing the use of hydrogen and renewable energy (da Costa et al. 2013; Piketty et al 2009; Norgate et al. 2011), introduce capture and storage technology for gas and particles with recycling facility, and improve the direct and smelting reduction processes. Individual industry can improve the short-term and long-term emission reduction targets based on resources and technologies to reduce the local and global impact on environment and human health.

3.8 Conclusions

The iron and steel industry is one of the most energy-intensive and atmospheric pollutant emitting industries. Steel industries in Australia have reduced their CO_2 emission trends by about 40% in the last 18 years by adopting energy efficient technologies. Particulates and heavy metal emissions also exhibit reducing trends though reduction of these pollutant emissions are still required to ensure industrial and environmental sustainability, and decrease the negative impacts on the environment and human health from local to global scale.

3.9 References

Arditsoglou, A., Samara, C. 2005, "Levels of total suspended particulate matter and major trace elements in Kosovo: a source identification and apportionment study", Chemosphere, Vol. 59, pp. 669–678.

Australian Bureau of Agricultural and Resource Economics (ABARE) 2009, "Data of energy consumption from iron and steel industries in Australia from 1980 to 2008", Access on: April 20 – 25, 2010.
<http://www.abare.gov.au/publications_html/energy/energy_10/energy_10.html>

Berggren, D., Bergkvist, B., Falkengrengrerup, U., Folkeson, L. and Tyler, G. 1990, "Metal solubility and pathways in acidified forest ecosystems of south Sweden", Science Total Environment, Vol. 96, pp. 103- 114.

da Costa, A.R., Wagner, D. & Patisson, F. 2013, "Modelling a new, low CO_2 emissions, hydrogen steelmaking process", Journal of Cleaner Production, Vol. 46, pp. 27-35.

Department Climate Change and Energy Efficiency (DCCEE) 2009, "National greenhouse gas inventory in Australia", Access on May 15, 2010.
<http://www.climatechange.gov.au/climate-change/emissions.aspx>

DeVries, W. and Bakker, D.J. 1996, "Manual for calculating critical loads of heavy metals for soils and surface waters", Report 114, DLO, Winland Staring Centre, Wageningen, The Netherlands.

EcoGeneration (EG) 2008, "Heat – the forgotten renewable energy, Article published on June 2008 by European Commission, Ecogeneration Publication, Victoria, Australia. Access on February 15, 2010, <http://ecogeneration.com.au/>

Hu, C., Chen, L., Zhang, C., Qi, Y., Yin, R. 2006, "Emission Mitigation of $C0_2$ in Steel Industry: Current Status and Future Scenarios", Journal of Iron and Steel Research, International, Vol. 13(6), pp. 38-42.

Lin, J. & Lee, L. 2004, "Characterization of the concentration and distribution of urban submicron (PM1) aerosol particles", Atmospheric Environment, Vol. 38, pp. 469–475.

Mazur, M., Bogacki, M., Oleniacz, R. 2003, "Assessment of Ecological Effects of the Implementation of Continuous Casting of Steel", Stahl und Eisen, Vol. 23(6/7), pp. 109-113.

National Pollutant Inventory (NPI) 2009, "Data of PM10 and heavy metal emission from iron smelting and steel manufacturing facilities in Australia (ANZSIC class 2110)", Department of the Environment, Water, Heritage and the Arts, Access on May 05-12, 2010. <http://www.npi.gov.au/cgi-bin/npidownload.pl?proc=fac>

Namdeo, A. & Bell, M. 2005, "Characteristics and health implications of fine and coarse particulates at roadside, urban background and rural sites in UK", Environment International, Vol. 31 pp. 565–573.

Norgate, T. & Langberg, D., 2009, "Environmental and economic aspects of charcoal use in steelmaking", ISIJ Int., Vol. 49, pp. 587-595.

Perez, P., Reyes, J. 2002, "Prediction of maximum of 24-h average of PM_{10} concentrations 30 hr in advance in Santiago", Atmospheric Environment, Vol. 36, pp. 4555–4561.

Piketty, M.-G., Wichert, M., Fallot, A., Aimola, L., 2009, "Assessing land availability to produce biomass for energy: the case of Brazilian charcoal for steel making", Biomass Bioenergy, Vol. 33, pp. 180-190.

Pope, C. 2000, "Review: epidemiological basis for particulate air pollution health standards", Aerosol Science Technology, Vol. 32, pp. 4–14.

Querol, X., Viana, M., Alastuey, Moreno, T., A., Castillo, S., Pey, J., Rodrıuez, S., Artinano, B., Salvador, P., Sachez, M., Garcia Dos Santos, S., Herce Garraleta, M.D., Fernandez-Patier, R., Moreno-Grau, S., Minguillo, M.C., Monfort, E., Sanz, M.J., Palomo-Marı, R., Pinilla-Gil, E., Cuevas, E. 2007, 'Source origin of trace elements in PM from regional background, urban and industrial sites of Spain', Atmospheric Environment, Vol. 41, pp. 7219-7231.

Querol, X., Alastuey, A., Viana, M., Rodriguen, S., Artinano, B., Salvador, P., Santos, S., Patier, R., Ruiz, C., Rosa, J., Campa, A., Menendez, M., Gil, J. 2004, "Speciation and origin of PM_{10} and $PM_{2.5}$ in Spain", Journal of Aerosol Science, Vol. 35, pp. 1151–1172.

Research Institute for Innovative Technology for the Earth (RITE) 2008, "International Comparisons of Energy Efficiency: Sectors of Electricity Generation, Iron and steel, Cement", Report published by RITE, Japan.

Seaton, A., MacNee, W., Donaldson, K. and Godden, D. 1995, "Particulate air pollution and acute health effects", Lancet Vol. 345, pp. 176-178.

World Steel Association (WSA) 2009, "Data of crude steel production in Australia from 1980 to 2008". Access on March 15, 2010.
<http://www.worldsteel.org./?action=stats_search>

Chapter 4

Characterisation of trace metals in atmospheric particles in the vicinity of iron and steelmaking industries in Australia

Preface

This chapter describes the mass and elemental content of atmospheric particles in PM_{10}, $PM_{2.5}$, and PM_1. The metal correlations and enrichment factors are also discussed in this chapter. This chapter refers to the Journal article [J1] and the thesis objective [A3]. This study will provide the comprehensive assessment of the particle chemistry which is not regulated, with an exception of lead.

4.1 Introduction

Steel has a significant role in modern society with continued demand due to diverse applications of steel products. Production of iron and steel is associated with a number of significant environmental challenges, one of which is emission of particles to the atmosphere. Iron and steel industries generate a significant amount of coarse particles mainly originating from mechanical processes such as moving piles of iron ore, coal and iron ore loading, and release of and reactions of fine particles in high temperature processes such as cokemaking, sinter plants, blast furnaces and basic oxygen furnaces. Atmospheric particles can have potential adverse impacts on human health through inhalation and respiratory deposition, with children, the elderly and people with respiratory problems being especially vulnerable groups of the population. Metals associated with atmospheric particles can cause harmful effects on human health (Lippmann and Chen, 2009; Lippmann et al., 2006; Bollati et al., 2010) and ecosystems (Berggren et al., 1990; de Vries et al., 2007).

The impact of atmospheric particles on human health and environment depends on their physical and chemical properties. In the atmosphere, particles can change their size, adsorb gaseous molecules onto their surface, coalesce with each other and can be removed

by deposition processes. Epidemiological investigations strongly suggest that human mortality and morbidity is increased due to higher concentration of inhalable particles (Pope III, 2000; Lin and Lee, 2004; Querol et al., 2004; Arditsoglou and Samara, 2005; Dominici et al., 2005; Namdeo and Bell, 2005; Ning and Sioutas, 2010), but respirable particles in the size range of $PM_{2.5}$ and PM_1 are particularly hazardous as they can be transported deep into the alveolar region of the lungs and the bloodstream (Krombach et al., 1997; Park and Wexler, 2008; Valiulis et al., 2008).

Apart from the particle size distribution, the chemical composition of particles is particularly important for environmental assessment of specific emissions. Inhalation of iron dust has been linked to chronic bronchitis, breathlessness, chronic cough (Xu et al., 1992), chronic phlegm (Chen et al., 2006), pneumoconiosis (Kuo et al., 1998), reduced lung function (Banks et al., 1999), and can lead to chronic obstructive pulmonary disease (COPD) (Driscoll et al., 2005). Previous studies showed the chemical properties of atmospheric particles were related to iron emissions with different industrial processes including iron and steel industries (Querol et al., 2004; Garimella and Deo, 2008). Atmospheric particulates generated from iron and steel industries have high concentrations of Cd, Cr, Fe, Mn, Ni and Zn (Machemer, 2004; Querol et al., 2007). Pope III (1996) described how the closure of a Utah Valley steel mill resulted in an overall decrease in PM_{10} concentrations and associated Fe, Cu and Zn content. Hutchison et al. (2005) found increasing inflammation of rat's lungs with increasing metal content in atmospheric particles released from steelworks. In addition, the Fe-bearing particles in total suspended particles and PM_{10} are found in higher concentrations nearby steel plants (Ledoux et al., 2006; Mazzei et al., 2006; Choël et al., 2007), however there are uncertainties in trace metals, including iron associated with size resolved air particles, especially fine and submicron size particles, in the vicinity of iron and steel industries in Australia.

The objective of this study was to investigate the metals associated with atmospheric PM_{10}, $PM_{2.5}$ and PM_1 particles and to reveal the dominant particle size and marker elements in the vicinity of iron and steel industries in Australia. To achieve this, the concentration of selected trace metals Ti, V, Cr, Mn, Fe, Co, Ni, Cu and Zn in atmospheric PM_{10}, $PM_{2.5}$ and PM_1 collected near three iron-steel plants and an urban background sites in Australia were analysed. This work aims to improve the understanding of the dominant size and trace metals, physicochemical characteristics, and human exposure

levels of air particles in the vicinity of different iron and steel processing plants in Australia when compared to the results from a non-industrial urban background site.

4.2 Methods

4.2.1 Sampling sites

Four sampling sites were selected from different areas in Australia to investigate concentration of metals in atmospheric particles collected near different iron and steelmaking plants. These sites were Cringila (CR), Rooty Hill (RT) and Macquarie Park (MQ) located in New South Wales and Whyalla (WH) site located in South Australia. CR and WH sampling sites were located in the vicinity of integrated iron and steel processing industries. The processing route of these industries is blast furnace (BF) - basic oxygen furnace (BOF). RT sampling site was located near an electric arc furnace (EAF) steelmaking process. MQ site was located in an urban area near to the sports field at Macquarie University, about 20 kms from the Sydney CBD. This sampling location was selected for comparison as there should be little very near field influence by industrial activity as the closest significant industrial site is more than 5 km from this location. The CR and WH are described as urban-industrial sites, RT as an industrial site and MQ as an urban-background site. Meteorological conditions especially wind speed and direction at all sampling sites are important influential factors for particle deposition and for their transportation range. Figure 4.1 shows the windroses at CR, RT, WH and MQ sites during PM sampling campaign which indicates the multi directional wind gust at the sampling sites in addition to the downwind direction from Wollongong steelworks (WOS), Rooty Hill steelworks (ROS) and Whyalla steelworks (WHS) as an important parameter for short and long term air particle transportation from multiple sources.

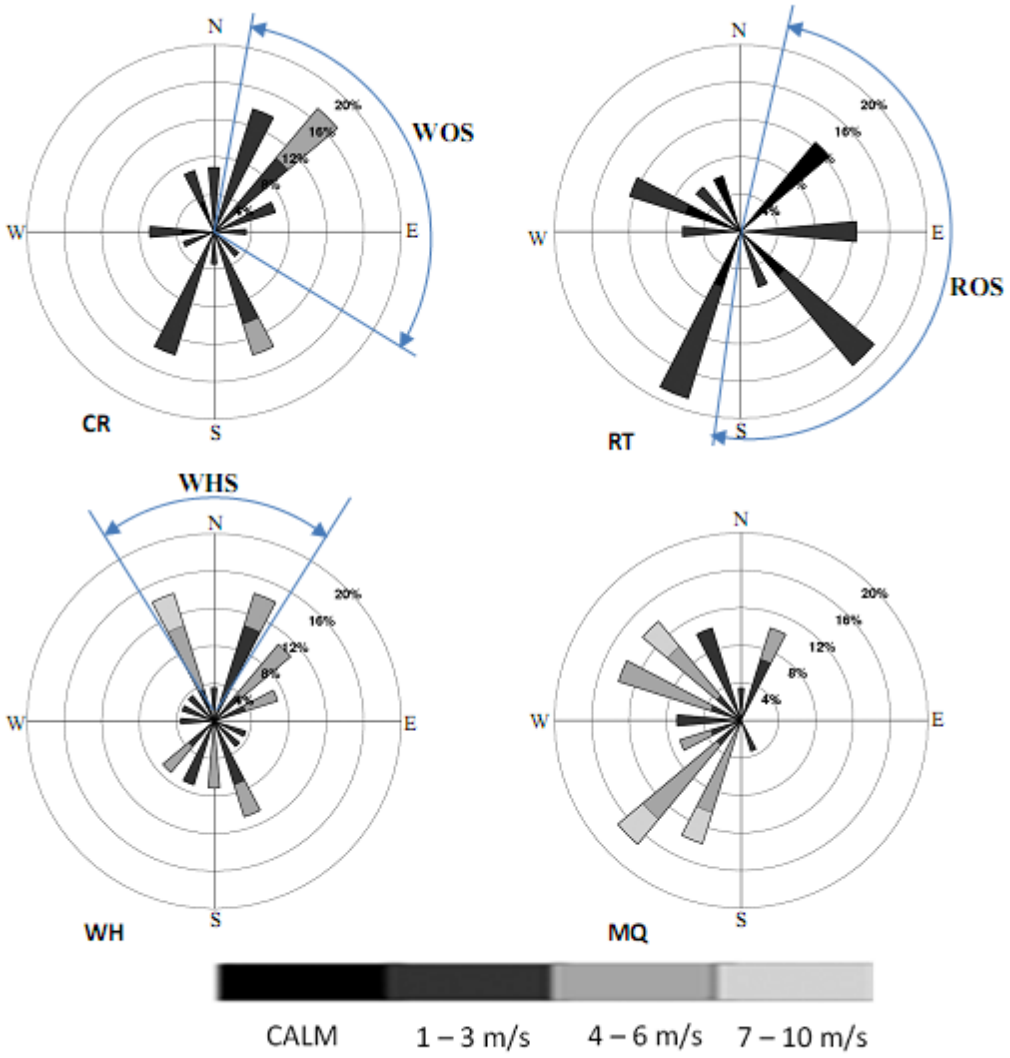

Figure 4.1 Windrose plots at CR, RT, WH and MQ sites. These windroses were constructed during the PM sampling campaign using 96 hours meteorological data starting from May 22, June 27, August 03 and November 04, 2011 at MQ, RT, CR and WH sites respectively.

4.2.2 *Sampling equipment*

An eight staged Micro Orifice Uniform Deposit Impactor (MOUDI) model M100-R was deployed at the sampling sites to collect the atmospheric particles from April 2011 to November 2011. The eight staged MOUDI sampler is sensitive to particle deposition characteristics due to their aerodynamically designed sharp cut-off diameter, and minimum particle loss on the wall. The overall particle collection efficiency across all stages is more than 95% (Marple et al., 1991). The range of aerodynamic diameter of atmospheric particle (D_P) was used to present the size distribution of particle population as coarse (10>Dp>2.5µm), intermodal (2.5>Dp>1µm) and submicron (Dp<1µm) particles. The 50% cut off diameters (D_{50}) of the MOUDI stages were 10.0, 5.6, 3.2, 1.8, 1.0, 0.56, 0.32

and 0.18 µm including an inlet (18 µm) and exit stage (<0.18 µm) (Marple et al. 1991). The sampling flow rate of 30 l/min was used for the entire sampling campaign. The inlet level of MOUDI sampler was at 1.5 m height from the ground. Stretched Teflon filters (PTFE membrane, 2 µm pores, 47 mm diameter, Pall Corporation) were used as substrate in all stages of the MOUDI sampler. Seven sets (10 samples per set from inlet and exit stage in addition to eight stages of MOUDI sampler) of air particulate samples of different size fractions were collected from each sampling site for at least 24 h particle loading.

4.2.3 Sample analysis

Teflon substrates were weighed before and after the atmospheric sampling at the Australian Nuclear Science and Technology Organisation (ANSTO) using Mettler Toledo MX5 microbalance with repeatability of 1.0 µg. Both blank and loaded Teflon substrates were conditioned for 24 h by maintaining humidity of 45 ± 5% and temperature of 22 ± 1.5^{o}C to reach equilibrium. Laboratory standard weights of 50 and 20 mg were measured before, during and after each weighing session to ensure accuracy of the weight measurements. The mass and elemental concentrations of PM_{10}, $PM_{2.5}$ and PM_{1} were calculated by summing the concentrations of the corresponding stages.

The collected atmospheric particle samples were analysed by Ion Beam Analysis (IBA) method on the Small Tandem Accelerator for Research (STAR) at the ANSTO using multi-elemental accelerator based Proton Induced X-ray Emission (PIXE) technique with a 22 mm diameter proton beam of 2.6 MeV energy and 10-15 nA target current. This technique can measure the following most commonly occurring elements in atmospheric particles: Al, Si, P, S, Cl, K, Ca, Ti, V, Cr, Mn, Fe, Co, Ni, Cu and Zn and have been described in detail elsewhere (Cohen, 1993; 1998; Cohen et al., 1996). The trace metals of particular interest related to iron and steel processing industries such as Ti, V, Cr, Mn, Fe, Co, Ni, Cu and Zn are analysed and discussed in this study. The total particle deposition area was measured using a dot grid method assuming the particle deposition under each nozzle is uniform. After acquiring the digital images of particles on Teflon substrates, the total surface area was calculated using transparent plastic sheet with imprinted dot grid lines.

4.3 Results and Discussion

4.3.1 Mass analysis

The PM fractions measured in the selected four sampling sites are shown in Table 4.1. RT site showed the highest mass concentration for PM_{10}, $PM_{2.5}$ and PM_1 compared to other sampling sites. This is because the RT site is located within a distance of 500 m from the EAF steelmaking plant which is likely to have significant fugitive emissions from raw materials handling and the slag processing plant, in addition to the emission from the electric arc furnace processes. Both $PM_{2.5}$ and PM_1 mass concentration fractions in the urban industrial sampling sites at CR and WH were found to be of a similar order or less than the mass concentration of the background MQ sampling site. The air quality index value was calculated according to the Office of Environment and Heritage guidance (Office of Environment and Heritage, 2013) and was rated as "very good" at CR, RT and MQ sites and "good" at RT site.

Table 4.1 PM_{10}, $PM_{2.5}$ and PM_1 mass concentrations, $\mu g/m^3$

	CR	**RT**	**WH**	**MQ**	**Air quality index level**
PM_{10}	7.6±6.2	26.9±10.4	13.6±6.3	10.9±3.7	Very good (CR, WH, MQ), Good (RT)
$PM_{2.5}$	3.6±3.1	14.5±6.3	4.8±2.6	6.8±1.8	Very good (CR, WH, MQ), Good (RT)
PM_1	2.3±2.2	10.6±5.3	2.7±1.3	5.0±1.6	--

In case of the industrial RT location, the concentration of fine and submicron particles was significantly greater than that observed at the other sites. The higher $PM_{2.5}$ and PM_1 mass concentration at the MQ site compared with the CR and WH sites is not significant as the sampling program employed in this study has not been extensive enough to encompass all potential source contributions and meteorological conditions which will affect long term PM concentrations at these sites.

Figure 4.2 presents mass concentrations of atmospheric PM_{10}, $PM_{2.5}$ and PM_1 for the four sampling sites selected in this study. Due to the higher standard deviation in PM fractions, the data is presented in box and whisker plots to show the variation of statistical parameters. The industrial sites CR, RT and WH showed significantly larger variation in PM_{10} and $PM_{2.5}$ mass concentration, particularly for the RT site due to the higher particle loading during calm atmospheric conditions shown in Figure 4.1. In case of PM_1, the background MQ site showed reasonably high variation in mass concentration compared

to CR and WH sites, which appears to be due to the variation of atmospheric conditions of wind speed and humidity during the sampling campaign.

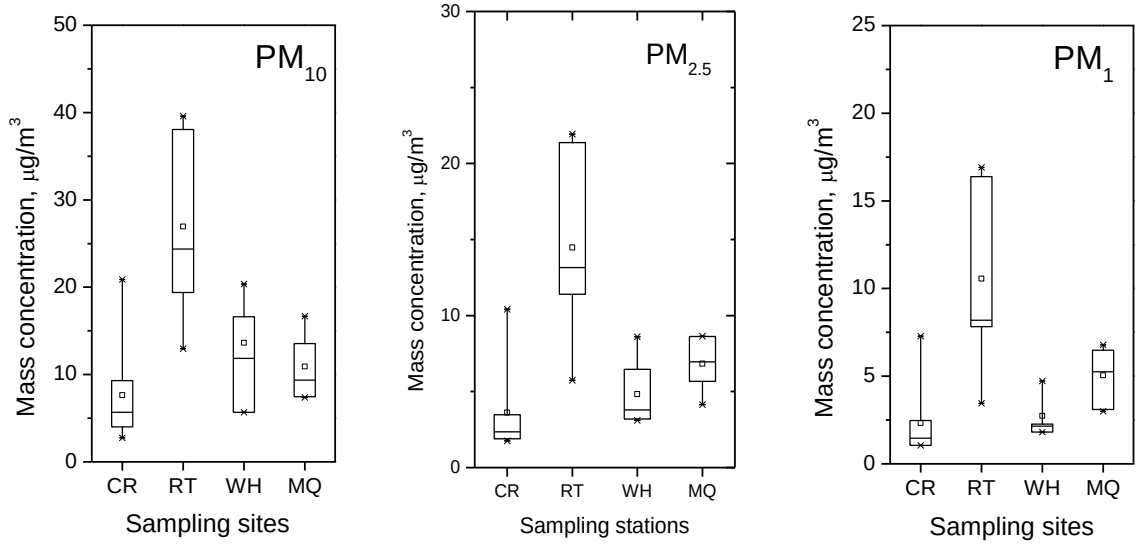

Figure 4.2 Mass concentration of PM_{10}, $PM_{2.5}$ and PM_1 for all sampling sites

The "coarse" (particles between 2.5 µm and 10 µm (10>Dp>2.5µm)), "intermodal" (particles between 1 µm and 2.5 µm (2.5>Dp>1µm)), and "submicron" (particles less than 1 µm (Dp<1µm)) particles fraction for each sampling site are compared in Figure 4.3. Considerable amount 35 to 62% of fine particles (Dp<2.5 µm) were observed. The fine particle range measured in our study was larger than the range of 37-42% measured in Australian urban cities of Sydney, Melbourne, Brisbane and Adelaide (Chan et al., 2008). The range of submicron particle (Dp<1 µm) contribution to the total PM_{10} concentration varied from 20 to 46%. The intermodal particle size shows a little variation of mass concentration at all sampling sites which implies the variation in fine particles at all sampling sites is not affected by the intermodal size particles having smaller PM size range from 1 to 2.5 µm. The regression analysis of $PM_{2.5}$ to PM_1 is presented in Figure 4.4; a strong correlation (R^2=0.99) was observed at the sampling sites indicates the mass concentration of fine particles are mostly dominated by submicron particles.

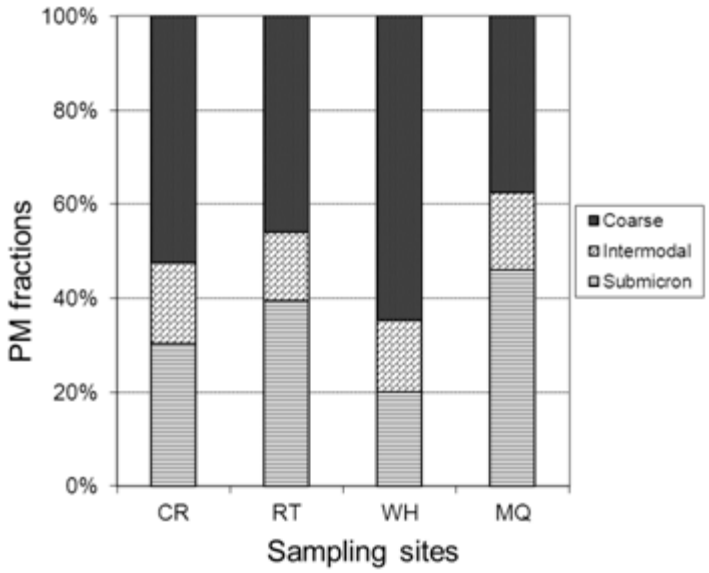

Figure 4.3 Coarse, Intermodal and Submicron PM fractions to PM_{10} mass

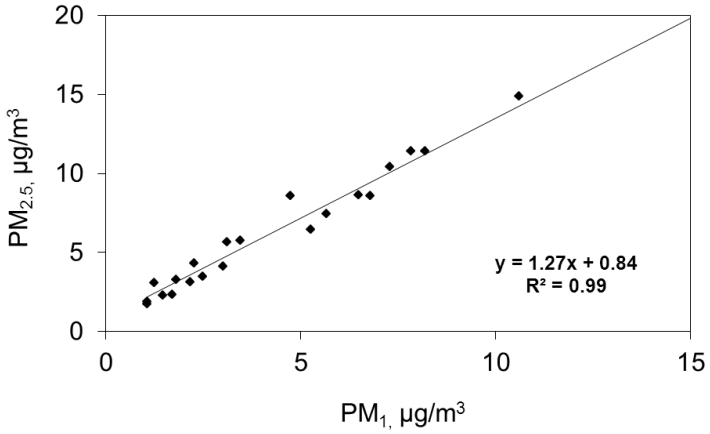

Figure 4.4 Correlation between $PM_{2.5}$ and PM_1 at sampling sites

4.3.2 Elemental concentrations

The elemental concentrations of selected elements in PM_{10}, $PM_{2.5}$ and PM_1 for the four sampling sites are shown in Table 4.2. It is observed that the elements studied in this work, Ti, V, Cr, Mn, Fe, Co, Ni, Cu and Zn had significantly higher concentrations in the atmospheric particles collected nearby the iron and steelmaking industries compared to the MQ sampling site. Approximately 78% of the anthropogenic atmospheric particle emissions in the Wollongong area (CR sampling site in this work) originate from the Wollongong steelworks (DECC NSW, 2007). In this work, the EAF site at Rooty Hill (RT) exhibited the highest concentration of all trace metals in the PM_{10} particles compared to the other iron-steelmaking sites. The possible reason for this could be the wind direction with calm to low wind speed and the location of the RT sampling site, which was within

Table 4.2 Average elemental concentrations of selected elements in PM_{10}, $PM_{2.5}$ and PM_1 from the four sampling sites [range of values determined in (brackets)], ng/m^3

		RT	CR	WH	MQ
Ti	PM_{10}	29.1 (18.4 – 46.2)	7.2 (2.0 – 24.9)	7.6 (5.8 – 12.8)	3.5 (1.3 – 5.4)
	$PM_{2.5}$	8.9 (7.0–12.5)	2.3 (0.8 – 6.2)	3.8 (1.9–6.2)	0.8 (0.3 – 1.8)
	PM_1	2.9 (2.1 – 3.7)	0.9 (0.2 – 1.4)	2.3 (1.2 – 3.0)	Nd
V	PM_{10}	2.9 (1.7 – 4.8)	1.8 (0.6 – 5.6)	1.9 (0.6 – 3.3)	1.0 (0.5 – 1.8)
	$PM_{2.5}$	2.0 (1.5– 3.3)	1.2 (0.5 – 3.0)	1.3 (0.3–2.4)	0.8 (0.2 – 1.8)
	PM_1	1.4 (0.7 – 2.2)	0.9 (0.2 – 2.0)	1.1 (0.2 – 2.2)	0.6 (0.3 – 1.5)
Cr	PM_{10}	10.7 (4.1 – 19.1)	1.9 (0.9 – 3.9)	2.7 (2.3 – 3.1)	Nd
	$PM_{2.5}$	5.5 (2.1–9.9)	1.3 (0.6–2.2)	1.9 (1.4–2.6)	Nd
	PM_1	3.7 (1.3 – 7.1)	0.9 (0.5 – 1.5)	1.5 (0.9 – 2.3)	Nd
Mn	PM_{10}	91.6 (45.8 – 136.2)	8.1 (2.1 – 32.8)	20.6 (3.7 – 36.8)	1.8 (0.7 – 4.6)
	$PM_{2.5}$	47.2 (17.3–78.5)	3.1 (1.1–9.5)	8.3 (2.6–20.7)	1.0 (0.1 – 2.8)
	PM_1	32.3 (6.5 – 56.0)	1.7 (0.7 – 3.8)	4.6 (1.7 – 11.9)	0.6 (0.2 – 2.0)
Fe	PM_{10}	2931.5 (919.6 – 6514.9)	224.1 (33.7 – 1100.1)	1236.1 (86.8 – 3200.5)	96.1 (58.3 – 123.9)
	$PM_{2.5}$	1767.9 (486.8–3973.5)	82.9 (13.2–368.9)	254.2 (46.2–566.2)	36.5 (18.4 – 55.9)
	PM_1	1272.1 (143.2 – 3293.5)	33.9 (6.2 – 139.8)	99.7 (29.6 – 238.6)	9.7 (2.1 – 16.3)
Co	PM_{10}	8.6 (2.5 – 19.8)	1.3 (0.2 – 5.9)	5.5 (1.6 – 12.7)	0.4 (0.2 – 0.7)
	$PM_{2.5}$	5.1 (1.2–13.4)	0.5 (0.1–1.9)	1.2 (0.7–2.1)	0.3 (0.1 – 0.5)
	PM_1	3.4 (0.1 – 10.4)	0.2 (0.1 – 0.5)	0.7 (0.6 – 1.0)	0.2 (0.1 – 0.4)
Ni	PM_{10}	6.8 (3.9 – 12.2)	3.5 (0.8 – 5.6)	3.5 (2.9 – 4.4)	1.2 (0.9 – 1.6)
	$PM_{2.5}$	5.6 (2.8–10.2)	3.0 (0.8–5.1)	2.4 (1.5–3.2)	1.0 (0.8 – 1.2)
	PM_1	3.6 (1.6 – 5.3)	2.9 (0.5 – 5.1)	1.8 (0.9 – 2.9)	0.8 (0.5 – 0.9)
Cu	PM_{10}	36.6 (7.1 – 96.2)	2.9 (0.7 – 7.5)	2.0 (1.5 – 3.0)	2.9 (1.4 – 4.1)
	$PM_{2.5}$	30.6 (5.0–86.4)	1.7 (0.6–3.7)	1.3 (0.4–2.7)	0.9 (0.3 – 1.6)
	PM_1	25.2 (2.1 – 79.5)	1.0 (0.5 – 1.9)	1.0 (0.4 – 2.0)	Nd
Zn	PM_{10}	397.6 (174.4 – 1183.2)	33.2 (1.8 – 180.3)	8.4 (2.1 – 21.3)	7.0 (1.2 – 12.1)
	$PM_{2.5}$	284.4 (81.4–1043.9)	23.0 (1.3–122.1)	6.3 (1.6–17.5)	5.3 (0.8 – 9.5)
	PM_1	145.6 (20.1 – 552.7)	13.1 (1.0 – 62.8)	4.1 (0.8 – 12.5)	3.0 (1.6 – 5.8)

500 m of the steelmaking facility compared to the other sampling sites (Figure 4.1). When the atmospheric particles collected in the sampling sites CR and WH, located in close proximity to the two integrated (BF/BOF) steelmaking industries are compared with each other, the elemental concentrations of Fe, Mn and Co at WH were found to be 2.5 to 5.5 times higher than at CR, whereas the elemental concentration of Ni, Cu and Zn at the Cringila CR site was found to be higher than at the Whyalla WH site.

$PM_{2.5}$ collected at the MQ sampling site exhibited metal (Co, V, Mn, Cu, Ti, Zn, Ni, Fe) concentrations in the range from 0.1 to 55.9 ng/m^3; these values were the lowest of those observed at all the sites. The concentrations for the same trace metal species detected in the sites located downstream of the iron and steel industries (RT, CR and WH) were up to 18 times above the MQ site. The $PM_{2.5}$ particles collected at the CR sampling site had lower concentrations of the examined trace metals, compared to $PM_{2.5}$ collected at RT and WH sites. Cohen et al. (2002) documented data for $PM_{2.5}$ particles sampled at the Warrawong sampling site from 1992-2000. This site is located close to the Cringila CR site used in this work and downwind, under some conditions, of the same steel industry in Wollongong. The concentrations of all elements, except for Ni, at the Warrawong site during 1992-2000 were higher than the measured concentrations in this work at CR (Cohen et al., 2002).

The trace metal composition of PM_1 particles determined at the RT site showed a similar trend of metal concentrations compared to the other sampling sites. The WH site showed higher concentrations of Ti, V, Cr, Mn, Fe and Co in PM_1compared with the CR site. Zn in PM_1 at the CR site had higher concentrations than those observed at WH. The MQ site had the lowest trace metal concentrations in PM_1 compared to the other sampling sites.

4.3.3 Particle fraction of trace elements

Figure 4.5 shows the relative percent of each trace element concentration in the coarse, inter-modal and submicron fractions. Ti is mainly associated with coarse particles at all sites, whereas V and Ni are predominantly associated with submicron particles. Mn, Fe and Co are associated with coarse particles at the WH and CR sites. The concentrations of Ti, Mn, Fe, Co and Cu in the inter-modal size particles are higher than for the other elements. In addition, the elemental fraction of coarse and submicron sized particles is substantial compared to inter-modal fractions, which indicates the focus particle group of coarse and submicron sizes in the vicinity of iron and steel industries.

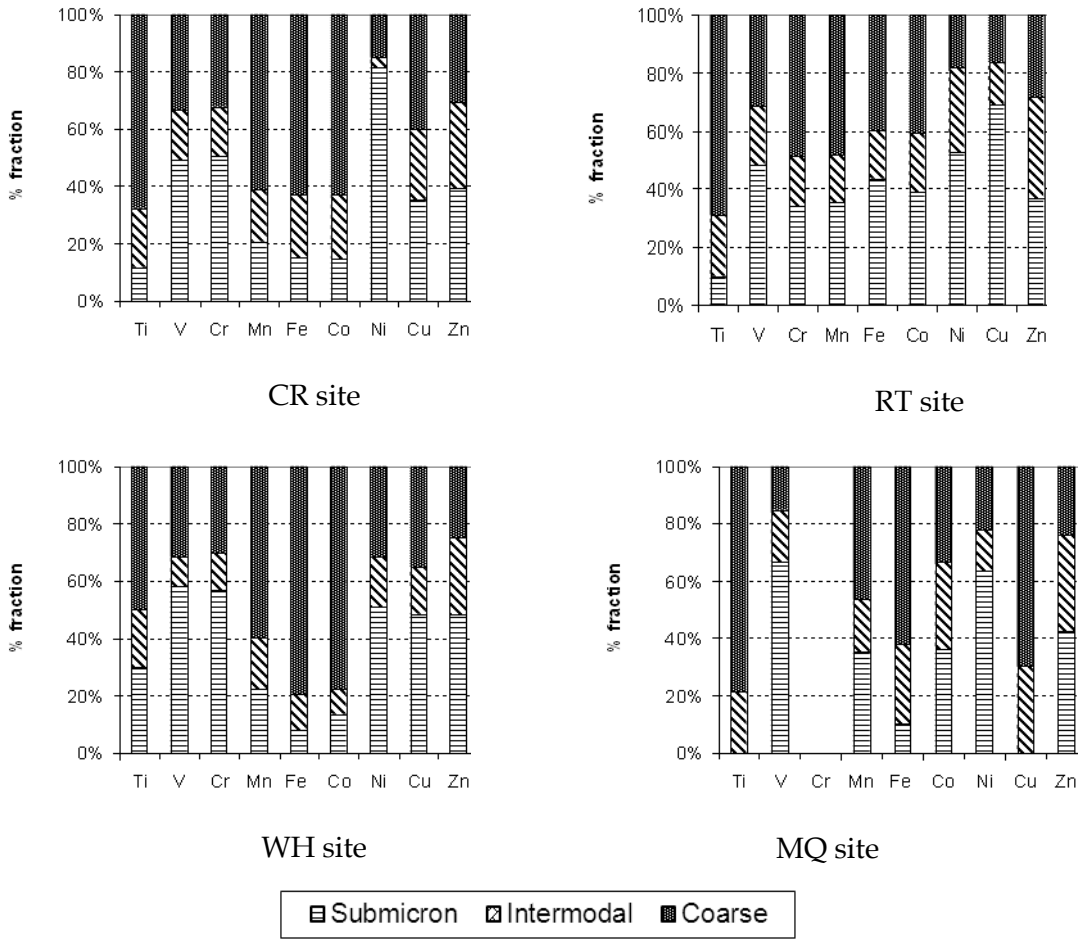

Figure 4.5 Coarse, Intermodal and Submicron fractions of trace elements; Cr was below detection limits at the MQ site

4.3.4 Inter-elemental correlation

Table 4.3 shows the correlation matrix of Ti, V, Cr, Mn, Fe, Co, Ni and Zn for coarse, intermodal and submicron particles obtained from the CR, RT and WH sites and the value represents the linear squared correlation coefficient (R^2) between two elements. The linear correlation coefficient was calculated using the straight line constructed from the scattered data plot between two elements from elemental data set of each particle. The possible sources which contribute to the atmospheric elemental loads around the sampling sites are qualitatively identified from the correlation matrix. The results show that Fe and Co have a very high correlation (R^2>0.93) in coarse particles at the industrial RT, CR and WH sites which demonstrates that the air particles most likely originated from the same source of iron and steel industries, as described by Cohen (2002) during analysis of Fe-Co correlation from industrial sites. The MQ site has no significant metal correlation, except for the Ti-Fe correlation in coarse particles, which indicates particle association from natural sources of soil dust. The strong association among Ti, V, Cr, Mn, Fe, Co metals for

coarse particle at CR site suggests the significant contribution of these metals from industrial activities in the Wollongong area. Coarse particles at the RT site also show strong correlation with Ti-Mn, Ti-Cu, Fe-Cr, Fe-Co and Co-Cr metals whereas the WH site shows strong metal correlation between Cr, Mn, Fe, Co and Cu. Fe and Co association at RT site was found to be less profound for coarse particles compared to the same for CR and WH sites, and may be due to the additional loading of Fe-bearing coarse particles to the total PM loading from open and uncontrolled sources nearby the EAF steelmaking facility.

Table 4.3 Inter-elemental correlations of coarse particles (10>Dp>2.5 μm)

		Ti	**V**	**Cr**	**Mn**	**Fe**	**Co**	**Ni**	**Cu**
	CR	**0.92**							
V	RT	0.04							
	WH	0.14							
	CR	**0.91**	0.84						
Cr	RT	0.67	0.22						
	WH	0.06	0.30						
	CR	**0.98**	**0.97**	**0.92**					
Mn	RT	**0.94**	0.10	0.84					
	WH	0.27	0.12	**0.92**					
	CR	**0.96**	**0.98**	**0.90**	**0.99**				
Fe	RT	0.43	0.35	**0.88**	0.65				
	WH	0.07	0.18	**0.97**	**0.91**				
	CR	**0.95**	**0.99**	**0.89**	**0.98**	**0.99**			
Co	RT	0.56	0.45	**0.88**	0.76	**0.93**			
	WH	0.09	0.16	**0.97**	**0.92**	**0.99**			
	CR	0.35	0.38	0.20	0.38	0.39	0.37		
Ni	RT	0.10	0.33	0.05	0.02	0.20	0.08		
	WH	0.79	--	0.44	0.72	0.45	0.48		
	CR	**0.93**	0.76	0.86	0.86	0.81	0.83	0.29	
Cu	RT	**0.93**	0.01	0.73	0.88	0.45	0.50	0.05	
	WH	0.02	0.09	0.85	0.76	**0.94**	**0.93**	0.31	
	CR	**0.93**	**0.99**	0.86	**0.98**	**0.99**	**0.98**	0.41	0.76
Zn	RT	0.52	0.01	0.79	0.61	0.57	0.48	0.02	0.70
	WH	**0.81**	0.01	0.41	0.70	0.44	0.47	**0.99**	0.32

Table 4.4 Inter-elemental correlations of intermodal particles (2.5>Dp>1 μm)

		Ti	V	Cr	Mn	Fe	Co	Ni	Cu
	CR	0.55							
V	RT	0.30							
	WH	0.04							
	CR	**0.75**	0.50						
Cr	RT	**0.86**	0.30						
	WH	0.78	0.41						
	CR	**0.93**	0.77	0.68					
Mn	RT	0.17	0.10	0.30					
	WH	0.78	0.03	0.35					
	CR	**0.88**	0.82	0.62	**0.99**				
Fe	RT	0.50	0.26	0.78	0.40				
	WH	0.47	0.28	0.07	**0.86**				
	CR	0.83	**0.85**	0.58	**0.94**	**0.97**			
Co	RT	**0.88**	0.34	**0.91**	0.17	**0.66**			
	WH	0.86	0.03	0.62	0.87	**0.54**			
	CR	0.02	0.19	0.13	0.05	0.05	0.06		
Ni	RT	--	0.14	0.14	0.02	0.32	0.06		
	WH	0.06	0.01	--	0.30	0.27	0.35		
	CR	**0.91**	0.63	0.69	**0.95**	**0.91**	0.80	0.04	
Cu	RT	0.51	0.08	0.77	0.41	0.73	0.77	0.23	
	WH	0.14	0.57	0.47	0.01	0.14	--	0.38	
	CR	**0.81**	**0.85**	0.53	**0.96**	**0.99**	**0.98**	0.05	0.85
Zn	RT	0.14	0.60	0.04	0.46	--	0.12	0.01	--
	WH	0.64	0.08	0.21	**0.97**	**0.93**	0.79	0.39	0.06

Table 4.4 shows the trace metal association in the intermodal particles in the vicinity of iron and steel processing industries is very high compared to the urban MQ site. The metals detected in the intermodal particles from the industrial RT, CR and WH sites also have similar correlation trend observed in the coarse particles. The most apparent strong correlation in the intermodal particles that can be attributed to the iron and steelmaking activities is that of Fe-Co. Intermodal and coarse particles at the MQ site show no significant metal correlations except for Ti-Fe.

The metal correlations in submicron particles, as shown in Table 4.5, have no significant correlation for the MQ site. However, in the case of the RT site there is a strong observed metal correlation in Fe-Co (0.96), Fe-Cr (0.94) and Co-Cr (0.87) suggesting contribution of the high temperature activities of the metal industry to the submicron particle emissions. The submicron particles from the CR and WH sites show similar metal correlation with strong Fe-Mn, Fe-Zn and Mn-Zn correlation. Hence, the results indicate the submicron particles in the vicinity of iron and steel industries have strong correlation with metal emissions from industrial and combustion activities.

Table 4.5 Inter-elemental correlations of submicron particles (Dp<1.0μm)

		Ti	**V**	**Cr**	**Mn**	**Fe**	**Co**	**Ni**	**Cu**
	CR	0.24							
V	RT	0.01							
	WH	0.04							
	CR	0.42	0.05						
Cr	RT	0.52	0.35						
	WH	--	0.13						
	CR	0.36	0.57	0.52					
Mn	RT	--	0.26	0.23					
	WH	0.28	0.04	0.59					
	CR	0.37	0.69	0.46	**0.92**				
Fe	RT	0.61	0.25	**0.94**	0.29				
	WH	0.17	0.02	0.69	**0.98**				
	CR	0.04	0.42	0.12	0.38	0.56			
Co	RT	0.76	0.16	0.87	0.21	**0.96**			
	WH	0.10	0.66	0.63	0.06	0.11			
	CR	--	0.13	--	0.16	0.01	--		
Ni	RT	0.10	0.51	0.09	0.04	0.11	0.10		
	WH	0.12	0.18	0.26	0.28	0.38	0.02		
	CR	0.14	0.15	0.39	0.50	0.28	--	0.36	
Cu	RT	0.51	0.01	0.54	0.27	0.75	0.74	0.03	
	WH	0.05	0.61	0.01	0.14	0.17	0.09	0.79	
	CR	0.29	0.72	0.40	0.85	**0.97**	0.65	0.02	0.20
Zn	RT	0.36	0.03	0.05	0.48	0.05	0.07	--	0.03
	WH	0.33	0.06	0.53	**0.99**	**0.96**	0.03	0.25	0.13

4.3.5 Percent metal fraction and metal enrichment factor

Table 4.6 shows the percent metal fraction (PMF) for PM_{10}, $PM_{2.5}$ and PM_1 from all sampling sites based on average of all samples. The metal fraction is calculated by dividing the elemental concentration with the total mass concentration. The lowest PMF value for all of the studied trace elements was found at the MQ background site. The RT site exhibited the highest PMF value for all elements, except for V and Ni. The distance between RT sampling site and the steel industry (500 m) may be one of the main reasons for the elemental loading by accumulating the particles from both point and diffuse sources. Also the atmospheric conditions of wind direction and mostly calm wind speed, shown in Figure 4.1, have a potentially significant effect in increasing the elemental PMF value at the RT site. Ni was found at higher concentrations in the atmospheric particles from the CR and WH sites, which have similar influences from integrated iron and steel processing. Fe (0.20-12.2%) and Zn (0.05-2.0%) are the leading contributors to the total PM_{10}, $PM_{2.5}$ and PM_1 concentrations for all sites.

Table 4.6 Percent Metal Fraction for PM_{10}, $PM_{2.5}$ and PM_1 at CR, WH, RT and MQ sites

		Ti	V	Cr	Mn	Fe	Co	Ni	Cu	Zn	Sum
PM10	CR	0.09	0.02	0.02	0.11	2.95	0.02	0.05	0.04	0.44	3.7
	RT	0.11	0.01	0.04	0.34	10.90	0.03	0.03	0.14	1.48	13.1
	WH	0.06	0.01	0.02	0.15	9.09	0.04	0.03	0.01	0.06	9.5
	MQ	0.01	0.01	nd	0.01	0.33	<0.01	0.01	0.01	0.05	0.4
PM2.5	CR	0.06	0.03	0.04	0.09	2.30	0.01	0.08	0.05	0.64	3.3
	RT	0.06	0.01	0.04	0.33	12.19	0.04	0.04	0.21	1.96	14.9
	WH	0.08	0.03	0.04	0.17	5.30	0.03	0.05	0.03	0.13	5.9
	MQ	0.02	0.01	nd	0.02	0.77	<0.01	0.01	0.02	0.08	0.9
PM1.0	CR	0.04	0.04	0.04	0.07	1.47	0.01	0.13	0.04	0.57	2.4
	RT	0.03	0.01	0.03	0.31	12.00	0.03	0.03	0.24	1.37	14.1
	WH	0.08	0.04	0.06	0.17	3.69	0.03	0.07	0.04	0.15	4.3
	MQ	Nd	0.01	nd	0.01	0.19	<0.01	0.02	nd	0.06	0.3

nd: not detected

Table 4.7 shows the metal enrichment factor (MEF) for PM_{10}, $PM_{2.5}$ and PM_1 at the three industrial sites. The MEF value provides information about the anthropogenic influence on particulate matter in these industrial sites. The MEF value is calculated according to the following expression:

MEF(A) = C(A)/PM (ambient) : C(A)/PM (background) (4.1)

Where MEF(A) is the metal enrichment factor for element A, C(A) is the concentration of the element A and PM is the total particulate matter concentration. In this case the MQ site is assumed to represent background conditions although it has some limitations as a true background site.

Table 4.7 Metal enrichment factor (MEF) for PM_{10}, $PM_{2.5}$ and PM_1 at CR, WH, RT sites

		Ti	**V**	**Cr**	**Mn**	**Fe**	**Co**	**Ni**	**Cu**	**Zn**	**Avg± SD**
	CR	9.0	2.0	nc	11.0	8.9	nc	5.0	4.0	8.8	5.4 ± 4.2
PM_{10}	RT	11.0	1.0	nc	34.0	33.0	nc	3.0	14.0	29.6	14.0 ± 14
	WH	6.0	1.0	nc	15.0	27.5	nc	3.0	1.0	1.2	6.1 ± 9.3
	CR	3.0	3.0	nc	4.5	3.0	nc	8.0	2.5	8.0	3.6 ± 2.9
$PM_{2.5}$	RT	3.0	1.0	nc	16.5	15.8	nc	4.0	10.5	24.5	8.4 ± 8.9
	WH	4.0	3.0	nc	8.5	6.9	nc	5.0	1.5	1.6	3.4 ± 3.0
	CR	nc	4.0	nc	7.0	7.7	nc	6.5	nc	9.5	3.9 ± 3.9
PM_1	RT	nc	1.0	nc	31.0	63.2	nc	1.5	nc	22.8	13.3 ± 22
	WH	nc	4.0	nc	17.0	19.4	nc	3.5	nc	2.5	5.2 ± 7.6

nc: not calculated as metal fraction at MQ site is less than 0.01% or not detected

The average metal enrichment for the three industrial sites was found to be of the order of 5.4-14.0 for PM_{10}, 3.4-8.4 for $PM_{2.5}$ and 3.9-13.3 for PM_1. The variance in average MEF varies with specific metals. Mn, Fe and Zn have high metal fraction and enrichment value, most likely associated with the iron and steel industries by releasing large amounts of these elements to the atmosphere. Due the atmospheric conditions, the MEF value of Ti, Mn, Fe, Cu, Zn for the RT site was found to be higher than for the other industrial sites, although the RT site was located near the smaller size steelmaking industry, compared to Wollongong and Whyalla steelworks. The contribution of iron and steel plant sources to the mass and elemental loading of air particles collected in the vicinity of iron and steel processing industries was found qualitatively significant with the fingerprint elements of trace metal correlations and atmospheric conditions.

The mass concentration, as discussed earlier, in the three studied industrial sites is about 0.5 to 2.5 times higher for PM_{10}, $PM_{2.5}$ and PM_1 whereas the metal concentration is about 3.4 to 14 times higher compared to the MQ site. Lead (Pb) in atmospheric particles is the only metal regulated internationally and in Australia. The other metals detected in this study are not separately regulated from PM. Considering this study found levels of magnitudes of up to 14 times difference in concentration levels among some of the metals present in the particles, monitoring and reporting of atmospheric metal composition should also be encouraged.

4.4 Conclusions

This study revealed that the $PM_{2.5}$ fractions in the PM_{10} particles at all sites were in the range from 35 to 62%. Similarly, PM_1 to the total PM_{10} at all sites varies from 20 to 46% contributing significantly to the PM_{10} mass loading. The MQ sampling site generally had lower PM_{10} concentrations than the industrial sampling sites.

The trace metals Co, Cr, Cu, Fe, Mn, Ni, Ti, V and Zn had significantly higher concentrations in the atmospheric particles collected nearby the iron and steelmaking industries compared to the background site and various associations with the size fractions. Ti was mainly associated with the coarse particles, whereas V and Ni were predominantly associated with the submicron particles. Mn, Fe and Co elements were also associated with the coarse particles at one of the industrial sites. The intermodal particles size range exhibited higher trace metal Co, Cu, Fe, Mn, and Ti concentrations.

The metal correlation results showed that Fe and Co have very strong correlation in coarse particles at all three industrial sites, most likely generated from iron and steel processing industries, whereas the MQ site had no significant metal correlation except for the Ti-Fe correlation, which may indicate particle association due to a contribution from a natural source (soil dust) at the background site.

Iron (0.20-12.2%) and zinc (0.05-2.0%) were the leading contributors in the total PM_{10}, $PM_{2.5}$ and PM_1 concentrations for all sites, according to the percent metal fraction (PMF) value. The average metal enrichment of the atmospheric particles in the vicinity of iron and steel industries was found to be about 3.4 to 14 times higher compared to the background site. This finding shows that the chemical composition of particles, which is

currently not regulated, may be as important as the particle size range concentration, in order to provide comprehensive risk assessment of atmospheric particles.

4.5 References

Arditsoglou, A. & Samara, C. 2005. Levels of total suspended particulate matter and major trace elements in Kosovo: a source identification and apportionment study. *Chemosphere,* 59**,** 669-678.

Banks, D. E., Shah, A. A., Lopez, M. & Wang, M.-L. 1999. Chest illnesses and the decline of FEV1 in steelworkers. *Journal of occupational and environmental medicine,* 41**,** 1085-1090.

Berggren, D., Bergkvist, B., Falkengren-Grerup, U., Folkeson, L. & Tyler, G. 1990. Metal solubility and pathways in acidified forest ecosystems of south Sweden. *Science of the Total Environment,* 96**,** 103-114.

Bollati, V., Marinelli, B., Apostoli, P., Bonzini, M., Nordio, F., Hoxha, M., Pegoraro, V., Motta, V., Tarantini, L. & Cantone, L. 2010. Exposure to metal-rich particulate matter modifies the expression of candidate microRNAs in peripheral blood leukocytes. *Environmental health perspectives,* 118**,** 763.

Chan, Y.-C., Cohen, D. D., Hawas, O., Stelcer, E., Simpson, R., Denison, L., Wong, N., Hodge, M., Comino, E. & Carswell, S. 2008. Apportionment of sources of fine and coarse particles in four major Australian cities by positive matrix factorisation. *Atmospheric Environment,* 42**,** 374-389.

Chen, P.-C., Doyle, P. E. & Wang, J.-D. 2006. Respirable dust exposure and respiratory health in male Taiwanese steelworkers. *Industrial health,* 44**,** 190-199.

Choël, M., Deboudt, K., Flament, P., Aimoz, L. & Mériaux, X. 2007. Single-particle analysis of atmospheric aerosols at Cape Gris-Nez, English Channel: Influence of steel works on iron apportionment. *Atmospheric Environment,* 41**,** 2820-2830.

Cohen, D. D. 1993. Applications of simultaneous IBA techniques to aerosol analysis. *Nuclear Instruments and Methods in Physics Research Section B: Beam Interactions with Materials and Atoms,* 79**,** 385-388.

Cohen, D. D. 1998. Characterisation of atmospheric fine particles using IBA techniques. *Nuclear Instruments and Methods in Physics Research Section B: Beam Interactions with Materials and Atoms,* 136**,** 14-22.

Cohen, D. D., Bailey, G. M. & Kondepudi, R. 1996. Elemental analysis by PIXE and other IBA techniques and their application to source fingerprinting of atmospheric fine particle pollution. *Nuclear Instruments and Methods in Physics Research Section B: Beam Interactions with Materials and Atoms,* 109**,** 218-226.

Cohen, D. D., Stelcer, E. & Garton, D. 2002. Ion beam methods to determine trace heavy metals concentrations and sources in urban airsheds. *Nuclear Instruments and Methods in Physics Research Section B: Beam Interactions with Materials and Atoms,* 190**,** 466-470.

De Vries, W., Lofts, S., Tipping, E., Meili, M., Groenenberg, J. E. & Schütze, G. 2007. Impact of soil properties on critical concentrations of cadmium, lead, copper, zinc, and mercury in soil and soil solution in view of ecotoxicological effects. *Reviews of environmental contamination and toxicology*. Springer.

Decc Nsw 2007. Air Emissions Inventory for the Greater Metropoliton Region in New South Wales: Industrials Emissions Module, ISBN 978 1 74122 378 1. Prepared by Department of Environment and Climate Change NSW, Technical Report No. 6.

Dominici, F., Mcdermott, A., Daniels, M., Zeger, S. L. & Samet, J. M. 2005. Revised analyses of the National Morbidity, Mortality, and Air Pollution Study: mortality among residents of 90 cities. *Journal of Toxicology and Environmental Health, Part A,* 68**,** 1071-1092.

Driscoll, T., Nelson, D. I., Steenland, K., Leigh, J., Concha-Barrientos, M., Fingerhut, M. & Prüss-Üstün, A. 2005. The global burden of disease due to occupational carcinogens. *American journal of industrial medicine,* 48**,** 419-431.

Garimella, S. & Deo, R. N. 2008. Characterization of aerosols generated in a steel processing factory. *The South Pacific Journal of Natural and Applied Sciences,* 25**,** 78-82.

Hutchison, G. R., Brown, D. M., Hibbs, L. R., Heal, M. R., Donaldson, K., Maynard, R. L., Monaghan, M., Nicholl, A. & Stone, V. 2005. The effect of refurbishing a UK steel plant on PM. *Respiratory research,* 6**,** 43.

Krombach, F., Münzing, S., Allmeling, A.-M., Gerlach, J. T., Behr, J. & Dörger, M. 1997. Cell size of alveolar macrophages: an interspecies comparison. *Environmental health perspectives,* 105**,** 1261.

Kuo, H.-W., Chang, C.-L., Lai, J.-S., Lee, F.-C., Chung, B.-C. & Chen, C.-J. 1998. Prevalence of and factors related to pneumoconiosis among foundry workers in central Taiwan. *Science of the total environment,* 222**,** 133-139.

Ledoux, F., Laversin, H., Courcot, D., Courcot, L., Zhilinskaya, E., Puskaric, E. & Aboukais, A. 2006. Characterization of iron and manganese species in atmospheric aerosols from anthropogenic sources. *Atmospheric research,* 82**,** 622-632.

Lin, J. J. & Lee, L.-C. 2004. Characterization of the concentration and distribution of urban submicron (PM< sub> 1</sub>) aerosol particles. *Atmospheric Environment,* 38**,** 469-475.

Lippmann, M. & Chen, L.-C. 2009. Health effects of concentrated ambient air particulate matter (CAPs) and its components. *Critical reviews in toxicology,* 39**,** 865-913.

Lippmann, M., Ito, K., Hwang, J.-S., Maciejczyk, P. & Chen, L.-C. 2006. Cardiovascular effects of nickel in ambient air. *Environmental health perspectives,* 114**,** 1662.

Machemer, S. D. 2004. Characterization of airborne and bulk particulate from iron and steel manufacturing facilities. *Environmental science & technology,* 38**,** 381-389.

Mazzei, F., D'alessandro, A., Lucarelli, F., Marenco, F., Nava, S., Prati, P., Valli, G. & Vecchi, R. 2006. Elemental composition and source apportionment of particulate

matter near a steel plant in Genoa (Italy). *Nuclear Instruments and Methods in Physics Research Section B: Beam Interactions with Materials and Atoms,* 249**,** 548-551.

Namdeo, A. & Bell, M. 2005. Characteristics and health implications of fine and coarse particulates at roadside, urban background and rural sites in UK. *Environment international,* 31**,** 565-573.

Ning, Z. & Sioutas, C. 2010. Atmospheric processes influencing aerosols generated by combustion and the inference of their impact on public exposure: a review. *Aerosol and Air Quality Resarch,* 10**,** 43-58.

Office of Environment and Heritage. 2013. *Air Quality Index* [Online]. Available: http://www.environment.nsw.gov.au/AQMS/dataindex.htm.

Park, S. & Wexler, A. 2008. Size-dependent deposition of particles in the human lung at steady-state breathing. *Journal of Aerosol Science,* 39**,** 266-276.

Pope Iii, C. 1996. Particulate pollution and health: a review of the Utah valley experience. *Journal of exposure analysis and environmental epidemiology,* 6**,** 23.

Pope Iii, C. A. 2000. Review: Epidemiological basis for particulate air pollution health standards. *Aerosol Science & Technology,* 32**,** 4-14.

Querol, X., Alastuey, A., Viana, M., Rodriguez, S., Artiñano, B., Salvador, P., Garcia Do Santos, S., Fernandez Patier, R., Ruiz, C. & De La Rosa, J. 2004. Speciation and origin of PM10 and PM2. 5 in Spain. *Journal of Aerosol Science,* 35**,** 1151-1172.

Querol, X., Viana, M., Alastuey, A., Amato, F., Moreno, T., Castillo, S., Pey, J., De La Rosa, J., Sánchez De La Campa, A. & Artinano, B. 2007. Source origin of trace elements in PM from regional background, urban and industrial sites of Spain. *Atmospheric environment,* 41**,** 7219-7231.

Valiulis, D., Šakalys, J. & Plauškaitė, K. 2008. Heavy metal penetration into the human respiratory tract in Vilnius. *Lithuanian Journal of Physics,* 48.

Xu, X., Christiani, D. C., Dockery, D. W. & Wang, L. 1992. Exposure—Response relationships between occupational exposures and chronic respiratory illness: a community-based study. *American Review of Respiratory Disease,* 146**,** 413-418.

Chapter 5

Mass and elemental distribution of atmospheric particles nearby blast furnace and electric arc furnace operated industrial areas in Australia

Preface

This chapter describes the mass modality, elemental modality, mass and elemental fraction in size resolved atmospheric particles. The chapter also shows the relative particle number and surface area distribution in the size resolved atmospheric particles. It refers to the thesis objectives [A4] and published journal articles [J2]. This chapter also presents the iron contribution from industrial sectors.

5.1 Introduction

The industrial sectors contribute approximately 59% of PM_{10} and 45% of $PM_{2.5}$ emissions to the atmosphere in New South Wales (NSW), Australia (NSW EPA, 2012), which can potentially impact the health and environment of the nearby communities. To reduce the impacts from particle emissions and meet the standards and goals set by the National Environment Protection Measure (NEPM), the NSW government has operated an extensive air particle monitoring program for PM_{10} and $PM_{2.5}$ in urban and industrial areas using both continuous tapered element oscillating microbalance (TEOM) technique and gravimetric high volume sampling. However, monitoring of particle mass is not sufficient as the impact of particles on human health and the environment is highly dependent on particle size distribution and associated chemistry (Spurny, 1996; Koliadima et al., 1998; Lighty et al., 2000; Seinfeld and Pandis, 2012; Portin et al., 2013; Mohiuddin et al., 2014).

Understanding the mass and elemental distribution of atmospheric particles are important parameters, as the toxicity of particles depends on their size and chemical composition, specifically the concentration of metals in the particles. Coarse particles can be deposited in the upper respiratory tract, fine particles can penetrate into the lungs, whereas ultrafine particles ≤ 0.1 μm can further reach into the alveolar region of the lungs (Krombach et al., 1997; Park and Wexler, 2008; Valiulis et al., 2008). Particles ≤ 3 μm can enter the lower airways during breathing and can deposit in the tracheobronchial and

pulmonary regions of the lungs and the highest deposition of particles having size range of 1 to 3 μm can occur in the pulmonary region (ICRP, 1995; NCRP, 1997). Metals associated with the particles can mediate toxicity depending on their chemical properties present in the particles (Oberdörster, 1993; Spurny, 2010; Dick et al., 2003). For example, Fe is an essential element for the human body but not in the form of inhalable particles as Fe-bearing particles can stimulate reactive oxygen species on the lung surface, which may further lead to scarring of the lung tissue (Knaapen et al., 2004). Iron and steel industries can generate large amounts of coarse to ultrafine range particles associated with high concentration of Cr, Fe, Mn, Ni, and Zn (Machemer, 2004; Querol et al., 2004; Querol et al., 2007; Garimella and Deo, 2008). These particles can impact the surrounding areas and the residents can be exposed to elevated levels of atmospheric particles of different mass and concentration of metals. Workers in industries are protected by occupational health and safety regulations; however residents living in close proximity to the industrial boundaries have no separate zoning or regulation protection arrangements, other than the NEPM goals.

The focus of this study was to investigate the mass and elemental distribution of particles collected nearby steelmaking industrial areas that operate under blast furnace and electric arc furnace operating regimes, and compare to one background urban site. Detailed elemental modality was examined in this work, including the elemental mass median aerodynamic diameter (MMAD) and geometric standard deviation (GSD) to standardise particle characterisation. Four sampling sites in Australian urban and industrial areas were selected and ten different size distributions of particles ranging from ≤ 0.18 μm to 18 μm were collected and analysed for particle mass and elemental composition of Al, Si, P, S, K, Ca, Ti, V, Cr, Mn, Fe, Co, Ni, Cu, Zn, Br, Sr and Pb. This study provides the fundamental information of particle mass and elemental distribution in the vicinity of iron and steelmaking industries. The outcomes of this study may assist the development of improved particle monitoring programs in the vicinity of industrial areas and also establish an elemental modality dataset which can be incorporated in the exposure and risk assessments of atmospheric particles.

5.2 Materials and methods

Three sites in the vicinity of Australian iron and steel industries and one site in the urban area, shown in Figure 5.1, were selected for sampling of the size resolved air particle samples: (1) Cringila (CR) sampling site was located in the vicinity of the Port Kembla

integrated iron and steelworks (blast furnace and basic oxygen furnace), with moderate traffic and strong industrial influence; (2) Rooty Hill (RT) sampling site was located in close proximity to the Rooty Hill mini-mill steelworks (electric arc furnace), with moderate traffic and strong industrial influence; (3) Whyalla (WH) sampling site was located nearby to the Whyalla integrated iron and steelworks (blast furnace and basic oxygen furnace), with moderate traffic and strong industrial influence; and (4) Macquarie Park (MQ) sampling site, which was located in the sports field of Macquarie University, surrounded by residential areas, one highway and commercial activities, has little or no industrial influence nearby to the sampling site. CR, RT and WH sites are highly influenced by atmospheric conditions during downwind flow from iron and steelmaking industries.

The samples were collected with an eight staged micro orifice uniform deposit impactor (MOUDI: model M100-R) for the period from April 2011 to November 2011. The eight stages had 50% cut diameters of 10.0, 5.6, 3.2, 1.8, 1.0, 0.56, 0.32 and 0.18 μm. In addition to the eight stages, two additional stages representing the inlet and exit particles were also used in the sampling. A sampling flow rate of 30 l/min was maintained during the entire sampling campaign. The air particles were collected on stretched Teflon filters (Pall corporation: PTFE membrane) substrates for at least a 24 hr particle loading period. Each sample set contained 10 atmospheric particle samples and 23 sets of samples were collected from the locations, CR (7 sets), RT (6 sets), WH (4 sets) and MQ (6 sets) site.

The particle mass was measured by weighing each Teflon substrate before and after the air particle sampling using a microbalance with 1.0 μg precision. Proton induced X-ray emission (PIXE) technique at Australian Nuclear Science and Technology Organisation (ANSTO) was performed on each particle sample to measure the elements Al, Si, P, S, K, Ca, Ti, V, Cr, Mn, Fe, Co, Ni, Cu, Zn, Br, Sr and Pb. The details of the PIXE technique are described elsewhere (Cohen, 1993; 1998; Cohen et al., 1996; Mohiuddin et al., 2014).

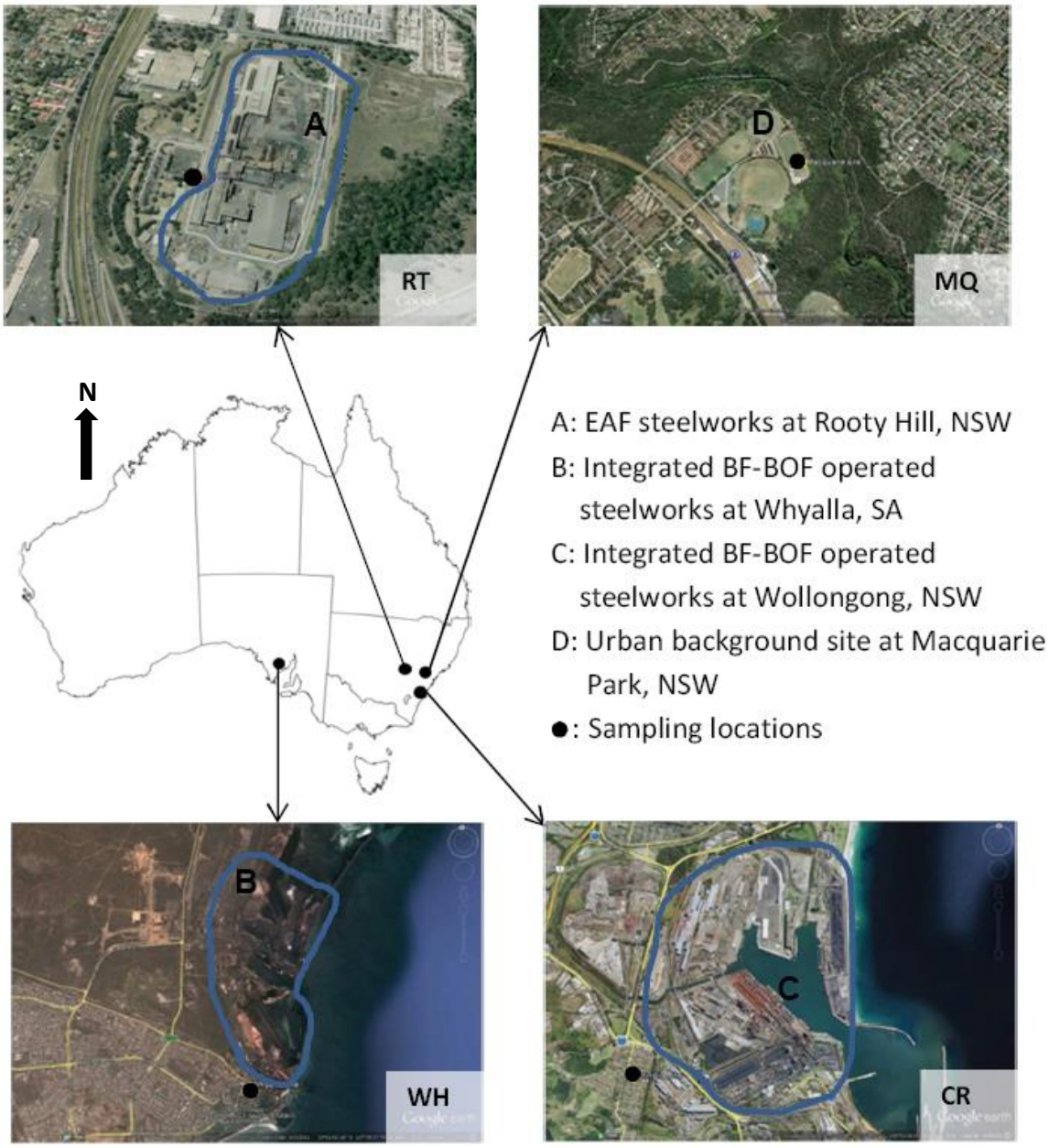

Figure 5.1 Map of sampling locations in Australia

5.3 Results and Discussion

5.3.1 Particle size distribution

Figure 5.2 shows that particle size distribution had the highest abundance in the range of aerodynamic diameter from 1.4 to 4.4 µm, for all sites except for the MQ (urban) site, which is characterised by two peaks with the same height. The highest peak in unimodal distribution at all sampling sites also occurred within this particle size range. The next relative abundance was found with the particle size range from 0.1 to 1.0 µm associated with the particles in the accumulation mode. The multimodal distribution also occurred in the particle size range from 0.1 to 10.0 µm.

Kao and Friedlander (1995) have described how the frequency distribution and statistical properties of atmospheric particles can reveal similarities and differences among particle components which may indicate the sources and stochastic processes influencing the atmospheric particle levels. The geometric standard deviation shows the spread of data around the geometric mean which may reflect the influence and effect of physical processes, for instance dry deposition, and also chemical processes, such as the equilibrium relationship with chemical species (Kao and Friedlander, 1995).

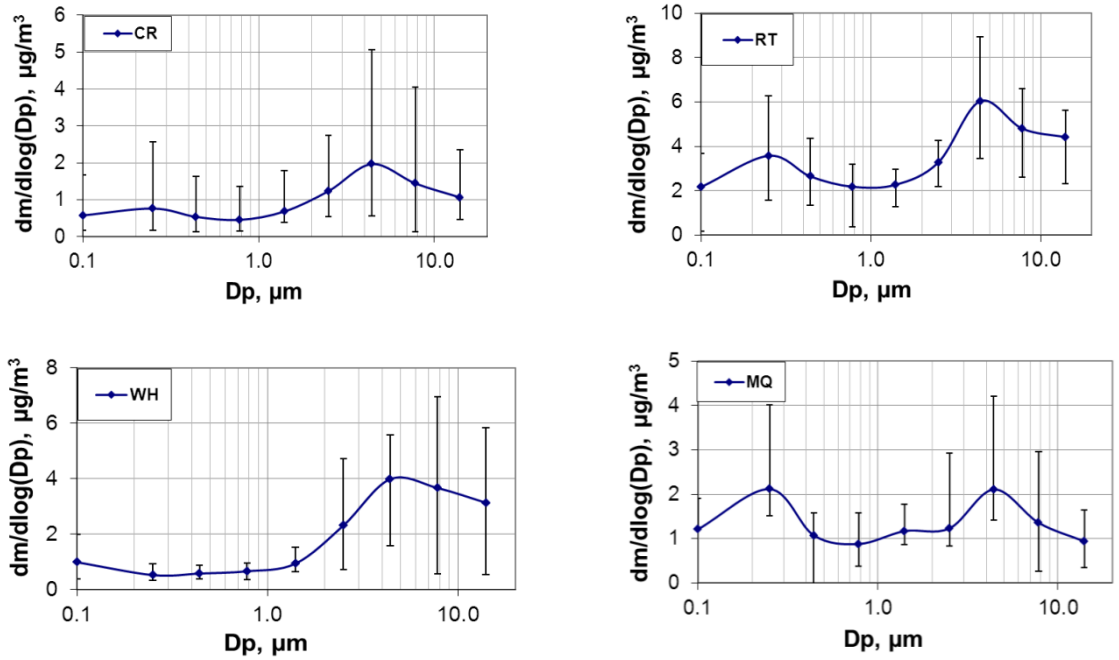

Figure 5.2 Average particle size distribution (expressed as mass per increment in log particle diameter) at CR, RT, WH and MQ sites; vertical line shows the lowest and highest concentration values

Table 5.1 Cumulative mass distribution calculation

stage	Cut-off diameter, µm	PM size range, µm d_{p_s} - d_{p_e}	PM mean size, $(d_{p_s} + d_{p_e})/2$	Mass concentration, µg/m³(C_i)	Mass fraction, % (f_i)	Cumulative distribution, %
S0	18	>18		C_1	$f_1 = {C_1}/{C_T}$	$\sum_2^{10} f_i$
S1	10	10 – 18	14.00	C_2	$f_2 = {C_2}/{C_T}$	$\sum_3^{10} f_i$
S2	5.6	5.6 – 10	7.80	C_3	$f_3 = {C_3}/{C_T}$	$\sum_4^{10} f_i$
S3	3.2	3.2 – 5.6	4.40	C_4	$f_4 = {C_4}/{C_T}$	$\sum_5^{10} f_i$
S4	1.8	1.8 – 3.2	2.50	C_5	$f_5 = {C_5}/{C_T}$	$\sum_6^{10} f_i$
S5	1	1 – 1.8	1.40	C_6	$f_6 = {C_6}/{C_T}$	$\sum_7^{10} f_i$
S6	0.56	0.56 – 1	0.78	C_7	$f_7 = {C_7}/{C_T}$	$\sum_8^{10} f_i$
S7	0.32	0.32 – 0.56	0.44	C_8	$f_8 = {C_8}/{C_T}$	$\sum_9^{10} f_i$
S8	0.18	0.18 – 0.32	0.25	C_9	$f_9 = {C_9}/{C_T}$	f_{10}
SP	0.02	0.02 – 0.18	0.10	C_{10}	$f_{10} = {C_{10}}/{C_T}$	0
				$C_T = \sum_{i=1}^{10} C_i$		

The normal distribution is not appropriate for the statistical analysis of particle size distribution data. Hinds (2012) showed the PM size distribution model as log-normal distribution which can be represented by cumulative or differential distribution. The cumulative size distribution was constructed using the method described in Table 5.1. The mass median aerodynamic diameter (MMAD) and the geometric standard deviation (GSD) parameters were calculated using regression lines from the log-probability graph of PM size versus cumulative mass distribution. The MMAD value is the particle size corresponding to the 50% cumulative distribution expressed as $\%50d_p$. Figure 5.3 shows the cumulative mass distribution with PM size for the four sampling sites. Coarse particles showed higher abundance at the CR and WH sites situated nearby the integrated steelmaking industries, whereas fine particles were found higher at the RT and MQ sites.

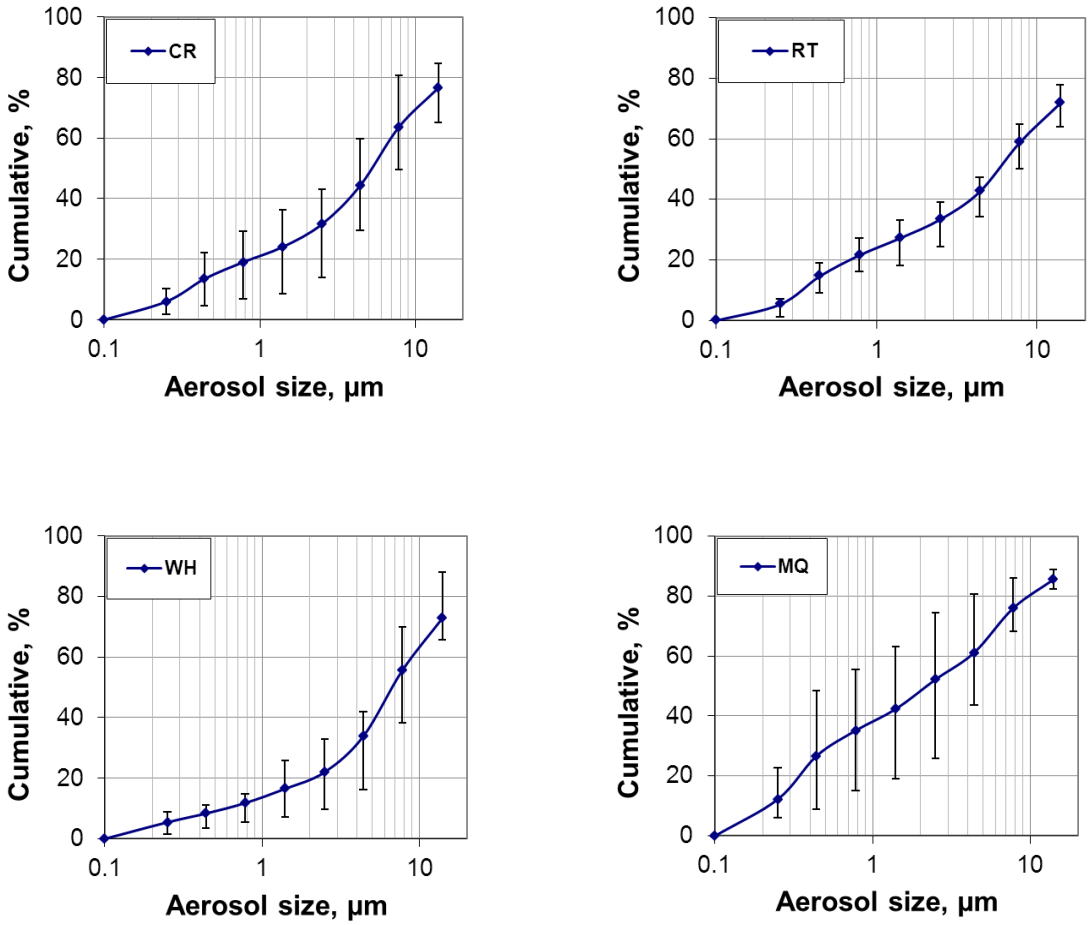

Figure 5.3 Average cumulative mass distribution of atmospheric particles; vertical line shows the lowest and highest percentage values

The geometric standard deviation (GSD) was calculated for the particles in unimodal, bimodal and trimodal distribution from the log-probability plot using the following formula:

For unimodal distribution (Hinds, 2012; O'Shaughnessy and Raabe, 2003):

$$GSD\ (\sigma_g) = \frac{\%84.13 d_p}{\%50 d_p} = \frac{\%50 d_p}{\%15.87 d_p} \qquad (5.1)$$

For bimodal and trimodal distribution (Wang et al., 2002; Nag et al., 2005):

$$GSD\ (\sigma_g) = \sqrt{\frac{\%84.13 d_p}{\%15.87 d_p}} \qquad (5.2)$$

Table 5.2 shows the MMAD and GSD values for the PM samples collected from all sampling sites. The MMAD values are dominated by coarser particles in the vicinity of iron and steel processing industries. The highest average MMAD value of 7.0 µm was found at the WH site while the MQ background site showed the lowest average value of 2.9 µm which indicates the dominancy of coarse particles at WH site and fine particles at MQ site. In addition, similar MMAD values are obtained at CR and RT sites of 5.4 µm and 5.8 µm respectively which display the higher particle loading at the three upper MOUDI stages (S0, S1 & S2). At the RT and MQ sites, the GSD values were found higher than MMAD because of the additional mode that occurred in the submicron particle size range with the same and/or considerable height compared to coarse particle mode. This resulted in significantly lower GSD fraction of $\%15.87d_p$ whereas the MMAD values are independent to the particle behaviour in the lower and higher distribution size range. The PM frequency variation in coarse and fine particles, as shown in Figure 5.3, for all sampling sites indicates the importance of individual particle size monitoring and analysis in urban and industrial areas. The meteorological conditions during the sampling period and source emission distribution might be the key factors for increasing the variation of particle frequency distribution of individual particle sizes.

Table 5.2 MMAD and GSD values for all PM samples; Mean (Min – Max)

	MMAD, µm	GSD (dimensionless)
CR	5.4 (3.2 – 8.0)	4.8 (3.0 – 8.2)
RT	5.8 (4.8 – 7.8)	8.0 (7.0 – 9.0)
WH	7.0 (5.3 – 10.0)	3.5 (2.7 – 4.5)
MQ	2.9 (0.5 – 5.1)	5.9 (4.2 – 6.8)

5.3.2 Particle mass concentration

The PM_{10} (<10 µm), $PM_{2.5}$ (<2.5 µm) and PM_1 (<1 µm) represents the accumulated mass of different particle size ranges from which the variability of PM_{10}, coarse PM ($PM_{10-2.5}$), fine PM ($PM_{2.5}$) and submicron PM (PM_1) is calculated, as shown in Table 5.3. The PM variability was calculated by the ratio of standard deviation with mean ratio values for the corresponding PM size. The PM mass concentration at the background MQ site was higher than in the industrial CR and WH sites, possibly due to the meteorological conditions, long range transport particles and dominating urban source categories, such as domestic combustion particles, transport particles and soil dust. The detailed analysis of PM_{10}, $PM_{2.5}$ and PM_1 mass concentrations for these four sites has been presented

elsewhere (Mohiuddin et al., 2014). The PM variability for fine PM ($PM_{2.5}$) and submicron PM (PM_1) is increased compared to PM_{10} and $PM_{10-2.5}$ in the vicinity of the iron and steel industries at CR, RT and WH sites. The fluctuating variability of PM groups indicates the importance of individual particle size distribution. For this, the PM mass concentration and distribution was carried out by the MOUDI sampler which provided ten different PM size ranges (<18, 10-18, 5.6-10, 3.2-5.6, 1.8-3.2, 1-1.8, 0.56-0.32, 0.18-0.32, <0.18 µm). Figure 5.4 shows the average PM mass concentration of the ten MOUDI stages from all sampling sites. The RT site had higher average PM mass concentrations in all of the stages, when compared to the other sampling sites. The dominant mass in the coarse particle size was found in stage 3 (3.2-5.6 µm) whereas PM mass collected in stage 8 (0.18-0.32 µm) was the dominated among fine particle stages for all sampling sites.

Table 5.3 Total mass concentration (in µg/m³) and variability (dimensionless) of PM

	PM_{10}, µg/m³	$PM_{2.5}$, µg/m³	PM_1, µg/m³	PM_{10} variability	$PM_{10-2.5}$ variability	$PM_{2.5}$ variability	PM_1 variability
CR	7.6	3.6	2.3	0.82	0.83	0.86	0.96
RT	26.9	14.5	10.6	0.39	0.34	0.43	0.50
WH	13.6	4.8	2.7	0.46	0.55	0.54	0.48
MQ	10.9	6.8	5.0	0.34	0.75	0.26	0.32

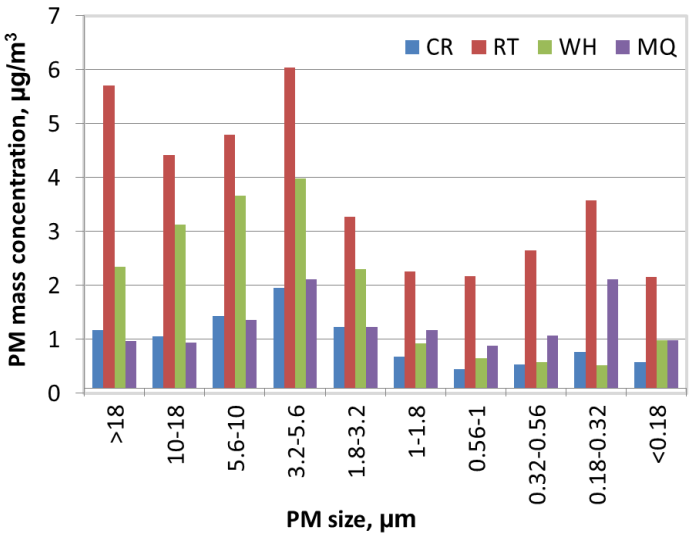

Figure 5.4 PM mass concentration for different PM size distributions

5.3.3 Elemental distribution

As the effect of particles on human health and the environment depends not only on their size and mass but also their chemical constituents, the elemental modal distribution of the particulate matter is important for risk assessment. The modality types are found highly variable between the mass and elements, and among elements in the urban and industrial areas. For example, the typical RT sample has unimodal mass distribution of coarse particles, however, only Al, Si and Ca of the studied elements have unimodal character, while the remaining elements, P, S, K, Ti, V, Cr, Mn, Fe, Co, Ni, Cu, Zn, Br, Sr, Pb represent bimodal and trimodal distribution. The mean elemental modal distribution for all particle samples is shown in Figure 5.5. Modality differs with the variation of mass and elemental fraction in the coarse, fine, intermodal, submicron and ultrafine particles. The cumulative percentage frequency for all elements from the studied sites was calculated and for the selected elements it is shown in Figure 5.6. When the PM mass fraction in the coarse size range is very high compared to fine or submicron size particles, then the modality in fine or submicron particle regions tend to disappear as the smaller peaks are found negligible compared to the higher peaks. The same observation is apparent for the elemental modal distribution.

Depending on their occurring modal types, the studied elements can be divided into three categories: a) Group I elements with a single mode distribution, b) Group II elements, with at least two modes in the particle size range, and c) Group III elements exhibiting both single and several modes of particle size distribution. The modal analysis method was consistent with other studies published elsewhere (Toscano et al., 2011; Waheed et al., 2011; Onat et al., 2012; Şahin et al., 2012).

5.3.3.1 Group I elements (Si, Ca)

The elements Si and Ca showed single mode distribution, mostly in the coarse particle size range, with the exception of some CR and WH samples for Si. The Si and Ca mode distributions are largely distributed in the range from 2.5 – 7.8 μm indicating that the elements mainly originated from physical formation processes such as windblown dust. However, coarse particles can also be emitted from industrial activities mainly from raw materials and stockpile handling, which is likely to have contributed to large particle breakdown in the CR, WH and RT industrial areas, as the particles were collected within 1.5 km of the iron and steelmaking plants. RT site has the highest coarse fraction for Si (82.5%) and Ca (90.7%) whereas the lowest coarse fraction for Si (69.4%) and Ca (78.8%) was found at the WH site.

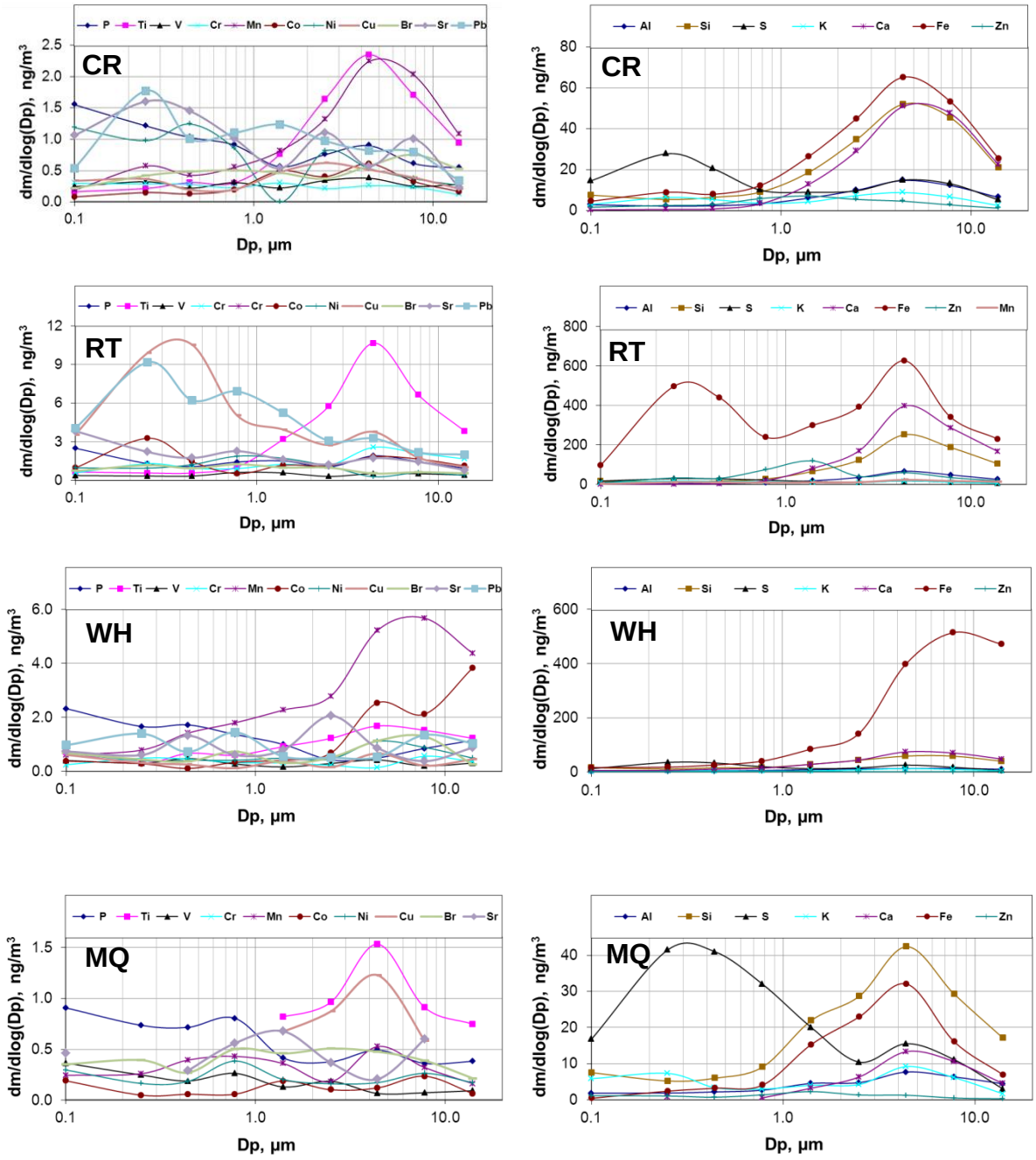

Figure 5.5 Mean elemental modal distribution of atmospheric particles

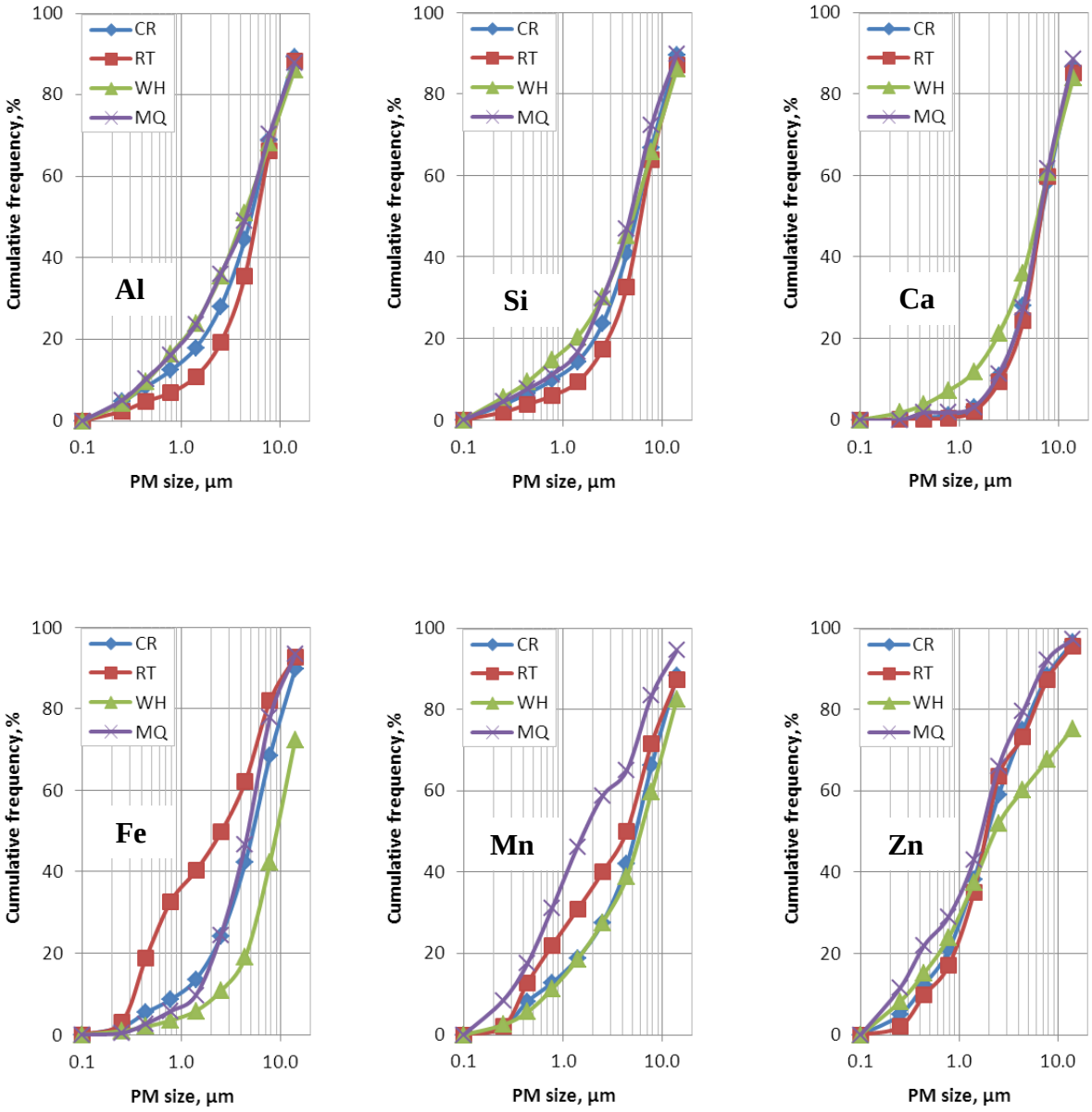

Figure 5.6 Cumulative frequency of selected elements

5.3.3.2 Group II elements (S, K, V, Ni, Pb)

The group II elements showed bimodal distribution exhibiting one mode at coarse particle range of 2.5 – 7.8 µm and different mode at the submicron particle size range of 0.25 – 0.78 µm. However, there are some exceptions in modal distribution found in the urban and industrial samples. For example, an additional mode for Ni and Pb in some CR samples indicates the different mechanisms of industrial particle input at the CR site. In contrast, some MQ samples have increasing trend with decreasing fine particle size range which tends to form an additional mode towards the ultrafine particle size range in the urban areas at MQ. The dominant mode in the group II elements S, K, V, Ni and Pb at the three industrial sites (CR, WH and RT) occurred in the submicron particle size range. The fine

particle size fraction is very high in this group ranging from 68.7% (Ni) to 47.6% (K) at CR site, from 75.5% (Pb) to 56% (V) at RT site, from 64.1% (S) to 34.2% (K) at WH site and from 79% (S) to 52.6% (K) at MQ site. The maximum coarse fraction was found for K (65.8%) at the WH site whereas the lowest was for S (21%) at the MQ site.

5.3.3.3 Group III elements (Al, P, Ti, Cr, Mn, Fe, Co, Cu, Zn, Br, Sr)

The elements Al, P, Ti, Cr, Mn, Fe, Co, Cu, Zn, Br and Sr present a variable modal distribution exhibiting unimodal, bimodal and/or trimodal distribution at the different sampling sites. Both unimodal and bimodal distributions occurred for Al that is one of the important earth crust reference elements, used to determine the metal enrichment in urban and industrial environment. In the most CR samples, Al exhibits two modes at the coarse and fine particle size range, with no apparent association to Si during the fine particle mode. This observation indicates on the likely industrial Al contribution in addition to the mineral dust influence. Similarly, both unimodal and bimodal particle size distribution was observed for Ti, Mn, Fe, Cu and Zn in the same CR samples which are most likely influenced by particles generated from the nearby steelworks along with other industrial activities. In general, the group III elements, Al, P, Ti, Cr, Mn, Fe, Co, Cu, Zn, Br and Sr, showed coarse mode at 2.5 – 7.8 µm and one or two fine modes at 0.1 – 0.78 µm and/or at 0.78 – 2.5 µm, which indicates likely multiple sources of atmospheric particle emission. Two successive modes can also occur in the submicron particle size range at 0.1 – 0.78 µm.

The fine particle size fraction is prevalent for P (65.2%), Cr (63%), Zn (59%) and Sr (66.2%) at the CR site, P (59.3%), Co (56.4%), Cu (77.8%), Zn (63.5%), Br (65%) and Sr (69.2%) at RT, P (73.4%), Cr (58.8%), Cu (53.2%) and Zn (52%) at WH and P (69%), Mn (58.6%), Zn (66%), Br (55.3%) and Sr (63.3%) at the MQ site. In addition, the coarse particle size fraction in group III was found to range from 79% (Ti) to 33.8% (Sr) at the CR site, from 82% (Ti) to 22.2% (Cu) at the RT site, from 89.1% (Fe) to 26.2% (P) at the WH site and from 83.6% (Ti) to 31% (P) at the MQ site.

Table 5.4 MMAD [in μm] and GSD [dimensionless] values at all sampling sites

	CR	RT	WH	MQ
	MMAD (GSD)	MMAD (GSD)	MMAD (GSD)	MMAD (GSD)
Al	5.3 (4.7)	5.8 (2.9)	4.2 (5.8)	4.5 (6.0)
Si	5.4 (3.5)	6.0 (2.6)	5.0 (5.7)	4.7 (5.6)
P	0.9 (5.9)	1.6 (6.4)	0.7 (3.7)	0.9 (5.6)
S	0.8 (5.2)	0.9 (4.6)	1.0 (4.6)	0.7 (3.8)
K	2.8 (4.9)	1.4 (4.7)	4.6 (4.3)	2.1 (5.4)
Ca	6.7 (2.3)	6.7 (2.1)	6.1 (3.4)	6.4 (2.2)
Ti	5.3 (2.9)	5.6 (2.5)	4.4 (7.1)	5.8 (2.3)
V	2.3 (7.0)	2.0 (5.3)	1.3 (5.8)	0.8 (4.6)
Cr	1.4 (5.3)	4.5 (5.3)	1.5 (6.1)	--
Mn	5.4 (3.5)	4.4 (4.8)	6.0 (4.8)	1.7 (4.5)
Fe	5.2 (3.3)	2.5 (4.7)	9.1 (2.6)	4.7 (2.6)
Co	3.4 (3.8)	1.7 (5.8)	9.2 (3.2)	2.4 (7.0)
Ni	0.7 (5.0)	1.2 (3.5)	3.5 (5.9)	1.3 (6.1)
Cu	2.7 (5.1)	0.7 (2.2)	2.1 (7.6)	4.7 (2.1)
Zn	2.0 (3.5)	1.9 (3.1)	2.3 (5.0)	1.7 (5.3)
Br	2.7 (5.2)	1.3 (4.8)	3.6 (5.6)	1.9 (5.0)
Sr	0.9 (5.0)	0.9 (5.9)	2.6 (4.2)	1.8 (4.2)
Pb	1.3 (4.6)	0.9 (4.2)	1.2 (6.5)	0.8 (3.8)

5.3.4 Elemental MMAD and GSD

Table 5.4 shows the elemental Mass Median Aerodynamic Diameter (MMAD) and Geometric Standard Deviation (GSD) values for all sampling sites. Elemental MMAD of air particles is significant for exposure assessment as it explains the behaviour of particles in an air flow. The MMAD values are divided into three categories, submicron-MMAD at ≤ 1.0 μm, intermodal-MMAD for the particle size range of >1.0 – 2.5 μm and coarse-MMAD for the particle size range greater than 2.5 μm. The elements P (at CR, WH), S (at CR, WH), Ni (at CR), Cu (at RT), Sr (at CR, RT) and Pb (at RT) are found as submicron-MMADs. The submicron particles are formed from high temperature anthropogenic processes and natural bushfires, and the likely sources of these particles for the studied sites are iron and steelmaking industries, coal combustion and vehicle exhaust (Wang et al., 2005; Samara and Voutsa, 2005). At the MQ site the intermodal-MMADs are dominant for K, Mn, Co, Ni, Zn, Br and Sr, whereas P, S, V and Pb are found as submicron-MMADs

which may be due to biomass burning, vehicle exhaust and long range transport of particles (Yue et al., 2007), while the non-crustal V can be emitted from fuel oil combustion (Gao et al., 2002). In addition, the elements Al, Si, Ca, Ti and Mn are represented as coarse-MMADs, which is likely due to the mineral dust contribution. All elements are categorised as polydispersed particles (GSD > 1.2), suggesting significantly high variability in particle size distribution.

5.3.5 Elemental mass fraction of atmospheric particles

Figure 5.7 shows the elemental fraction (EF) of atmospheric particles in percentage collected on each of the MOUDI stages, S0, S1, S2, S3, S4, S5, S6, S7, S8 and SP from CR, RT, WH and MQ sampling sites. Due to the high concentration of elemental mass in the coarse particles, compared to fine and submicron particles, the mass concentration dataset is normalised by calculating the elemental contribution to the total mass in each stage which will provide the elemental percent loading in each MOUDI stage. Four categories were considered essential for their elemental contribution to the particle mass, such as EF ≥ 10%, 1% ≤ EF < 10%, 0.1% ≤ EF < 1.0% and 0.01% ≤ EF < 0.1%. In general, stage S2 and S3 in coarse particle size range and stage S5 and S6 in fine particle size range showed higher elemental mass fraction.

MQ site has the lowest elemental mass fraction due to low industrial influence, compared to the industrial activities in the surrounding areas of CR, RT and WH sites. The elemental concentrations of Mn, Fe, Cu, Zn at the RT site were found to be higher than the other industrial sites, possibly due to the atmospheric conditions, closer distance from receptor site to the industry, stronger influence of fugitive emissions, and uncertain chemical input from the recycled raw steels in addition to the emissions from the electric arc furnace. Among two integrated (BF/BOF) steelmaking industries, the elemental concentrations of Fe, Mn and Co at WH at WH site were found higher than at CR site due to the atmospheric emissions from the pellet plant in addition to the iron ore handling and blast furnace emissions. The elemental concentrations of Ni, Cu and Zn at the CR site were found to be higher than at WH site due to the atmospheric input from the galvanizing processes, and other industrial inputs from the surrounding areas in addition to the blast furnace emissions. Fe is found as the dominant metal in CR, RT and WH sites in each MOUDI stage as these sampling sites are located in the vicinity of the respective steelworks plants. Fe in the WH site shows ≥10 % contribution in stages S1, S2 and S3, whereas Fe in the RT site contributes to the same amount in stages S4 to S8. This indicates

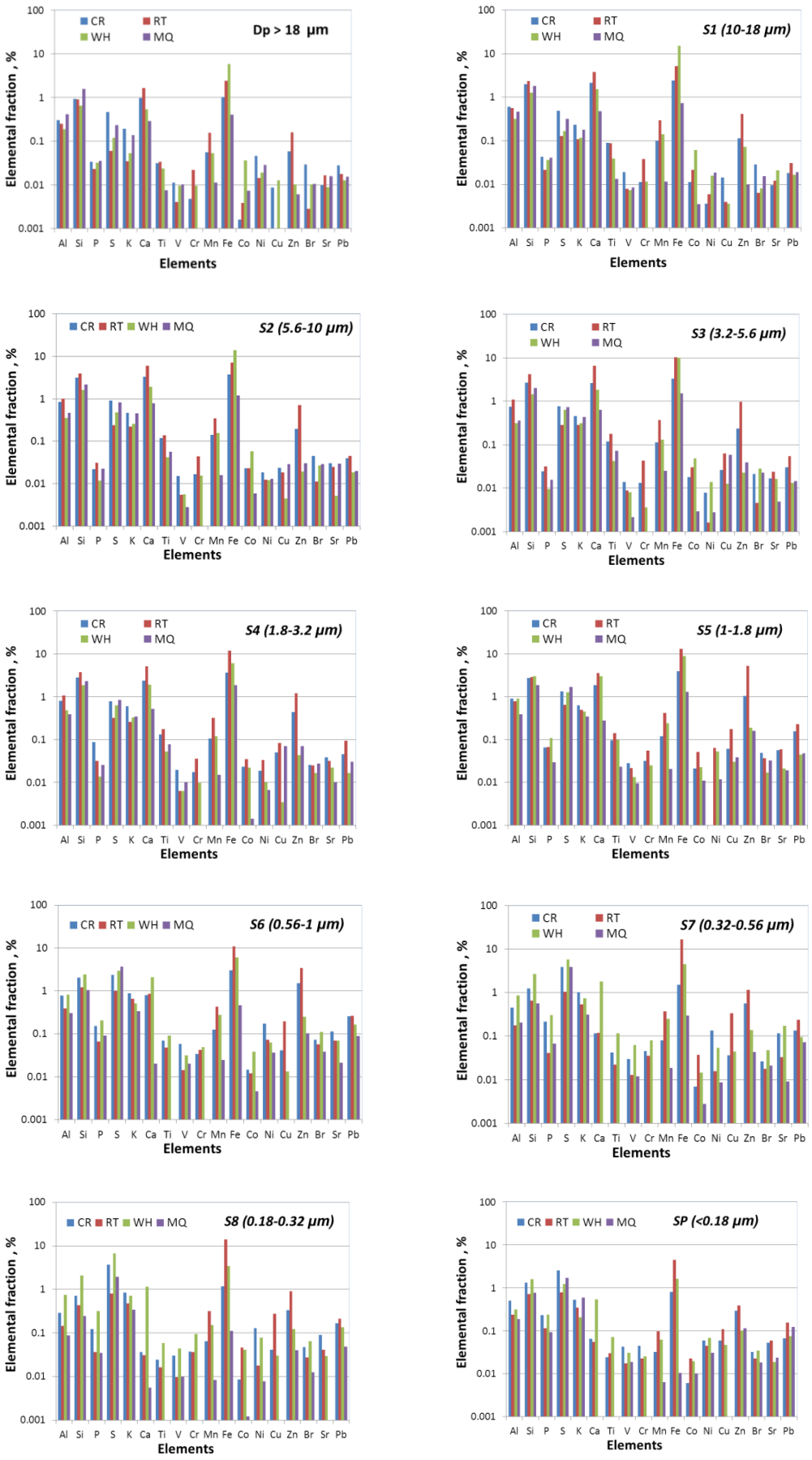

Figure 5.7 Elemental mass fraction (in percentage) of air particles at all MOUDI stages

that the Fe is dominant in the coarse particles at the WH site and in intermodal and submicron particles at the RT site. The WH site might be influenced by emissions from iron ore handling in addition to the Whyalla steelworks emissions. The RT site located in the close proximate to the electric arc-furnace steelworks might have additional influence by fine particles from point and fugitive emissions. S is found higher concentration in the CR site indicating the surrounding industrial influence from Wollongong area in addition to the Port Kembla steelworks emissions. Si, Ca and Fe elements are within the range of 1% ≤ EF < 10%, whereas Al, S, K, Ti, Mn and Zn elements are found in the range of 0.1% ≤ EF < 1.0%. In addition, P, Cr, Co, Ni, Cu, Br, Sr and Pb elements are in the category of 0.01% ≤ EF < 0.1% which are not significant in mass fraction.

5.3.6 Relative particle number and surface area distribution

The relative particle number and surface area distribution of atmospheric particles is characterised by assuming: a) the particles shape is spherical and b) the mean diameter of the particles size range in each stage is considered as reference particle size to calculate the particle number and surface area. The number of particles per volume of air and surface area particles per volume of air in each MOUDI stage for studied elements is calculated based on the following equations:

$$PM\ mass = \sum_{i=1}^{n}(volume \times mass\ density)_i$$

$$= Particle\ number\ (N) \times mean\ particle\ volume \times mass\ density \quad (5.3)$$

$$= \frac{1}{6} \times N \times mean\ surface\ area \times mean\ diameter \times mass\ density \quad (5.4)$$

Figure 5.8 shows the elemental particle number as a function of their mean diameters (both axis in logarithmic scales) from all sampling sites. Metals having mass density of ≥ 5.0 g/cm^3 are described in this study for PM number and surface area distribution. The number distribution of all studied metals is dominated by submicron and ultrafine particle size range. Elemental number distribution was found highly variable in the urban and industrial sampling sites which may depend on the distance from the emission sources and their atmospheric conditions. The elemental number distribution at all sites shows that the highest particle number occurs within the particle size of 0.1 µm whereas the highest PM mass occurs for the coarse particle size range. The industrial sites CR, RT and WH have higher elemental number distribution of V, Cr, Mn, Fe, Co, Ni, Cu, Zn and Pb compared with the urban background MQ site. Fe was found to exhibit the highest

number concentration for the 0.1 µm size particles at CR (1.1×10^{6} m^{-3}), RT (2.3×10^{7} m^{-3}) and WH (3.9×10^{6} m^{-3}), most likely originating from high temperature thermal activities. In addition, Zn (2.7×10^{5} – 2.2×10^{6} m^{-3}) and Mn (4.8×10^{4} – 5.4×10^{5} m^{-3}) had the next highest number concentrations for the 0.1 µm size particles at the industrial CR, RT and WH sites. However, the background MQ site shows higher Zn (3.0×10^{5} m^{-3}) concentration for the 0.1 µm size followed by Pb (2.0×10^{5} m^{-3}) and V (1.1×10^{5} m^{-3}). Overall, the ultrafine particles (≤ 0.1 µm) are found to be significant in particle number concentration and negligible mass concentration when compared with the total mass of PM_{10} and/or total suspended particles (TSP).

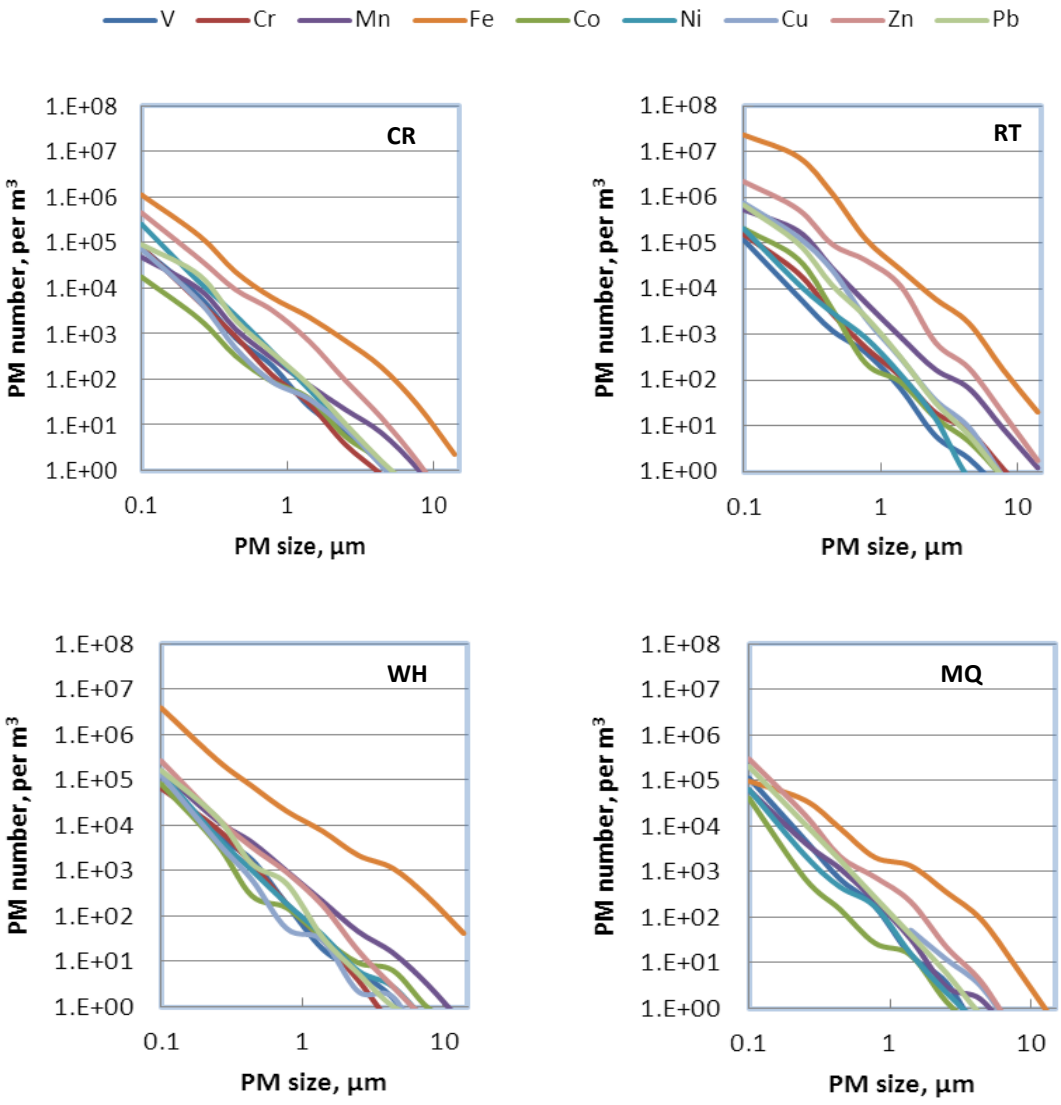

Figure 5.8 Elemental number distribution of atmospheric particles

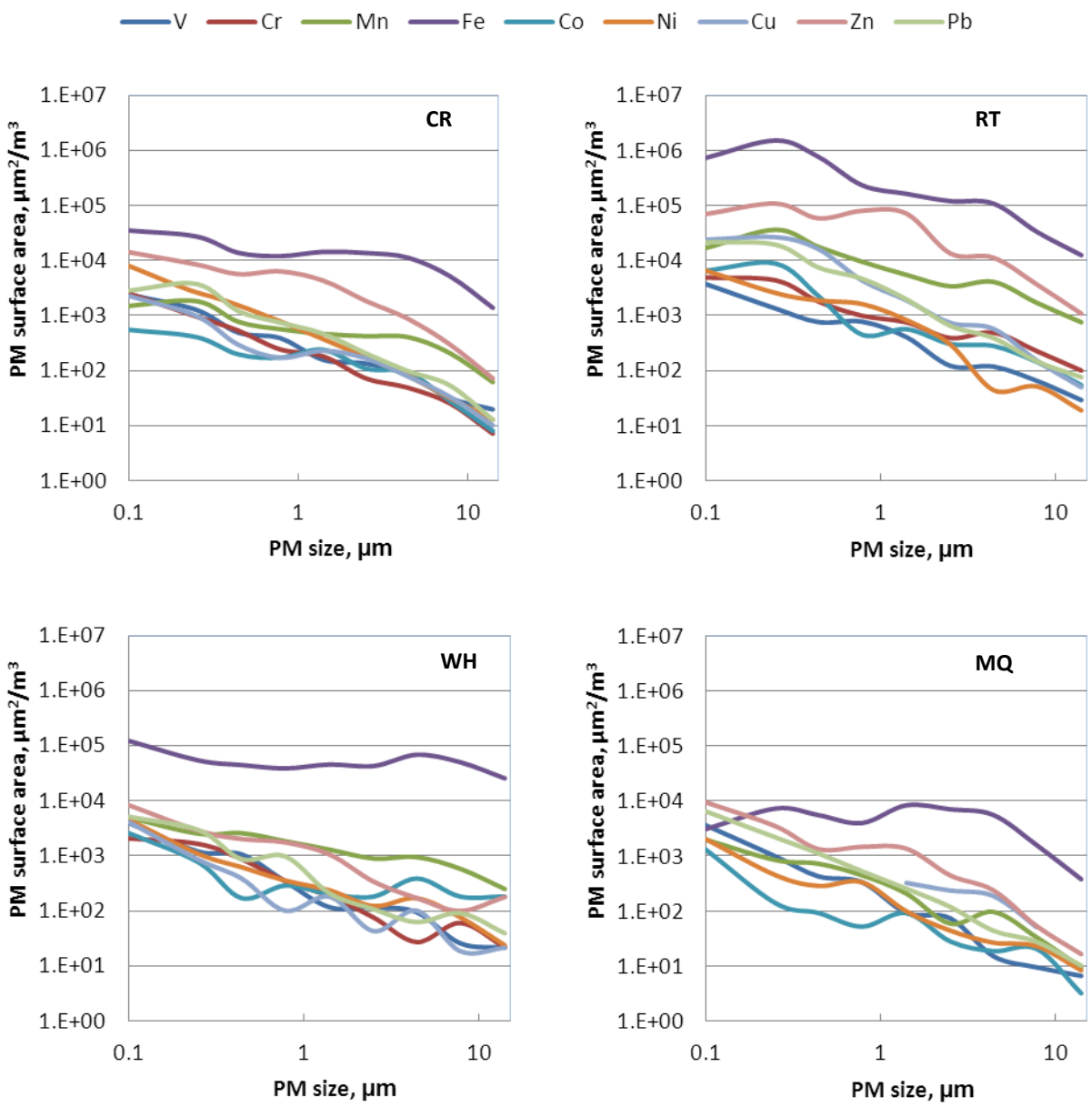

Figure 5.9 Elemental surface area distribution of atmospheric particles

PM surface area is an important parameter for gas phase interactions, such as partitioning, and heterogeneous reactivity as well as the health effects (Molina et al., 1996; Peter, 1997; Zondlo et al., 2000; Kolb and Worsnop, 2012). Figure 5.9 shows the elemental surface area distribution of the atmospheric particles (both axis in logarithmic scales) collected from the four sampling sites. Most of the particle surface areas for all studied elements were in the PM size range of 0.1 – 1.0 μm in the submicron and ultrafine particles. These particle sizes are first formed as nuclei and then grow to form accumulation mode particles. However, the higher surface area of Fe at the MQ site was found in the intermodal ($1.0 < D_p \geq 2.5$ μm) and coarse ($2.5 < D_p \geq 10$ μm) particle size ranges, which may be due to the

dominating primary source particles of mineral dust and the absence of heavy iron emitting industrial activities which can contribute to the iron fumes in the fine particle mass, as was the case with the industrial sites at CR, RT and WH. The particles collected at the RT site exhibited up to 1.5×10^{6} $\mu m^2.m^{-3}$ surface area for the 0.25 µm particle size. The highest surface area was found in Fe (3.5×10^{4} – 7.3×10^{5} $\mu m^2.m^{-3}$) for the PM size of 0.1 µm in the vicinity of iron and steel processing industries followed by Zn (8.3×10^{3} – 7.0×10^{4} $\mu m^2.m^{-3}$) and Mn (1.5×10^{3} – 1.7×10^{4} $\mu m^2.m^{-3}$) at CR, RT and WH sites.

5.3.7 Relative industrial contribution

The relative industrial contribution to the Fe in atmospheric particles was further estimated as Fe was found to be the dominant metal present in the particles collected in the vicinity of iron and steel processing industries for PM_{10}, $PM_{2.5}$ and PM_1 (Mohiuddin et al., 2014). According to the source emission categories the contribution from vehicular emission and sea spray on atmospheric Fe concentration is considered negligible as the source composition was not influenced by Fe. The relative industrial elemental contribution was further simplified by assuming: a) long range transport particles for all sampling sites are the same and b) secondary particle formations with associated atmospheric processes, such as dispersion, advection and chemical reaction in the local airshed from source to the receptor points of all industrial sampling sites are the same and/or negligible due to the close proximity within 1.5 km from the sampling sites. The formation of secondary particles can be affected by gaseous precursors and environmental conditions, such as temperature and humidity. The distance from source can be larger than 1.5 km depending on the wind speed and atmospheric reactions to form the secondary particles. Calculating the industrial contribution of the metals present in the atmospheric particles requires subtraction of the baseline metal content for the particles from the industrial sites. For this, MQ site is considered in this study as a background site which has very little influence from the industrial activities but similar influence from mineral dust compared to the industrial sites studied in this work. The Fe concentration for all sampling sites was normalised using their total mass concentration of each PM size range. The following equation was derived representing the worst case scenario to calculate relative industrial contribution to the total particle mass:

$$RIC = [(E/C)_{i+b} - (E/C)_b]/(E/C)_{i+b} \qquad \text{…….....(5.5)}$$

Where, RIC is the Relative industrial contribution; $(E/C)_{i+b}$ indicates the elemental fraction to the corresponding mass content at industrial sites of CR, RT and WH; and $(E/C)_b$ represents the background elemental fraction at the MQ site.

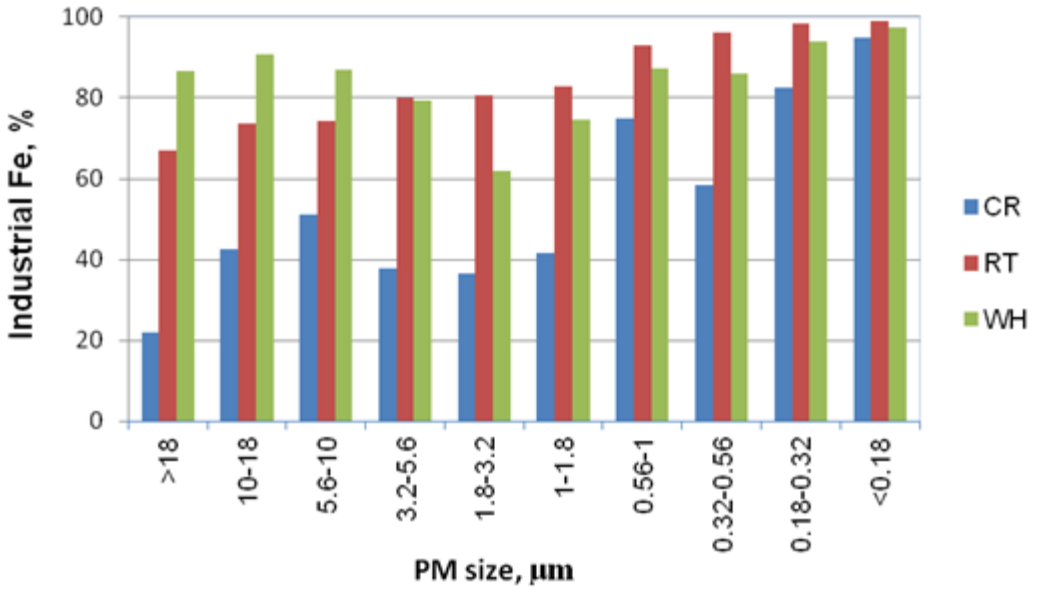

Figure 5.10 Industrial Fe contribution in percentage at CR, RT and WH site

Figure 5.10 shows the industrial Fe content in each MOUDI stage in the vicinity of iron and steelmaking industries at the CR, RT and WH sites. CR site shows the lowest industrial Fe fraction in all sampling stages particularly the stages with the PM size range of 1.0 – 18 µm indicating higher efficiency of the coarse particle reduction technologies installed by the steelworks. WH site shows the highest industrial Fe fraction in the coarse particles collected in the stages 0, 1 and 2. This may be due to the accumulation of higher mass fraction of coarse Fe from mechanical processes and raw material handling. Particles collected from the RT site exhibited significantly higher Fe fraction in all stages compared with the CR and WH sites with the exception of coarse PM size range of 5.6 – 18 µm at the WH site. The short distance (500 m) between Rooty Hill steelworks and the RH receptor sampling site is the possible reason for the higher Fe loading to the particle mass from both point and fugitive Fe sources. In addition, industrial Fe fraction at the submicron and ultrafine size particles at all sites are up to 95%. Higher industrial Fe fraction in submicron and ultrafine particles also indicates their higher number and surface area contribution in the vicinity of iron and steel processing industries.

5.4 Conclusions

The study analysed particulate matter distribution and modality of atmospheric particles collected in the vicinity of three industrial areas in Australia and compared these with results obtained for one background site. The results from this study showed that the modality types of atmospheric particles are highly variable between the particle mass and elements detected in the particles; and among elements in the particles collected from urban and industrial areas. Both unimodal and bimodal particle distribution was observed for the metals Mn, Fe and Zn in all industrial sampling sites which are most likely influenced by particles generated from the nearby steelworks. The mass median aerodynamic diameter (MMAD) of particles is found dominant in the coarser particles with the background site showing the lowest average value of 2.9 μm. At all of the sampling sites, the dominant mass concentration was found in the particle size range between 3.2 and 5.6 μm for the coarse particles, while for the fine particles, the dominant size range was 0.18 to 0.32 μm. The largest number of particles and surface area concentration were detected for the particle size of 0.1 μm, most likely originating from high temperature thermal activities. Particles collected at the background urban site were with the lowest elemental metal fraction, indicating strong local influence of the industrial activities on the elemental composition of the particles. Fe was found as the dominant metal in the three industrial ironmaking sites for each of the eight collected particle size ranges with contribution of more than 10% of the particle mass for some of the size ranges. In comparison, the particles collected from the background urban site had Fe concentration to the maximum of 1% of the particle mass. The industrial fraction of Fe was estimated assuming the background Fe concentration in the particles were those measured from the background site. The industrial fraction of Fe at the submicron and ultrafine size particles at the three industrial sites were estimated to range up to 95%, which is most likely a result of emissions from high temperature thermal activities.

5.5 References

Cohen, D. D. 1993. Applications of simultaneous IBA techniques to aerosol analysis. *Nuclear Instruments and Methods in Physics Research Section B: Beam Interactions with Materials and Atoms,* 79**,** 385-388.

Cohen, D. D. 1998. Characterisation of atmospheric fine particles using IBA techniques. *Nuclear Instruments and Methods in Physics Research Section B: Beam Interactions with Materials and Atoms,* 136**,** 14-22.

Cohen, D. D., Bailey, G. M. & Kondepudi, R. 1996. Elemental analysis by PIXE and other IBA techniques and their application to source fingerprinting of atmospheric fine

particle pollution. *Nuclear Instruments and Methods in Physics Research Section B: Beam Interactions with Materials and Atoms,* 109**,** 218-226.

Dick, C. A., Brown, D. M., Donaldson, K. & Stone, V. 2003. The role of free radicals in the toxic and inflammatory effects of four different ultrafine particle types. *Inhalation toxicology,* 15**,** 39-52.

Gao, Y., Nelson, E., Field, M., Ding, Q., Li, H., Sherrell, R., Gigliotti, C., Van Ry, D., Glenn, T. & Eisenreich, S. 2002. Characterization of atmospheric trace elements on PM< sub> 2.5</sub> particulate matter over the New York–New Jersey harbor estuary. *Atmospheric Environment,* 36**,** 1077-1086.

Garimella, S. & Deo, R. N. 2008. Characterization of aerosols generated in a steel processing factory. *The South Pacific Journal of Natural and Applied Sciences,* 25**,** 78-82.

Hinds, W. C. 2012. *Aerosol technology: properties, behavior, and measurement of airborne particles*, John Wiley & Sons.

Icrp 1995. International Commission on Radiological Protection. Conversion coefficients for use in radiological protection against external radiation. ICRP publication, 74, [Ann. ICRP 26 (3-4))].

Kao, A. S. & Friedlander, S. K. 1995. Frequency distributions of PM10 chemical components and their sources. *Environmental science & technology,* 29**,** 19-28.

Knaapen, A. M., Borm, P. J., Albrecht, C. & Schins, R. P. 2004. Inhaled particles and lung cancer. Part A: Mechanisms. *International Journal of Cancer,* 109**,** 799-809.

Kolb, C. E. & Worsnop, D. R. 2012. Chemistry and Composition of Atmospheric Aerosol Particles. *Annual Review of Physical Chemistry,* 63**,** 471-491.

Koliadima, A., Athanasopoulou, A. & Karaiskakis, G. 1998. Particulate matter in air of the cities of Athens and Patras (Greece): Particle-size distributions and elemental concentrations. *Aerosol science and technology,* 28**,** 292-300.

Krombach, F., Münzing, S., Allmeling, A.-M., Gerlach, J. T., Behr, J. & Dörger, M. 1997. Cell size of alveolar macrophages: an interspecies comparison. *Environmental health perspectives,* 105**,** 1261.

Lighty, J. S., Veranth, J. M. & Sarofim, A. F. 2000. Combustion aerosols: factors governing their size and composition and implications to human health. *Journal of the Air & Waste Management Association,* 50**,** 1565-1618.

Machemer, S. D. 2004. Characterization of airborne and bulk particulate from iron and steel manufacturing facilities. *Environmental science & technology,* 38**,** 381-389.

Mohiuddin, K., Strezov, V., Nelson, P. & Stelcer, E. 2014. Characterisation of trace metals in atmospheric particles in the vicinity of iron and steelmaking industries in Australia. *Atmospheric Environment,* 83**,** 72-79.

Molina, M. J., Molina, L. T. & Kolb, C. E. 1996. Gas-phase and heterogeneous chemical kinetics of the troposphere and stratosphere. *Annual review of physical chemistry,* 47**,** 327-367.

Nag, S., Gupta, A. & Mukhopadhyay, U. 2005. Size distribution of atmospheric aerosols in Kolkata, India and the assessment of pulmonary deposition of particle mass. *Indoor and Built Environment,* 14**,** 381-389.

Ncrp 1997. Uncertainties in fatal cancer risk estimates used in radiation protection, 126. National Council on Radiation Protection and Measurements report, [Bethesda MD].

Nsw Epa 2012. Technical report no 1. Air emissions inventory for the greater metropolitan region of New South Wales. 2008 calendar year. Consolidated natural and human-made emissions: results. Published by Environment Protection Authority, NSW, 978-1-74293-556-0.

O'shaughnessy, P. T. & Raabe, O. G. 2003. A comparison of cascade impactor data reduction methods. *Aerosol Science & Technology,* 37**,** 187-200.

Oberdörster, G. 1993. Lung dosimetry: pulmonary clearance of inhaled particles. *Aerosol science and technology,* 18**,** 279-289.

Onat, B., Şahin, Ü. A. & Bayat, C. 2012. Assessment of particulate matter in the urban atmosphere: size distribution, metal composition and source characterization using principal component analysis. *Journal of Environmental Monitoring,* 14**,** 1400-1409.

Park, S. & Wexler, A. 2008. Size-dependent deposition of particles in the human lung at steady-state breathing. *Journal of Aerosol Science,* 39**,** 266-276.

Peter, T. 1997. Microphysics and heterogeneous chemistry of polar stratospheric clouds. *Annual review of physical chemistry,* 48**,** 785-822.

Portin, H., Leskinen, A., Hao, L., Kortelainen, A., Miettinen, P., Jaatinen, A., Laaksonen, A., Lehtinen, K., Romakkaniemi, S. & Komppula, M. 2013. The effect of local sources on particle size and chemical composition and their role in aerosol-cloud interactions. *Atmospheric Chemistry and Physics Discussions,* 13**,** 32133-32173.

Querol, X., Alastuey, A., Viana, M., Rodriguez, S., Artiñano, B., Salvador, P., Garcia Do Santos, S., Fernandez Patier, R., Ruiz, C. & De La Rosa, J. 2004. Speciation and origin of PM10 and PM2. 5 in Spain. *Journal of Aerosol Science,* 35**,** 1151-1172.

Querol, X., Viana, M., Alastuey, A., Amato, F., Moreno, T., Castillo, S., Pey, J., De La Rosa, J., Sánchez De La Campa, A. & Artinano, B. 2007. Source origin of trace elements in PM from regional background, urban and industrial sites of Spain. *Atmospheric environment,* 41**,** 7219-7231.

Şahin, Ü. A., Scherbakova, K. & Onat, B. 2012. Size distribution and seasonal variation of airborne particulate matter in five areas in Istanbul, Turkey. *Environmental Science and Pollution Research,* 19**,** 1198-1209.

Samara, C. & Voutsa, D. 2005. Size distribution of airborne particulate matter and associated heavy metals in the roadside environment. *Chemosphere,* 59**,** 1197-1206.

Seinfeld, J. H. & Pandis, S. N. 2012. *Atmospheric chemistry and physics: from air pollution to climate change*, John Wiley & Sons.

Spurny, K. 1996. Aerosol air pollution its chemistry and size dependent health effects. *Journal of Aerosol Science,* 27**,** S473-S474.

Spurny, K. R. 2010. *Aerosol chemical processes in the environment*, CRC Press.

Toscano, G., Moret, I., Gambaro, A., Barbante, C. & Capodaglio, G. 2011. Distribution and seasonal variability of trace elements in atmospheric particulate in the Venice Lagoon. *Chemosphere,* 85**,** 1518-1524.

Valiulis, D., Šakalys, J. & Plauškaitė, K. 2008. Heavy metal penetration into the human respiratory tract in Vilnius. *Lithuanian Journal of Physics,* 48.

Waheed, A., Li, X., Tan, M., Bao, L., Liu, J., Zhang, Y., Zhang, G. & Li, Y. 2011. Size distribution and sources of trace metals in ultrafine/fine/coarse airborne particles in the atmosphere of Shanghai. *Aerosol Science and Technology,* 45**,** 163-171.

Wang, G., Huang, L., Gao, S., Gao, S. & Wang, L. 2002. Measurements of PM10 and PM2. 5 in urban area of Nanjing, China and the assessment of pulmonary deposition of particle mass. *Chemosphere,* 48**,** 689-695.

Wang, X., Sato, T., Xing, B., Tamamura, S. & Tao, S. 2005. Source identification, size distribution and indicator screening of airborne trace metals in Kanazawa, Japan. *Journal of Aerosol Science,* 36**,** 197-210.

Yue, W., Li, X., Liu, J., Li, Y., Zhang, G. & Li, Y. 2007. Source tracing of chromium-, manganese-, nickel-and zinc-containing particles (PM10) by micro-PIXE spectrum. *Journal of radioanalytical and nuclear chemistry,* 274**,** 115-121.

Zondlo, M. A., Hudson, P. K., Prenni, A. J. & Tolbert, M. A. 2000. Chemistry and microphysics of polar stratospheric clouds and cirrus clouds. *Annual review of physical chemistry,* 51**,** 473-499.

Chapter 6

Bonding structure and mineral analysis of size resolved atmospheric particles near steelmaking industrial sites

Preface

This chapter describes the basic functional groups of organic compounds and mineral content of inorganic compounds in different size fractions (coarse, fine, intermodal, submicron, and ultrafine) of atmospheric particles collected from Australian urban and industrial areas. It refers the thesis objectives [A5] and 'prepared for publication' article [P1] named as "Bonding structure and mineral analysis of size resolved atmospheric particles in the vicinity of iron and steelmaking industries in Australia".

6.1 Introduction

Atmospheric particles releasing from industrial sectors are posing significant challenges to the surrounding air quality. Industrial atmospheric particles are complex and heterogeneous, and may contain numerous organic and inorganic compounds. Characterisation of these particles are challenging due to their very low concentration in size resolved atmospheric particles, even though these particles can be hazardous for human health and environment. The level of toxicity also increases with the decrease of particle size, especially for fine and ultrafine particles (Braakhuis et al., 2014). Most of the particle characterisation studies are limited to mass and elemental concentration of bulk range particles (PM_{10}, $PM_{2.5}$) (Karlson et al., 2014; Cohen et al., 2014; Hibberd et al., 2013) and fewer studies for size resolved atmospheric particles (Radhi et al., 2010; Mohiuddin et al., 2014a; Mohiuddin et al., 2014b). Although elemental compositions of particles provide basic understanding of exposure and associated risks, further analysis on bonding structure and mineral content is required for comprehensive understanding of organic and inorganic compounds in atmospheric particles.

Organic compounds (carbonaceous and nitrogenous molecules) in atmospheric particles can have negative impacts on human health (Dockery et al., 1993; Alcock, 2003; Shah and Balkhair, 2011), and the ecosystem (Cupr et al., 2013). These compounds can be generated from both natural (biogenic) and anthropogenic (industrial process, vehicle exhaust, wood heaters) sources. Organic compounds can be examined using elemental analysis or gas chromatography–mass spectrometry (GC-MS), however about thousand to hundred thousand acyclic possible structures can be arranged for the same organic compound due to the diversity of carbon bonding (Roos, 1997). The behaviour of organic compounds also depends on the types of bonding structures. These structural bonding features of organic compounds in atmospheric particles can be identified and semi-quantified using Fourier transform infra-red (FTIR) technique (Allen et al., 1994; Maria et al., 2002; Ghauch et al., 2006). There are many studies focused on bonding structure in PM_{10} and $PM_{2.5}$ using FTIR method (Coury and Dillner, 2008; 2009; Ghauch et al., 2006), however, unregulated submicron (PM_1) and ultrafine particles ($PM_{0.1}$) are potentially the most hazardous. This study is the first attempt so far to analyse the bonding structure and their distribution in size resolved atmospheric particles collected nearby Australian blast furnace and electric arc furnace steelworks using FTIR technique.

Inorganic compounds in atmospheric particles can be constituted of both amorphous and crystalline materials. The elemental composition study of inorganic compounds in atmospheric particles can only provide the total elemental content, which may also originate from amorphous and/or crystalline materials. For example, total iron content in atmospheric particles can be contributed from amorphous metals and crystalline iron minerals, such as hematite, goethite, and magnetite. However, the behaviour of inorganic compounds is highly dependent on mineral phases (Reynolds et al., 2014; Calvo et al., 2013). Variety of minerals could be identified and semi-quantified by examining the unique characteristics (diffracted X-ray beam by crystalline atoms) of crystalline phases in atmospheric particles, which can be originated from both natural and anthropogenic sources. Some studies focus on mineral analysis of bulk samples of atmospheric particles (TSP, PM_{10}) (Hleis et al., 2013; Lu et al., 2007; Ohmsen, 2004a; b), however mineral types and quantity can be significantly varied with different size fractions of atmospheric particles. The process efficiency and environmental performance of iron and steelmaking industries are also dependent on emission of crystalline minerals generated from fugitive sources (raw materials handling), and point sources of high temperature processing plants, such as blast furnace, basic oxygen furnace, and electric arc furnace because

releasing these minerals at any stage of the steelmaking process could affect the production performance. Hence, it is essential to examine the mineral content of size resolved atmospheric particles in the vicinity of Australian iron and steelmaking industries using X-Ray Diffraction (XRD) technique.

This study was devoted to identifying and semi-quantifying the bonding structures of organic compounds and mineral contents of inorganic compounds, including their distribution in size resolved atmospheric particles. The Fourier Transform Infra-Red (FTIR) and X-Ray Diffraction (XRD) analysis was performed in ten different particle size ranges collected from three Australian industrial sites in the vicinity of iron and steelmaking industries and one urban background site. The outcome of this study will provide improved understanding of organic and inorganic compounds in atmospheric particles, and their source apportionment to reduce the particle pollution.

6.2 Materials and methods

6.2.1 Sampling details

Three industrial sites, highly influenced by iron and steel processing industries, and one background site, where little or no industrial influence is expected, were selected to sample the size resolved atmospheric particles in a sampling protocol described previously (Mohiuddin et al., 2014a; Mohiuddin et al., 2014b). Four sets of samples (ten samples per set) were selected for the FTIR and XRD analysis. Cringila (CR) site was located in the residential area in New South Wales (NSW) with highly industrial influence in surrounding areas including the Wollongong integrated blast furnace – basic oxygen furnace (BF-BOF) steelworks. Whyalla site was located in the residential area in South Australia, and in proximity to the Whyalla integrated BF-BOF steelworks. CR and WH steelworks have the same integrated BF-BOF process for iron and steel production with an exception of pellet plant at WH steelworks instead of sinter plant at the CR steelworks. Rooty Hill (RT) site in NSW is located in the industrial area nearby to the electric arc furnace (EAF) steelmaking plant. The background Macquarie Park (MQ) site in NSW is located near to the Macquarie University sports field surrounded by mainly residential areas. An eight staged Micro Orifice Uniform Deposit Impactor (MOUDI) sampler with Teflon substrate was deployed in the sampling sites to collect the atmospheric particles for at least 24 hrs sampling duration.

6.3.2 FTIR analysis

Attenuated Total Reflectance (ATR) technique equipped with ZnSe-Diamond crystal was applied using Nicolet 6700 series Fourier Transform Infra-Red (FTIR) spectrometer to analyse the collected atmospheric particles. The 32 numbers of scan with 4 cm^{-1} spectral resolution over the range of 4000 – 500 cm^{-1} were used to prepare the FTIR spectra for the atmospheric particles samples. The blank Teflon substrate was also tested by FTIR technique to confirm the Teflon bond structure and eliminate the overlapping spectra with the particle samples. During the sampling campaign, the atmospheric particles were deposited on to the surface of the Teflon substrates. Small portions in thickness of the Teflon substrate were subjected to the FTIR scan. 1 mm infra-red beam was used to pass the particle samples collected on Teflon filters to acquire FTIR scans. It was found difficult to subtract the blank Teflon spectra with the same that confused particle samples, as the scan intensity depends on the thickness of the samples under FTIR investigation. For this, the Teflon spectral peaks were excluded for bonding structure analysis of the atmospheric particle samples. The blank Teflon spectra had strong peaks at 1203.6, 553.5, 505.1 cm^{-1} position and bonding structure was matched with the reference Teflon structure [n(-CF_2-)]. The Omnic spectra software was used to perform the FTIR scan analysis including baseline corrections, spectra normalisation and peak integration.

6.3.3 XRD analysis

The atmospheric particle samples on Teflon substrate were examined for mineralogical composition using X-Ray diffractometry (XRD). The Teflon substrate was placed on a Si-crystal low background holder to avoid the diffraction peaks generated from aluminum based sample holder. PANalytical X'Pert Pro MPD diffractometer was used with the settings of sample stage (reflection-transmission spinner), CuKα radiation, X'Celerator detector, Bragg Brentano geometry, scan range (18.5 to 80^0 2Θ), generator (40mA, 45 kV), scan type (continuous), divergence slit type (fixed), divergence slit size (1^0), and a high resolution scan using step size of 0.02 2Θ with scan per step of 200 s. 20 mm square beam was used for XRD analysis to acquire XRD scans. Minerals identification and semi-quantification was performed using PANalytical's Highscore Plus software v2.2.4, coupled with ICDD PDF2 and PAN-ICSD mineral databases. The systematic Reitveld refinement technique was applied on identified minerals using Highscore Plus software.

6.4 Results and discussion

6.4.1 FTIR analysis

The spectra of the size resolved atmospheric particles collected from CR, RT, WH, and MQ sites are shown in Figures 6.1(a-d). The qualitative absorbance frequencies in the coarse, fine, intermodal and submicron size particles at all studied sites are presented in Table 6.1. The interpretation of the spectra was limited to the selected organic absorbance groups as mentioned below:

Table 6.1 Absorbance observed in FTIR spectra of air particles

Functionality		Absorption frequencies (cm^{-1})	Sampling site	Presence in air particle samples			
				Coarse >2.5µm*	Intermodal 1-2.5µm**	Submicron 0.18-1µm	Ultrafine <0.18µm
-CH	Aliphatic carbons	2850-3000, 1410	CR	H	H	H	nd
			RT	I	H	H	H
			WH	I	H	L	nd
			MQ	L	H	L	H
- OH	Hydroxyl	3250-3650, 1400-1450, 1000-1050	CR	H	H	L	nd
			RT	I	H	nd	nd
			WH	I	H	L	nd
			MQ	M	H	M	H
-NH	Amino	3300-3500, 1550-1650, 660-900	CR	M	H	L	nd
			RT	L	H	H	nd
			WH	M	H	M	H
			MQ	M	H	M	H
-CO	Carbonyl carbons	1640-1850	CR	Nd	H	L	H
			RT	L	H	nd	H
			WH	nd	H	M	H
			MQ	I	nd	M	H

**particle size range of >1.8µm was considered as coarse particles for qualitative analysis;*
***particle size range of 1-1.8µm was considered as intermodal particles for qualitative analysis;*
Occurrence frequency High, H: >75%; Moderate, M: 50-75 %; Intermediate, I : 25-50 %;
Low, L: <25%, and nd: not detected

6.4.1.1 Aliphatic carbon (-CH) group

The aliphatic carbon molecules can be constituted by $-CH_3$, $-CH_2$, and -CH carbon bonds which may include n-alkanes, branched alkanes, carbonyl containing molecules, alkanes, and aromatics aliphatic substituents (Roos, 1997). The characteristic IR spectra of aliphatic carbon bonds occur in the region of 2850–3000 cm^{-1}. The absorption at 2918 and 2850 cm^{-1} (Table 6.1, Figure 6.1) are attributed to $–CH_2$ asymmetric vibration. In addition, the absorption at 1410 cm^{-1} is assigned to the bending vibration with $–CH_2$ deformation which indicates the organic compound could be originated from alkane functional group

containing linear aliphatic chain (Coates, 2000). This aliphatic carbon bond was identified in the atmospheric particle size ranges from 0.18–10 µm at CR, RT, WH, and MQ sites. The stretching vibration at 2850-3000 cm^{-1} was selected for the relative quantification of the $–CH_2$ group.

6.4.1.2 Hydroxyl (-OH) group

Hydroxyl group mainly occurs at 3250-3650 cm^{-1} absorption range. Moderate to strong, and broad stretching vibrations were observed at 3350, 3390 cm^{-1} in this study (Table 6.1, Figure 6.1) which are assigned as free OH and hydrogen bonding of alcohol functional group (Coates, 2000). Moderate bending vibrations were also found in the region of 1400-1450 and 1000-1050 cm^{-1} which confirm the simple hydroxyl compound containing H-bonded alcohol functions in atmospheric particles. From the structural point of view, these alcohols may be derived by replacing H-atoms from a parent water molecule by a C-based alkyl group. The structural modification of alcohol when moving towards ether also may result significant changes in physical and chemical properties of these compounds depending on their hydroxyl content and ability to participate in H-bonding. This hydroxyl bond was mainly observed in the particle size ranges of 1-18 µm at all studied sites. The vibrations at 3250-3650 cm^{-1} were used to calculate the relative quantity of -OH group in the atmospheric particles.

6.4.1.3 Amino ($-NH_2$) group

Amino ($-NH_2$) group is regarded as an amino substituent derived from ammonia (NH_3), and similar sp3 structural features. Different amine classes (1^0 to 4^0) can be categorised according to their degree of substitution. Amino ($-NH_2$) groups can occur in different vibrations from 3300-3500, 1550-1650, 660-900 cm^{-1}. It appeared that weak N-H bond was overlapped and disappeared when strong O-H bond was identified at 3300-3500 cm^{-1}. The medium to strong bending vibration at 1621 cm^{-1} (Table 6.1, Figure 6.1) was attributed to the $–NH_2$ scissoring, and vibration at 873 cm^{-1} was assigned to NH_2 wagging, indicating these organic compounds originate from 2^0-amines functional group. This group was mainly observed in the particle size range of 0.56-10 µm at the CR, RT, WH, and MQ sites. The bending vibration at 1600-1660 cm^{-1} was selected for relative quantification of the $-NH_2$ group.

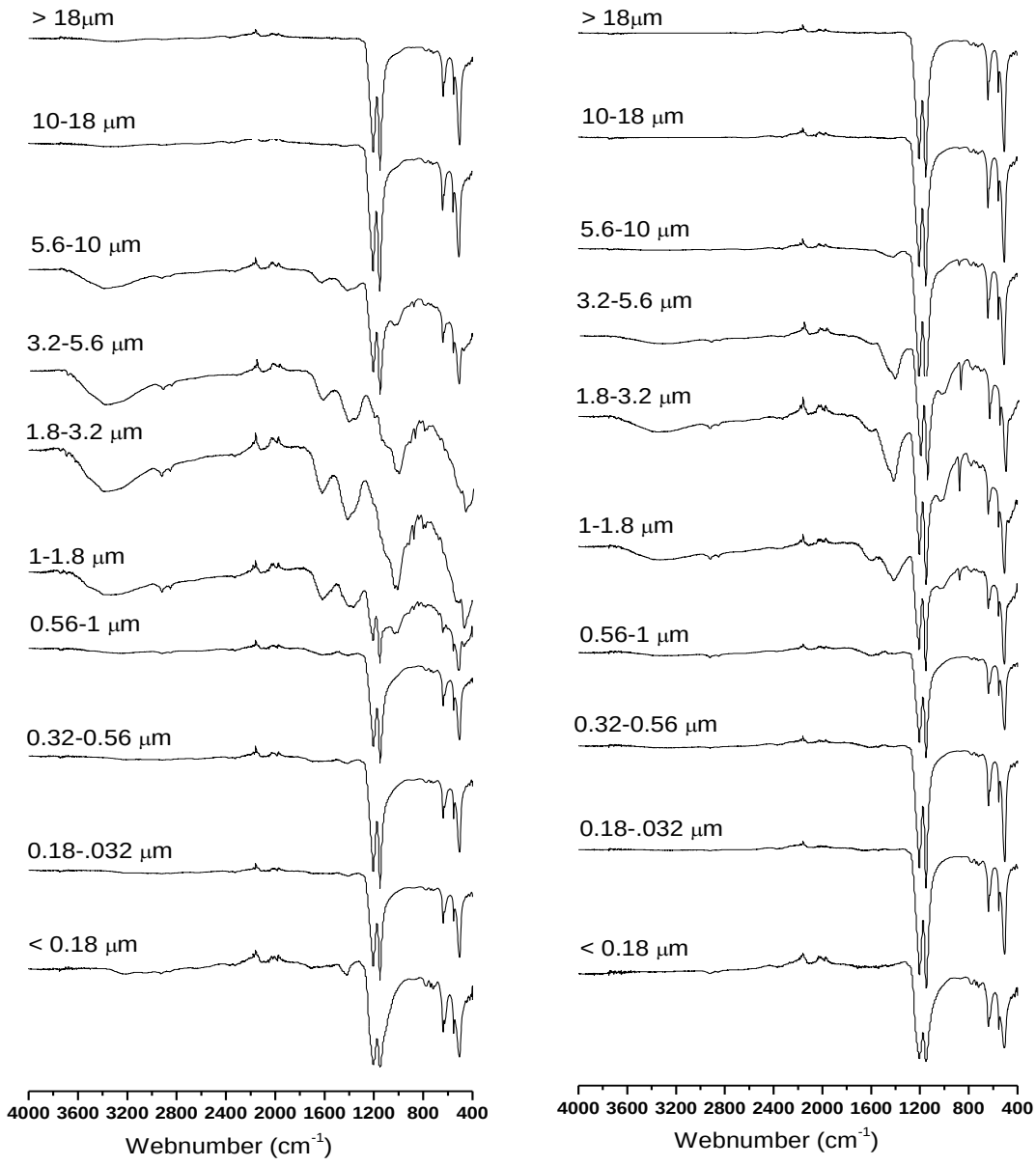

Figure 6.1 FTIR scans for size resolved aerosol samples at CR and RT sites

Carbonyl (-CO) group

The structural features of the carbonyl group can be found in several classes of organic compounds which impose very specific planar geometry associated with sp^2 hybridised carbon and oxygen, such as Aldehyde (R-COH), Ketone (R-CO-R), and Carboxylic acid (R-COOH). This group can blend with other functional groups resulting in properties and reactivities of combined functional groups. Carbonyl group can appear at a broad frequency range of 1640-1850 cm^{-1} (Table 6.1, Figure 6.1) with specific peaks from low to high frequencies depending on various functional groups from amide to open-chain acid anhydride. The absorption bands found at 1794 cm^{-1}, 1714 cm^{-1}, and 1695 cm^{-1} match well

with the reactive carbonyl compound (acid halide), simple carbonyl compound (Ketone), and conjugated carbonyl compound (conjugated ketone), respectively in the particle size below 1.8 μm at CR, RT, WH, and MQ sites. The vibration at 1680-1720 cm^{-1} was assigned to the relative quantification of –CO group.

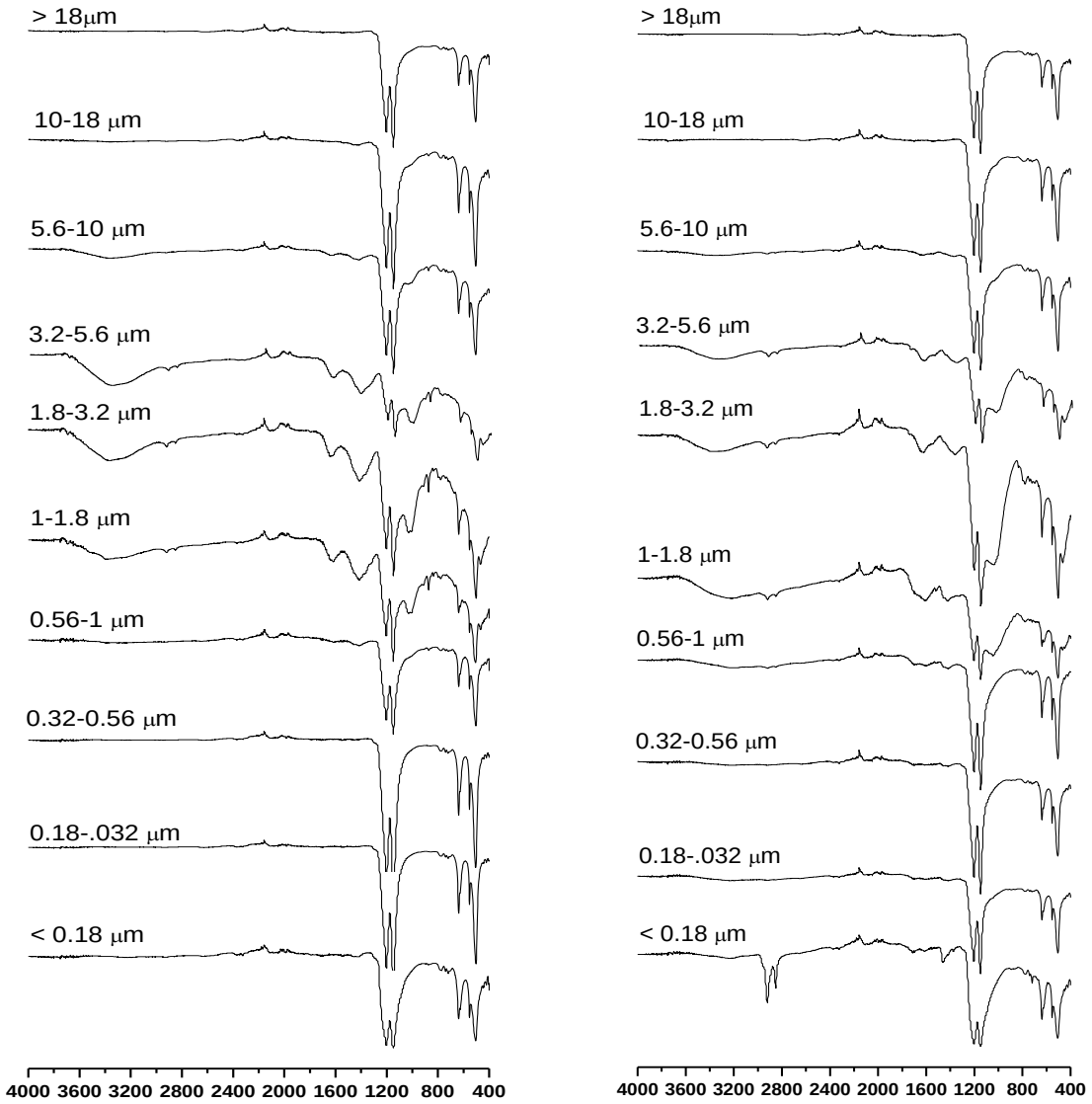

Figure 6.1 (contd). FTIR scans for size resolved aerosol samples at WH and MQ sites

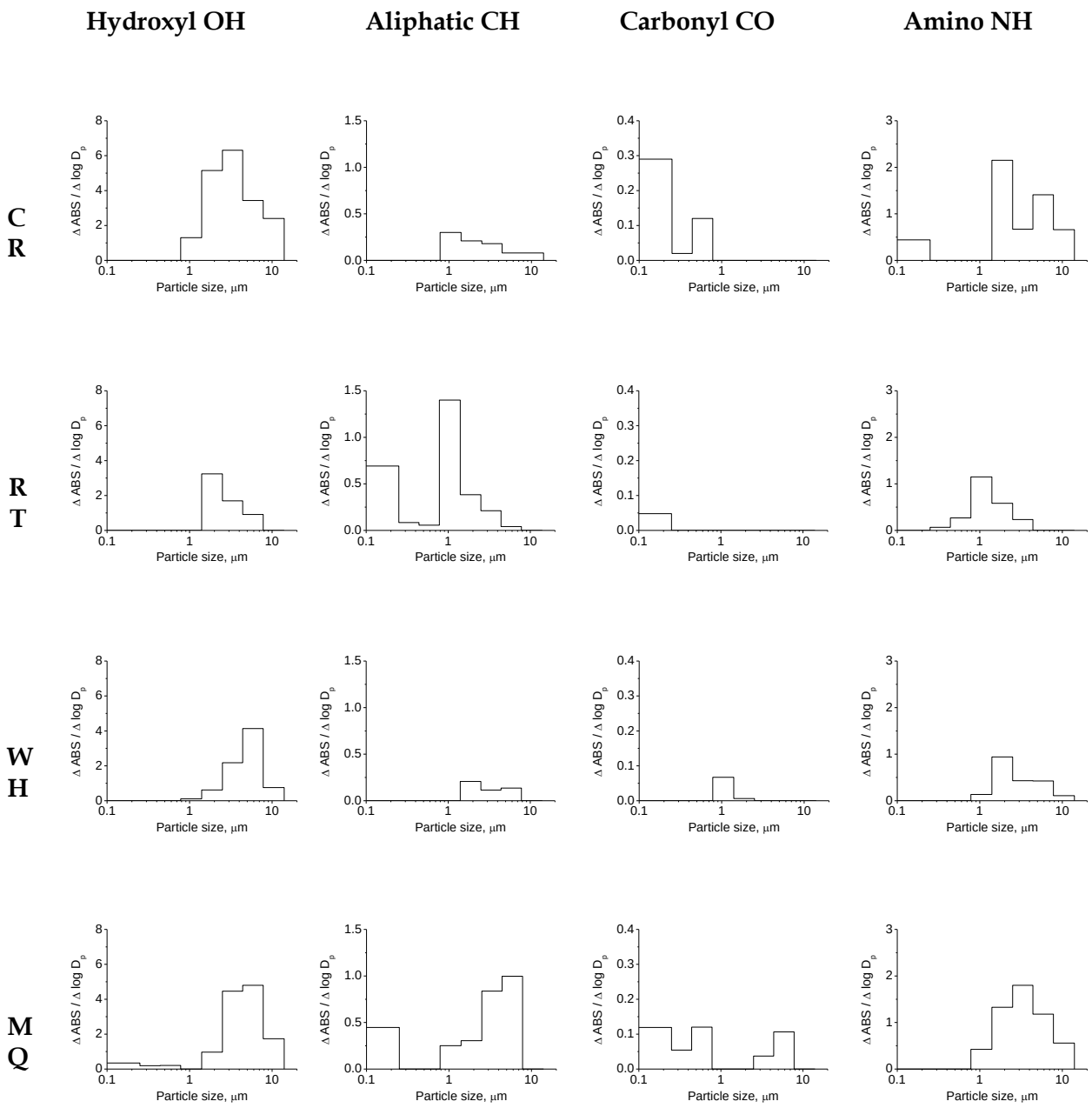

Figure 6.2 Functional group distribution as a function of particle size at CR, RT, WH and MQ sites

6.4.2 Functional group distribution

The strength, occurrence and modality type of functional groups are essential to understand the behaviour of organic compounds in atmospheric particles. Figure 6.2 shows the distribution of hydroxyl, aliphatic carbon, carbonyl, and amino functional groups in size resolved atmospheric particles collected from the CR, RT, WH, and MQ sites. The higher absorption value was found in -OH, -CH, -CO, and -NH groups at MQ site indicating their elevated concentration levels in the organic compounds in atmospheric particles. The functionality distribution was found variable between mass

and bonding groups, among bonding groups, and among urban and industrial areas. Single mode distribution was found predominant for -OH, -CH, -CO, and -NH groups at all industrial CR, RT, and WH sites whereas bimodal distribution was observed for -OH, -CH, and -CO groups at urban background MQ sites. The highest absorption peak occurred in the particle size range of 1.4 – 4.4 µm (-OH), 0.78 – 1.4 µm (-CH), 0.10 – 0.78 µm (-CO), and 0.78 – 4.4 µm (-NH) (Fig 2).

The -OH bonding in alcohol compounds, -CH bonding in n-alkane, -CO bonding in ketone, and –NH bonding in amine in the atmospheric particles in the industrial areas at CR, RT and WH sites can be attributed to mainly anthropogenic sources, such as iron and steelmaking industries (Environment Protection Authority, 2013), and motor vehicles exhaust (Xie et al., 2009). These compounds can also originate from microbiological processes from biogenic sources (Kavouras et al., 1999) in addition to the vehicle exhaust (Schauer and Cass, 2000), and wood heaters (Environment Protection Authority, 2013) especially in the winter time at the urban MQ site. The increasing amount of organic compounds in atmospheric particles in the urban background site compared to the industrial sites (Fig. 2) may be due to the strong influence of local biogenic emissions from surrounding plants covering large areas. The variation in bonding group distributions can also be influenced by atmospheric conditions, and atmospheric photochemical reactions.

6.4.3 Functional groups fraction

Figure 6.3 shows the relative percent of functional groups in the coarse, intermodal and submicron particles in urban and industrial areas. The –OH group is strongly associated with the coarse particles (at WH and MQ sites), and intermodal particles (at RT site), whereas the –CH group is associated with intermodal particles (at WH site), and submicron particles (at RT site). The –CO group is predominantly associated with submicron particles at all sampling sites. The –NH group is found substantial with submicron particles (at RT site), and intermodal particles (at WH site). The strong association of bonding groups with submicron particles may be associated to the vehicle exhaust, biogenic sources, and secondary organic particles from atmospheric photochemical reactions.

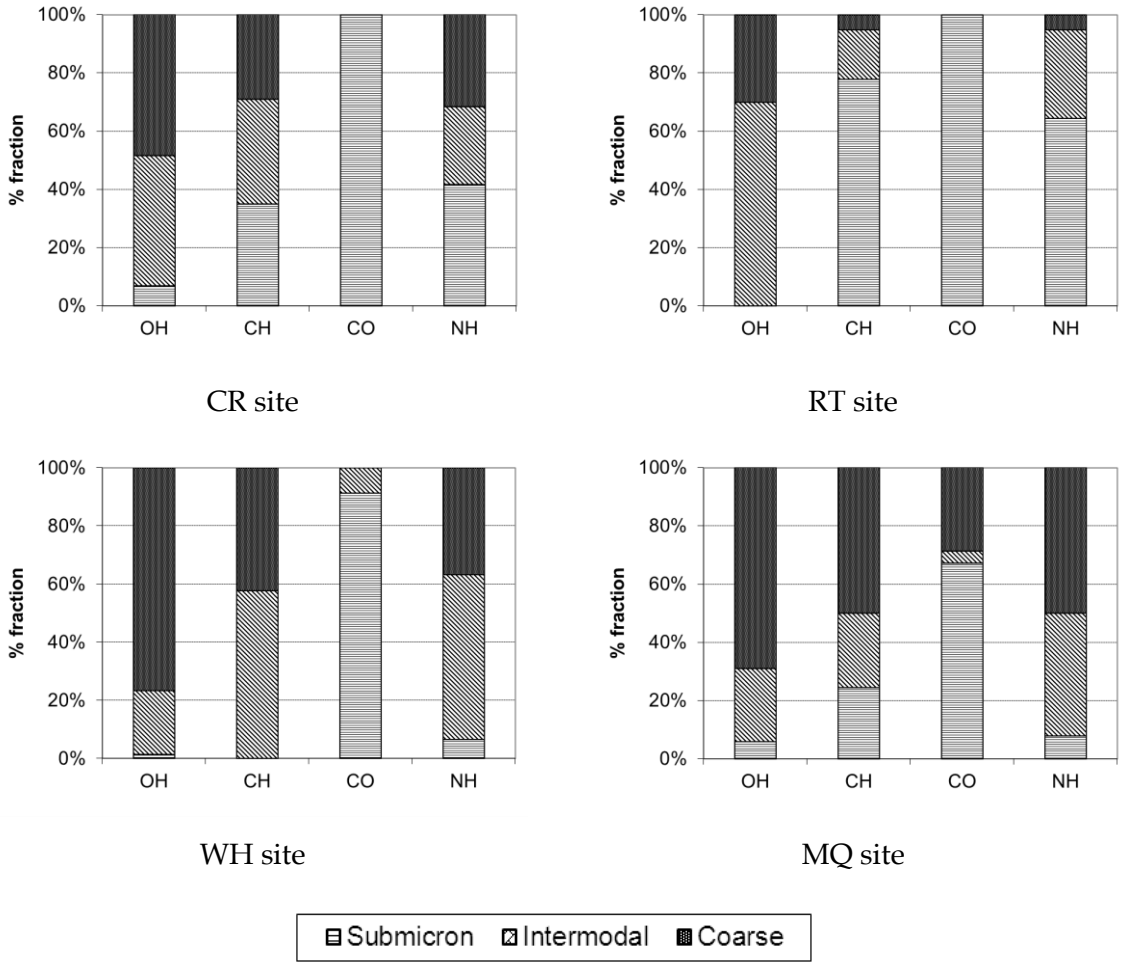

Figure 6.3 Coarse, intermodal and submicron PM functional group fractions

6.5 XRD analysis

6.5.1 Mineral identification and composition

The XRD analysis was performed on the atmospheric particles (0.10<Dp<18 μm), and the dominant minerals of quartz (SiO_2), hematite (α-Fe_2O_3), calcite ($CaCO_3$), goethite (FeO_2H), magnetite (Fe_3O_4), halite (NaCl), maghemite (γ-Fe_2O_3), iron titanium oxide ($FeTiO_3$), and franklinite ($ZnFe^{3+}{}_2O_4$) were identified in the inorganic fraction of the samples. Figure 6.4 shows the typical XRD diffraction pattern of the size resolved atmospheric particles at WH site. Fe-containing minerals (hematite, goethite, magnetite, maghemite, iron titanium oxide, and franklinite) dominate the atmospheric particles in the vicinity of iron and steelmaking industries at the CR, RT, and WH sites, whereas the background MQ site contained primarily quartz, calcite, and halite. Calcite minerals can be contributed from steelmaking sources as they are used as fluxing agents in addition to the natural mineral sources. Halite could originate from the sea spray at the CR, RT, and MQ sites; however the RT site was not influenced by the halite minerals, possibly due to the prevailing atmospheric conditions. Iron titanium oxide ($FeTiO_3$), and franklinite ($ZnFe^{3+}{}_2O_4$) were

found at the RT site where electric arc furnace steelmaking processes are operating. Maghemite was found at the WH site where integrated BF-BOF steelmaking process is operating, and the surrounding soils also contain variety of iron minerals.

Table 6.2 shows the mineral content (in percentage) of size resolved atmospheric particles considering total crystalline materials found in the particles apart from the amorphous materials. For this, the mineral content (Table 6.2) represents the relative percentage among all minerals identified and quantified in a particular atmospheric particle sample. It is observed that the increasing percentage in the different size fraction of particles does not necessarily indicate the higher mineral mass. For example, hematite is found in S2 stage (26%), and S5 stage (79%) at the WH site, but the mass concentration of hematite might be higher in the S2 stage compared with S5 stage. The relative mineral content can be discussed and compared considering the total crystalline materials in each sample as 100% regardless of their mass concentration. Hence, careful consideration is necessary for reporting the mineral quantification especially for the size resolved atmospheric particles. Ohmsen (2004b) reported that air-fall dust at Whyalla Wall Street contains about 18–45 % hematite, however these values represent the percent hematite content in total crystalline materials where the mass of total crystalline materials is unknown. In this case, the lower percentage of mineral content may represent higher significance in terms of their implication and effect on human health and environment.

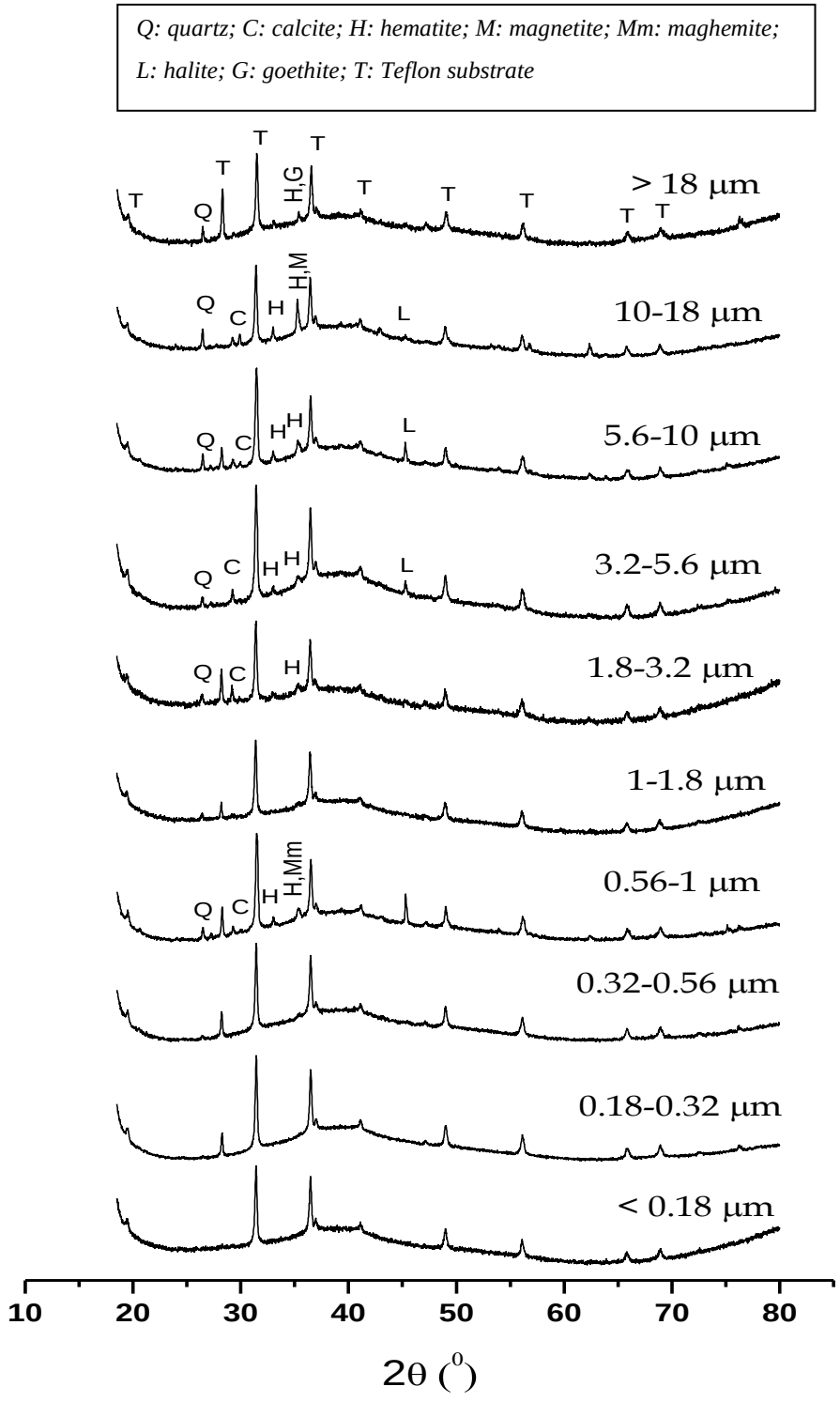

Figure 6.4 Typical XRD diffraction pattern of size resolved atmospheric particles at WH site

Table 6.2 Mineral content (%) as a function of total crystalline materials in size resolved atmospheric particles at CR, RT, WH, and MQ sites

Stage no	Particle Size, µm	Site	Quartz	Hematite	Calcite	Goethite	Halite	Iron titanium oxide	Franklinite	Magnetite	Maghemite
S0	>18	CR	80				20				
		RT	39	24	38						
		WH	21	76	1	2					
		MQ	9				91				
S1	10-18	CR	12	42	29		17				
		RT	39	32	28						
		WH	21	21	15		32			11	
		MQ	14		23		64				
S2	5.6-10	CR	10	21	33		36				
		RT	15		35			50			
		WH	16	26	29		30				
		MQ	15		13		72				
S3	3.2-5.6	CR	9	34	21	11	25				
		RT	15	17	28				40		
		WH	14	17	14		55				
		MQ	4		24		72				
S4	1.8-3.2	CR	10	53	13		24				
		RT	18	17	26				25	14	
		WH	14	16	21		49				
		MQ	9		29		63				
S5	1-1.8	CR	8	51	42						
		RT	20	57	2				21		
		WH	10	79	1						11
		MQ	43		58						
S6	0.56-1	CR	13	87							
		RT		92						2	
		WH	16								84
		MQ	54		46						
S7	0.32-0.56	CR		68	20	13					
		RT		99						1	
		WH	24								76
		MQ	nd								
S8	0.18-0.32	CR		58	26	16					
		RT		99						1	
		WH	nd								
		MQ	nd								
SP	<0.18	CR	nd								
		RT	nd								
		WH	nd								
		MQ	nd								

nd: not detected

The results of the XRD analysis of size resolved atmospheric particles (Table 6.2) showed the abundance of quartz, calcite, halite, and hematite minerals. Hematite was found the dominant mineral in the vicinity of iron and steelmaking sites at Cringila (CR), Rooty Hill (RT), and Whyalla (WH), whereas the background MQ site contributed from the quartz, calcite, and halite minerals most likely from the natural soil dust and sea spray. Apart from hematite minerals, considerable amount of iron minerals such as goethite, magnetite, iron titanium oxide, franklinite, and maghemite, were found nearby the steelmaking industrial sites, indicating the strong influence of iron and steelmaking processes on surrounding atmospheric particulate mineralogy.

At stages S0–S1 (>10 µm) halite (up to 91%) was found dominant at the background MQ site. Calcite (up to 38%) and quartz (up to 80%) minerals were found at all sampling sites. Fe-minerals of hematite (up to 76%), goethite (2%), and magnetite (11%) were dominant at the WH site, indicating the increasing amount of iron crystalline materials originating from raw materials handling. At stages S2-S4 (1.8-10 µm) the atmospheric particles contained both background and iron bearing minerals. These stages are particularly important as the dominant mass and elemental concentration occurred within these particle sizes at all sampling sites. The iron bearing minerals at RT site contained hematite (up to 17%), goethite (11%), iron titanium oxide (50%), franklinite (up to 40%), and magnetite (14%) minerals which shows the diverse crystalline materials originated from electric arc furnace (EAF) steelmaking processes compared with blast furnace-basic oxygen furnace (BF-BOF) steelmaking processes. Hematite was absent at the background MQ site, indicating the importance of distance between industries and receptor sites and how the surrounding atmospheric particles can be influenced by industrial processes at CR, RT, and WH sites. Halite (up to 72%), quartz (up to 16%), and calcite (up to 35%) minerals were found in these particle size range of 1.8 – 10µm at all sampling sites. At stages S5-S7 (0.32-1.8 µm) halite crystal phase was absent at all sampling sites. Fe-containing minerals at WH site constituted of hematite (up to 79%), and maghemite (up to 84%). The mass concentration in these particle sizes was found to be substantially lower compared to coarse particles. Among the crystalline materials, hematite (up to 99%) was found predominant at the RT site, whereas both hematite (up to 68%), and goethite (up to 16%) were found significant at the CR site. At stages S8-SP (< 0.32 µm) minerals are not detected in most samples, possibly due to the lower concentration of crystalline materials in these particle sizes.

The variation in the crystalline phases and their contents in industrial atmospheric particles could result from a number of factors, such as the distance between the industrial sources and receptor sites, prevailing atmospheric conditions including wind speed and direction, raw materials variation in EAF and BF-BOF steelmaking processes, processing variations, like pellet plants at WH site and sinter plant at CR site, the production and variability of emissions from iron and steelmaking point sources etc. The overall crystalline phases show that the dominant iron crystalline materials originate from both fugitive and point sources at CR, RT, and WH steelmaking sites. The fugitive emissions can be reduced significantly by introducing advanced dust free raw materials handling operations. The atmospheric iron particles were mixed in nature and originated from iron and steelmaking industries, soil dust and other sources. The amorphous iron content was not recognised in this study. Understanding the behaviour of Fe-nanocrystalline phases in atmospheric particles, which were mostly not detected in this study, generated from high temperature combustion processes in iron and steelmaking industries requires further attention to ensure the clean air quality, safe human health and environment.

6.6 Conclusions

Bonding structure and mineral content of atmospheric particles in the vicinity of Australian electric arc furnace and integrated steelmaking industries was investigated in this work, focusing on different size fractions from coarse to ultrafine particles. –OH, -CH, -NH, and –CO bonding was examined in the organic compounds in atmospheric particles at CR, RT, WH, and MQ sites, indicating the H-bonded alcohol, n-alkane, 2^0 amines, and conjugated ketone classes, respectively, occurred in organic compounds in atmospheric particles. The functional groups distribution were found variable between mass and bonding groups, among bonding groups, and among urban and industrial areas. These functional groups in organic compounds at CR, RT, and WH sites can be originated from iron and steelmaking industries and motor vehicle exhaust, whereas strong influence of organic functional groups at the urban background MQ site can be assigned to the local biogenic emissions. The –OH group was mostly associated with coarse particles, whereas –CH, -CO, and –NH groups were mostly associated with submicron particles, indicating strong influence of fine particle sources of combustion process, car exhaust, domestic wood burning and plants. Hematite mineral was found predominant in the vicinity of iron and steelmaking industries, which likely originates from the raw materials handling, and high temperature combustion processes, whereas the background minerals quartz,

calcite and halite, were found predominantly at the urban background site. The nanocrystalline iron minerals in ultrafine particles were not detected by the XRD analysis, likely due to the insufficient amount of crystalline materials present in the inorganic compounds of the ultrafine particles, which requires further investigation for comprehensive understanding of the atmospheric particle characterisation.

6.7 References

Alcock, R. E. Health risks of persistent organic pollutants from long-range transboundary air pollution. 2003. Joint WHO/Convention Task Force on the Health Aspects of Air Pollution.

Allen, D. T., Palen, E. J., Haimov, M. I., Hering, S. V. & Young, J. R. 1994. Fourier transform infrared spectroscopy of aerosol collected in a low pressure impactor (LPI/FTIR): method development and field calibration. *Aerosol Science and Technology,* 21**,** 325-342.

Braakhuis, H. M., Park, M. V., Gosens, I., De Jong, W. H. & Cassee, F. R. 2014. Physicochemical characteristics of nanomaterials that affect pulmonary inflammation. *Particle and fibre toxicology,* 11**,** 18.

Calvo, A., Alves, C., Castro, A., Pont, V., Vicente, A. & Fraile, R. 2013. Research on aerosol sources and chemical composition: Past, current and emerging issues. *Atmospheric Research,* 120**,** 1-28.

Coates, J. 2000. Interpretation of infrared spectra, a practical approach. *Encyclopedia of analytical chemistry*.

Cohen, D., Stelcer, E., Atanacio, A. & Crawford, J. 2014. The application of IBA techniques to air pollution source fingerprinting and source apportionment. *Nuclear Instruments and Methods in Physics Research Section B: Beam Interactions with Materials and Atoms,* 318**,** 113-118.

Coury, C. & Dillner, A. M. 2008. A method to quantify organic functional groups and inorganic compounds in ambient aerosols using attenuated total reflectance FTIR spectroscopy and multivariate chemometric techniques. *Atmospheric Environment,* 42**,** 5923-5932.

Coury, C. & Dillner, A. M. 2009. ATR-FTIR characterization of organic functional groups and inorganic ions in ambient aerosols at a rural site. *Atmospheric Environment,* 43**,** 940-948.

Cupr, P., Flegrová, Z., Franců, J., Landlová, L. & Klánová, J. 2013. Mineralogical, chemical and toxicological characterization of urban air particles. *Environment international,* 54**,** 26-34.

Dockery, D. W., Pope, C. A., Xu, X., Spengler, J. D., Ware, J. H., Fay, M. E., Ferris Jr, B. G. & Speizer, F. E. 1993. An association between air pollution and mortality in six US cities. *New England journal of medicine,* 329**,** 1753-1759.

Environment Protection Authority 2013. Managing particles and improving air quality in NSW. EPA NSW, Sydney.

Ghauch, A., Deveau, P.-A., Jacob, V. & Baussand, P. 2006. Use of FTIR spectroscopy coupled with ATR for the determination of atmospheric compounds. *Talanta,* 68**,** 1294-1302.

Hibberd, M., Selleck, P., Keywood, M., Cohen, D., Stelcer, E. & Atanacio, A. 2013. Upper Hunter Particle Characterisation Study: Final report. CSIRO, Australia.

Hleis, D., Fernández-Olmo, I., Ledoux, F., Kfoury, A., Courcot, L., Desmonts, T. & Courcot, D. 2013. Chemical profile identification of fugitive and confined particle emissions from an integrated iron and steelmaking plant. *Journal of Hazardous Materials*.

Karlson, L., Greene, R., Scott, K., Stelcer, E. & O'loingsigh, T. 2014. Characteristics of aeolian dust across northwest Australia. *Aeolian Research,* 12**,** 41-46.

Kavouras, I. G., Lawrence, J., Koutrakis, P., Stephanou, E. G. & Oyola, P. 1999. Measurement of particulate aliphatic and polynuclear aromatic hydrocarbons in Santiago de Chile: source reconciliation and evaluation of sampling artifacts. *Atmospheric Environment,* 33**,** 4977-4986.

Lu, S., Luan, Q., Jiao, Z., Wu, M., Li, Z., Shao, L. & Wang, F. 2007. Mineralogy of inhalable particulate matter (PM10) in the atmosphere of Beijing, China. *Water, air, and soil pollution,* 186**,** 129-137.

Maria, S. F., Russell, L. M., Turpin, B. J. & Porcja, R. J. 2002. FTIR measurements of functional groups and organic mass in aerosol samples over the Caribbean. *Atmospheric Environment,* 36**,** 5185-5196.

Mohiuddin, K., Strezov, V., Nelson, P. & Stelcer, E. 2014a. Characterisation of trace metals in atmospheric particles in the vicinity of iron and steelmaking industries in Australia. *Atmospheric Environment,* 83**,** 72-79.

Mohiuddin, K., Strezov, V., Nelson, P. F., Stelcer, E. & Evans, T. 2014b. Mass and elemental distributions of atmospheric particles nearby blast furnace and electric arc furnace operated industrial areas in Australia. *Science of The Total Environment,* 487**,** 323-334.

Ohmsen, G. 2004a. Characterisation and Source Apportionment of Air-Fall Dusts, Whyalla. Department of Health, South Australia.

Ohmsen, G. 2004b. Quantitative X-Ray Diffraction and Chemical Analysis of TSP and PM10 Filters collected from Hummock Hill, Walls Street and Civic Park, Wyalla. Department of Health, South Australia.

Radhi, M., Box, M., Box, G., Mitchell, R., Cohen, D., Stelcer, E. & Keywood, M. 2010. Size-resolved mass and chemical properties of dust aerosols from Australia's Lake Eyre Basin. *Atmospheric Environment,* 44**,** 3519-3528.

Reynolds, R. L., Cattle, S. R., Moskowitz, B. M., Goldstein, H. L., Yauk, K., Flagg, C. B., Berquó, T. S., Kokaly, R. F., Morman, S. & Breit, G. N. 2014. Iron oxide minerals in dust of the Red Dawn event in eastern Australia, September 2009. *Aeolian Research*.

Roos, G. 1997. *Organic Chemical Concepts*, Harcourt Brace & Company, Marrickville, NSW.

Schauer, J. J. & Cass, G. R. 2000. Source apportionment of wintertime gas-phase and particle-phase air pollutants using organic compounds as tracers. *Environmental Science & Technology,* 34**,** 1821-1832.

Shah, P. S. & Balkhair, T. 2011. Air pollution and birth outcomes: a systematic review. *Environment international,* 37**,** 498-516.

Xie, M., Wang, G., Hu, S., Han, Q., Xu, Y. & Gao, Z. 2009. Aliphatic alkanes and polycyclic aromatic hydrocarbons in atmospheric PM10 aerosols from Baoji, China: Implications for coal burning. *Atmospheric Research,* 93**,** 840-848.

Chapter 7

Speciation of size resolved iron containing particles in proximity of Australian steelmaking industries

Preface

This chapter describes morphology of iron containing particles, oxidation states of iron, and dispersion analysis of iron containing particles collected from Australian urban and industrial areas. The analysis of wind directions and back trajectories during sampling campaign are also presented in this chapter. It refers to the thesis objective [A6] and the 'prepared for publication' article [P2] titled as "Speciation of size resolved iron containing particles in proximity of Australian iron and steelmaking industries using K-edge XANES techniques".

7.1 Introduction

Atmospheric particles generated from industrial have negative effect on air quality, human health, and the environment. This effect largely depends on the concentration, size, shape and chemistry of the atmospheric particles. Previous studies in Australia have associated particles with a range of environmental and health effects, including increased premature mortality rates (Morgan et al., 1998a), increased hospital admissions due to chronic obstructive pulmonary disease and heart disease in elderly (Morgan et al., 1998b), and increased chest colds and night coughs in children (Lewis et al., 1998).

Iron and steel processing industry is one of the significant emitters of particles to the surrounding atmosphere. Of particular concern with the particles emitted from these industries is emission of heavy metals as they have known respiratory effects, and, in some cases, are known carcinogens (Andjelkovich et al., 1992). Querol et al. (2007) stated that iron and steel industries generate high concentrations of Fe, As, Cr, Cd, Ni, Pb, Mn, Zn, Mo, Se and Sc. The inhalation of iron dust has been linked with chronic bronchitis, breathlessness, chronic cough (Xu et al., 1992), chronic phlegm (Chen et al., 2006) and reduced lung function (Banks et al., 1999), and can lead to chronic obstructive pulmonary disease (Driscoll et al., 2005). Previous studies on chemical properties of atmospheric particles provided relationship between various metal fractions in particles with the associated industrial processes (Querol et al., 2004; Garimella and Deo, 2008).

Iron is one of the major trace metals emitted by the iron and steelmaking industries. It is expected that the concentration of iron in atmospheric particles in proximity to these industries would be substantial and would have significant effect on the surrounding air quality through dispersion and settling processes. Toxicity of iron in atmospheric particles has been identified to be closely related to its soluble fraction, which depends on the chemical speciation form of iron (Oakes et al., 2012). Chemical speciation of iron also may provide indication of its source of emission and potentially the process that contributes to its atmospheric emissions. The major limitation in the current state of knowledge is the lack of information on the types of iron species that are present in the atmospheric particles in vicinity of iron and steelmaking operations.

This study was focused on first stage speciation of iron to identify the iron oxidation states in size-resolved atmospheric particles collected in the vicinity of Australian iron and steelmaking industries. The synchrotron based X-ray emission near edge structure (XANES) technique was used for the speciation of iron. The morphology of iron containing particles is also analysed using scanning electron microscopy coupled with energy dispersive spectrometer (SEM-EDS) along with the windrose, backward trajectories, and dispersion analysis to facilitate this iron speciation study and their implications. The findings on iron speciation database coupled with atmospheric conditions can be incorporated into speciation-based exposure and risk assessment modelling of atmospheric particles.

7.2 Materials and methods

7.2.1 Sampling locations

Four sampling sites were selected in this study, which were Macquarie Park (MQ) site in New South Wales (NSW), Rooty Hill (RT) site in NSW, Cringila (CR) site in NSW and Whyalla (WH) site in South Australia (SA). Macquarie Park (MQ) site was selected near to the sports field of Macquarie University as a background site, because of its far distance (>10 km) from any major industrial activity. Three other sites were selected nearby (≤ 1.5 km) to the Australian iron and steelmaking industries. The CR and WH sites were located in the downwind of integrated iron and steel processing industries. The processing route of these industries is blast furnace–basic oxygen furnace (BF–BOF) steelmaking, with an exception of pellet plant at WH site instead of sinter plant at CR site. Rooty Hill (RT) site was located in close proximity (500 m) of the steel industry, having electric arc furnace (EAF) process route. The location of the sampling sites were: Macquarie Park site, NSW

(latitude 33^0 45′ 55.1″ S, longitude 151^0 7′ 3.2″ E, elevation 66.8 m); Rooty Hill site, NSW (33° 45' 59.6" S, 150° 50' 53.8" E, 40.75 m); Cringila site, NSW (34° 28' 12.5" S, 150° 52' 22.2" E, 25.24 m) and Whyalla site, SA (33° 2' 9.97" S, 137° 35' 9.9" E, 21.3 m). The CR and WH sites were categorised as urban-industrial type, RT site as an industrial type and MQ site as an urban-background site.

7.2.2 Sampling equipment

An eight staged Micro Orifice Uniform Deposit Impactor (MOUDI; M100-R, MSP Corporation) (Marple et al., 1991) was deployed to collect the atmospheric particles from all sampling sites for the period from April 2011 to November 2011. Operational parameters, including the cut-off and nozzle diameter, of MOUDI stages are presented in Table 7.1. Teflon filters (PTFE membrane, 47 mm diameter, Pall Corporation), with particle collection efficiency of 99%, were used as substrate materials at all stages of the MOUDI sampler. These stretched-type PTFE membrane filters, having supporting rings attached to clutch, provide additional adhesion to the atmospheric particles and reduce the particle bouncing effect compared to non-stretched type membrane filters. Four to seven sample sets (10 samples per set) were collected from all sampling sites for at least 24 hrs particles loading on Teflon substrate.

Table 7.1 Operational parameters of the MOUDI sampler (Marple et al., 1991)

Stage	**Nominal cut-off dia[a], µm**	**Particle size range, µm**	**Nozzle diameter, cm**	**No of nozzles**	**S/W[b]**	**P/P_0[c]**
Inlet, S0	18	>18	1.71	1	0.75	1.0
S1	10	10-18	0.889	3	0.5	1.0
S2	5.6	5.6-10	0.380	10	1.0	1.0
S3	3.2	3.2-5.6	0.247	10	1.0	1.0
S4	1.8	1.8-3.2	0.137	20	1.0	1.0
S5	1.0	1-1.8	0.072	40	1.0	0.99
S6	0.56	0.56-1	0.040	80	1.5	0.97
S7	0.32	0.32-0.56	0.0140	900	4.1	0.95
S8	0.18	0.18-0.32	0.0090	900	6.4	0.89
Exit, SP	0	<0.18	NA	NA	NA	NA

[a]Based on flow rate of 30 L/min which was maintained in this study;
[b]S: distance from impact jet to stage plate; W: nozzle diameter;
[c]P: pressure at exit stage; P_0: pressure at inlet stage;

7.2.3 Windrose and back trajectory analysis

Windrose was constructed by the software Windrose-NOAA (Rolph, 2013), using wind speed and wind direction data during sampling campaign at all sampling sites. Wind speed was categorised in seven types from calm (<1 m/s) to strong (>21 m/s), whereas wind direction was in 16 categories (such as N, NNE, NE, ENE, E, ESE, SE, SSE, S, SSW, SW, WSW, W, WNW, NW, and NNW). Backward air-mass trajectories were constructed at all sampling sites during sampling campaign using the NOAA HYSPLIT model (Draxler and Rolph, 2013). The model vertical velocity method was used to calculate the vertical motion. Three vertical levels of 200 m, 500 m, and 1000 m were considered to determine the trajectory plots. The aerial distances of the trajectories from sampling sites were considered to indicate the long range particle transport behaviour. The relative humidity and their variation at different levels during sample collection were also presented, which will provide the indication of wet deposition along with each trajectory.

7.2.4 PIXE analysis

The Teflon substrates were weighed before and after the particle sample collection using Mettler Toledo MX5 microbalance (accuracy ±1 µg) to measure the particle loading in each filter. Ion Beam Analysis (IBA) was performed using Proton Induced X-ray Emission (PIXE) technique (Johansson and Johansson, 1976; Cohen, 1993). The IBA was carried out with 22 mm diameter proton beam of 2.6 MeV energy and 10-15 nA target current. PIXE technique was used to quantify the Fe concentration in the collected atmospheric particles prior to their speciation study (Mohiuddin et al., 2014a; Mohiuddin et al., 2014b).

7.2.5 SEM-EDS analysis

The surface morphology (size, texture, and shape) and relative elemental composition (except C and F) of iron containing atmospheric particles were determined using scanning electron microscope (SEM: JEOL JSM-6480 LA) coupled with energy-dispersive spectrometer (EDS: EX-23000 BU). Atmospheric particles deposited on stretched Teflon filters were coated with a thin carbon film using the carbon coater (Quorum Q150T coater). Coated samples were analysed by SEM-EDS technique using an accelerating voltage of 15 kV in low-vacuum compartment for achieving the non-conductive behaviour of particles. The surface morphology was observed and photographed by SEM, and its relative elemental composition was analysed by EDS.

7.2.6 *XANES analysis*

Iron speciation was performed qualitatively using the X-ray absorption spectroscopy (XAS) technique at the Australian Synchrotron facility. The Australian Synchrotron XAS is a 3 GeV ring synchrotron facility with 1.9T wiggler source and a Si (111) double-crystal monochromator with the energy resolution of 1.5×10^{-4} ($\Delta E/E$). Four calibration standards, such as Fe(II) oxide, Fe(III) oxide, Fe(II) sulphide and Fe(II) hydroxide, were prepared and artificially loaded to the MOUDI filters. Sections of the artificially loaded MOUDI filters and filters from selected stages analysed for the iron content using PIXE analyser were prepared and loaded to the synchrotron holders. In the XAS technique, incident X-rays of sufficient energy bombard atoms, ejecting the electrons from an electron shell emitting a characteristic fluorescence signal which are collected as raw data against each element of the multi-element detector. In this study the incident X-ray energy was varied from 7000 to 7100 eV in 3 eV increments, from 7100 to 7160 eV in 0.3 eV increments and then from 7160 to 7400 eV gradually increasing from 1 to 2.4 eV increments. The energy spectra were subjected to smoothing and normalisation using the ATHENA software. Normalisation of the spectra is required in order to avoid mathematical discrepancies caused by directly dividing the fluorescence signal of incident X-ray beam by the signal in the upstream ionization chamber (Oakes et al., 2012). The critical step in normalisation is selecting appropriate pre-edge (region before Edge energy value, E0) and post-edge (region after E0 value).

7.2.7 *Particle dispersion analysis*

The dispersion of particles was analysed using Hybrid Single Particle Lagrangian Integrated Trajectory (HYSPLIT) particle dispersion model (Draxler and Hess, 1998; Draxler and Rolph, 2013) considering particle emission from point source at Whyalla steelworks during the sampling campaign. HYSPLIT, a dynamic simulation model has the capability of applying highest frequency of input atmospheric data and offers 1 min simulation step, which is required for particle dispersion modelling. The HYSPLIT particle dispersion model was widely used for dispersion modelling (Chen et al., 2013; Connen et al., 2013; Mcgowan et al., 2008) and the HYSPLIT particle dispersion model has been validated elsewhere (Wang et al. 2008, 2009a, 2009b). The particle dispersion takes into account the following assumptions: (i) in case of the puff model, the puffs expand and then split into several new puffs by sharing the mass when they reached the maximum size of the meteorological grid cell in horizontal or vertical direction, and (ii) in

case of the particle model, particles are advected by the mean wind field and spread by turbulent component, and 3-dimensional particle distribution is configured as default (Draxler and Hess, 1998). The model does not consider the effect of chemical reactions, dense gases, varying emission rate, and release of non-naturally buoyant materials. The model output provides particle hotspots and their concentration along with particle deposition.

7.3 Results and Discussion

7.3.1 Wind direction and back-trajectories analysis

Figure 7.1(a-d) shows the windrose plots at Cringila (CR), Rooty Hill (RT), Whyalla (WH), and Macquarie Park (MQ) site. Windrose at CR site presented that about 30% wind with a speed of 3-6 m/s occurred at N and NNE direction (Figure 7.1) where integrated BF-BOF steelmaking industry is situated. The wind at RT site was predominantly from the west direction (Figure 7.1), whereas the steelmaking point source is located in east direction, however, the fugitive emissions could affect the particle loading as the distance between the receptor site and fugitive emission sources is very close (about 50 m). At WH site, the wind was from N (6%) and NNE (18%) direction (Figure 1).

Figure 7.2 (a-d) shows the backward air-mass trajectories during the sampling campaign at CR, RT, WH, and MQ sites. The pathway of back trajectory at CR site can originate from the ocean followed by the Brisbane urban areas, farming areas, and regional areas in NSW to the Cringila receptor site. CR site is located in a coastal area, however, in this case the long range transport particles could originate from the inland areas up to 1000 km north of Sydney, indicating the strong influence of atmospheric conditions on particle loading. The trajectory at the RT site is from SW direction following the coastal areas with a distance travelled more than 400 km. The trajectory at the WH site can be followed about 900 km in NW direction through the desert, regional areas, and ocean, which could possibly contribute to the long range transport particles loading. Air-mass trajectories at the MQ site showed the spiral type trajectory at different levels of 200 m, 500 m and 1000 m, among which one circular trajectory occurred at 500 m level where the particles could originate from Sydney basin and travel about 600 km before returning to Sydney basin again. Trajectories at 200 m, and 1000 m levels could follow the inland pathway, which includes regional areas, farming land, and deserts. The relative humidity along with the trajectories showed the influence of wet deposition during loading of the long range transport particles. The wet deposition occurred at the MQ site where significant rain

episodes occurred during the sampling campaign, indicating the wet deposition of mostly coarser particles (Figure 7.3) and the accumulation of finer particles during the particle loading.

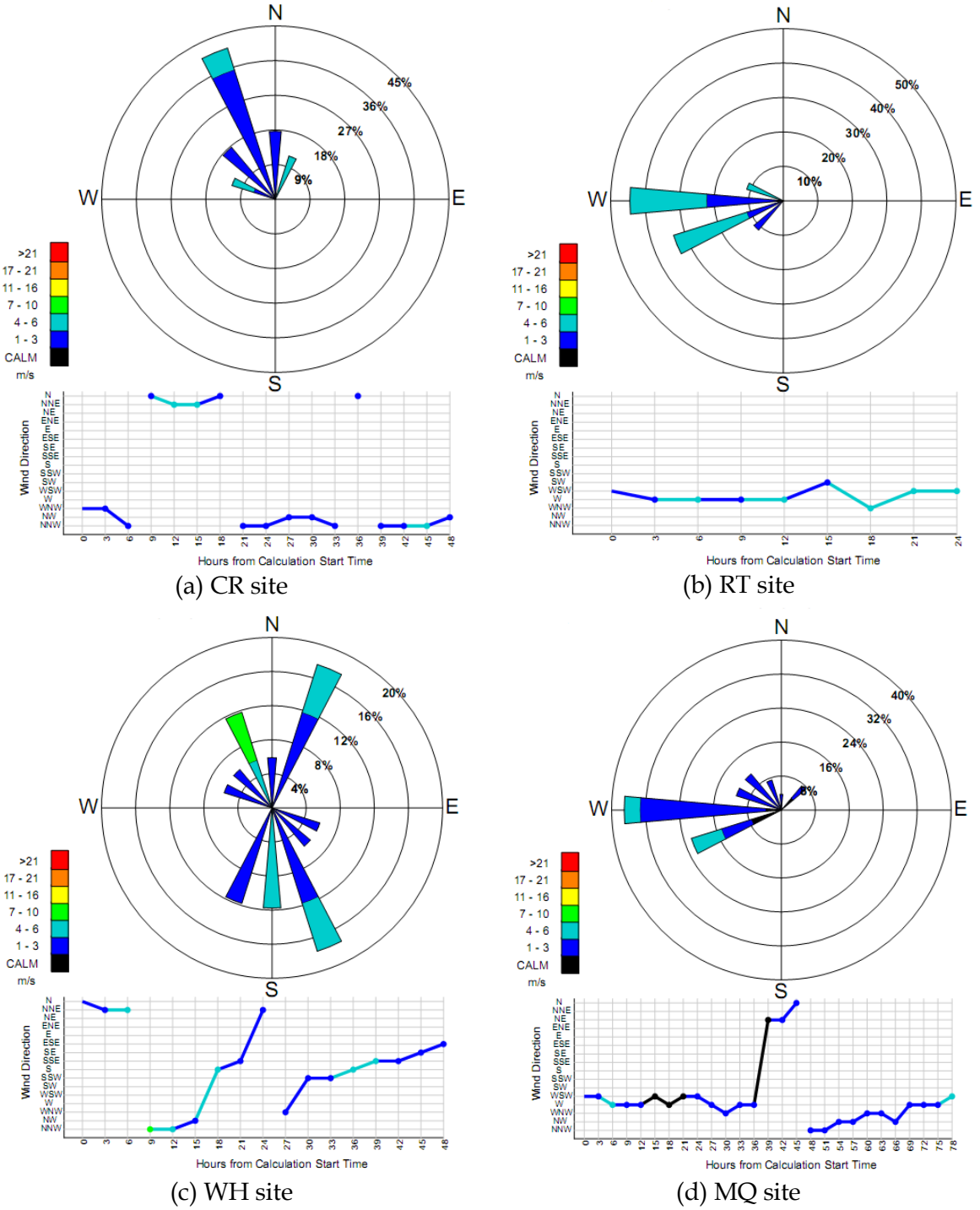

Figure 7.1(a-d) Windrose plots during sampling campaign at CR site (03 Aug 11, ending after 48 hrs), RT site (18 Jul 11, ending after 24 hrs), WH site (04 Nov 11, ending after 46 hrs), and MQ site (23 Jun 11, ending after 78 hrs); for the samples subjected to iron speciation study.

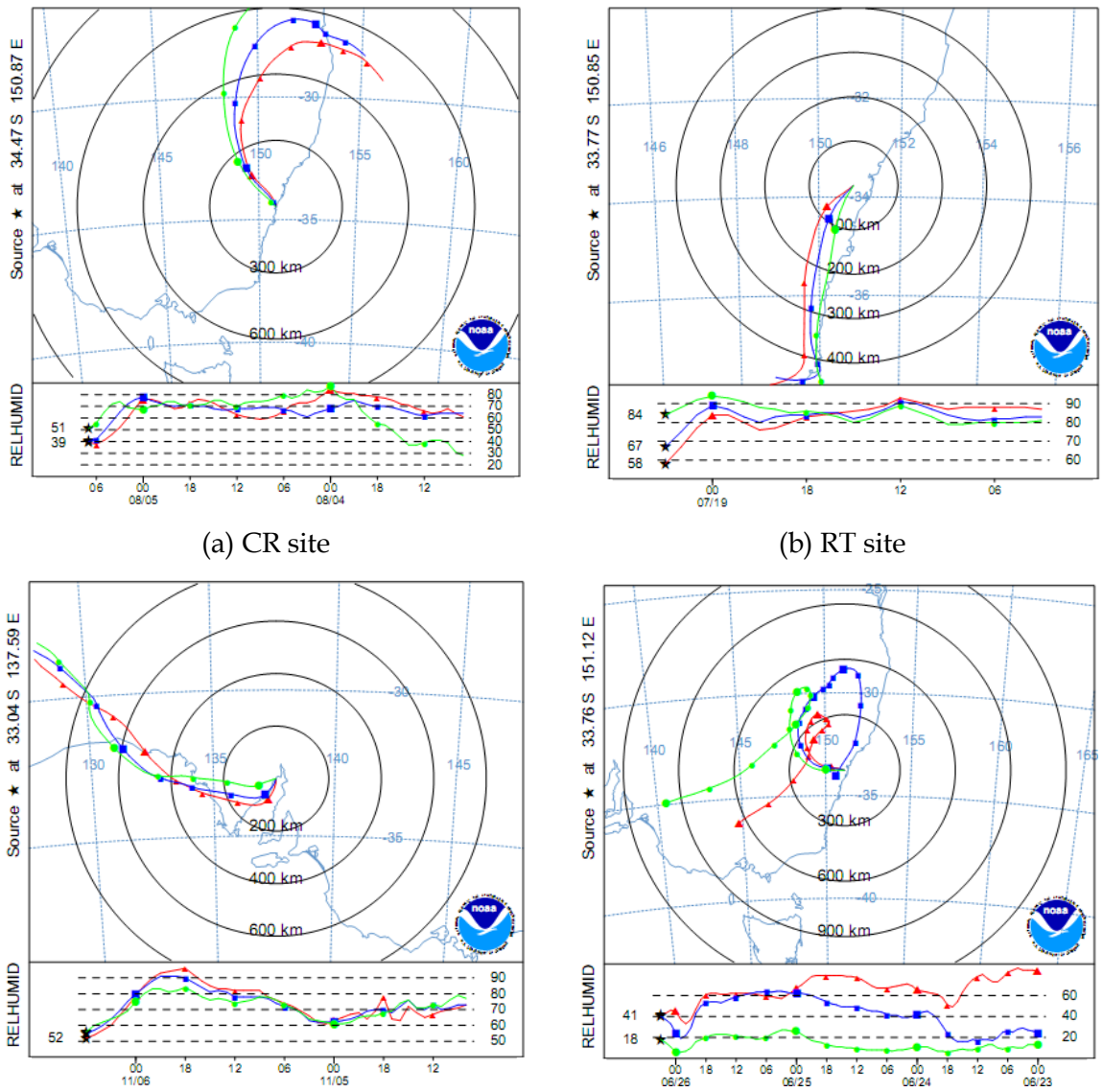

(a) CR site (b) RT site

(c) WH site (d) MQ site

Figure 7.2(a-d) Backward air-mass trajectories ending at level height of 200 m (red-colored line), 500 m (blue-colored line), and 1000 m (green-colored line) during sampling campaign at CR site (03 Aug 11, ending after 48 hrs), RT site (18 Jul 11, ending after 24 hrs), WH site (04 Nov 11, ending after 46 hrs), and MQ site (23 Jun 11, ending after 75 hrs), including the variation in relative humidity and relative distances of trajectories

7.3.2 Mass and iron concentration in atmospheric particles

Figure 7.3 shows the mass and iron concentration in atmospheric particles at all sampling sites analysed by PIXE technique. In case of the Cringila (CR) and Whyalla (WH) sampling sites nearby to the blast furnace and basic oxygen furnace operated facilities, the largest concentration of iron was detected in the coarse particles size ranges of 3.2 – 10 µm collected with the sampling stages 1 to 3. The increasing amount of iron concentration at Rooty Hill (RT) site was found in all particle size fractions, including the submicron (<1.0 µm) and ultrafine particles (<0.18 µm). The iron concentration in atmospheric particles

was found the lowest at the urban background MQ site. Particles collected in proximity to the iron and steelmaking plants (RT, CR and WH sites) showed larger mass concentration for the coarser and finer particle size ranges collected with stages 1 to 4, compared with ultrafine particles collected on stages 5 to SP, however the trend between the mass and iron concentration along with the particle size range was not apparent at the MQ site.

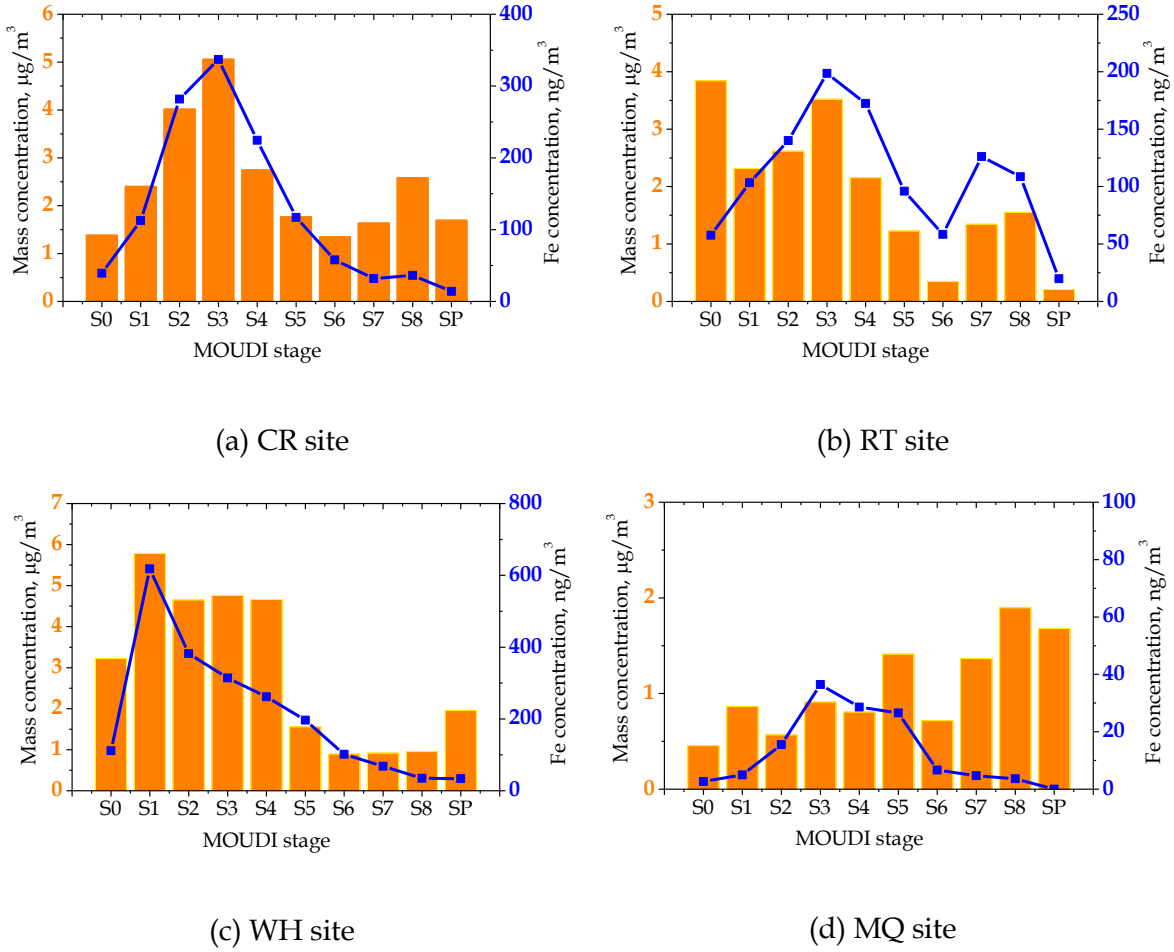

Figure 7.3(a-d) Mass (bar diagram: orange colored), and Iron (line graph: blue colored) concentration at each MOUDI stage in all sampling sites

7.3.3 Morphology of iron containing particles

Figure 7.4 shows the morphology and relative composition of iron containing particles collected from industrial sites at CR, RT, and WH sites. The brighter colour indicates the influence of back scattered spectroscopy on heavy metals, such as iron, compared to other light elements. Iron was found highly dominant fraction in the iron rich particles, indicating the likely direct influence of emissions from iron and steelmaking industries. The round shape particles in coarse and fine size fractions were found at all industrial sites (Figure 7.4c,h). Cracked and fractured particles were observed in the SEM images with high of iron content, possibly generated from high temperature processing activities.

Iron was found associated with Mn, Zn, Ca, and S confirming the particles contribution from iron and steelmaking industries at CR, RT, and WH sites. Cr was also found associated with iron in atmospheric particles, indicating the importance of toxicity assessment of iron containing particles in proximity of the iron and steelmaking industries in Australia.

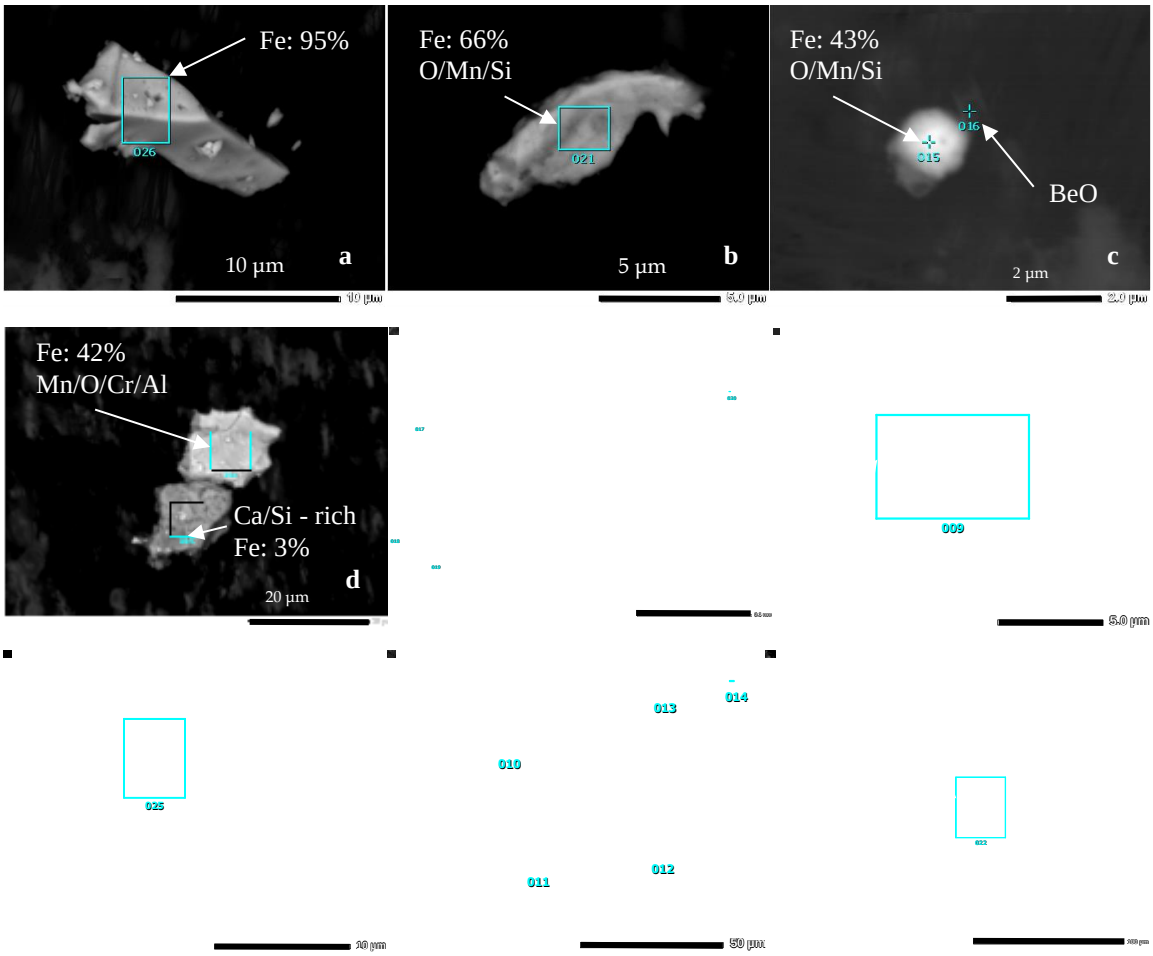

Figure 7.4(a-i) Morphology of iron containing particles identified by SEM-EDS at industrial CR, RT, and WH sites

7.3.4 Iron speciation

Figure 7.5 shows the normalised XANES spectra for iron based standards. By analysing the XANES spectra of the iron standards it was found that E0 for Fe(II) oxidation state is 7117 eV, while for Fe(III) it is 7127 eV. The edge energy (E0) value is the maximum value of the first derivative curve of the XANES spectrum. Shifting of E0 was associated with the oxidation state of elements under investigation. This makes XANES suitable as a qualitative or a semi-quantitative method for elemental speciation. Hence the Fe(II) and Fe(III) E0 values can be used to qualitatively understand Fe speciation in filters collected at each sampling site.

XANES spectra for the filters collected at the MQ, RT, CR and WH sites, and previously subjected to PIXE analysis, are presented in Figure 7.6. A table was then developed to tabulate E0 values of each sample collected from each sampling site, and performed spectra interpretation with respect to the speciation of iron (Table 7.2). The signal to noise (S/N) ratio for the XANES spectrum of each particle sample was proportional to the Fe concentration. As shown in Table 7.2, Fe speciation on the substrates with 'SP' size fraction (ie. particle size range with less than 0.18 μm in diameter) at all sampling sites was not possible to determine, possibly due to their inadequate iron content resulting in poor signal to noise (S/N) ratio.

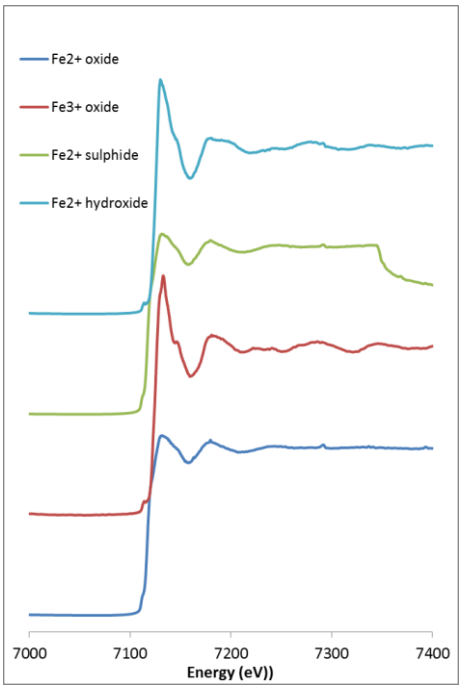

Figure 7.5 Fe K-edge XANES spectra for the set of calibration standards applied in this study

At RT site, iron was found mainly in Fe(III) oxide form in all substrates of atmospheric particles (Table 7.2), where the nearby-steel industry is equipped with electric arc furnace. The likely sources of iron emissions at RT site are direct emissions from the furnace and other processing equipment and/or fugitive dust from materials handling and stockpiles on site.

For Cringila (CR) samples, particles collected with the MOUDI stages 2, 5 and 7 indicate the presence of a mixture of Fe(II) and Fe(III) forms. Particles collected with the sampling stage 7 were in ultrafine size range and therefore their likely source might be fumes from

furnace exhaust. Iron in particles from filters collected with the sampling stages 3, 4, 6 and 8 indicate the iron is present only in Fe(III) form. For Whyalla (WH) samples, filters collected with the sampling stages 1, 2 and 5 indicate the presence of both Fe(II) and Fe(III) iron phases, while for the other stages Fe(III) was the dominant form of iron.

The samples collected from CR and WH sites were similar in qualitative iron speciation, as these two sampling sites were located downstream of iron and steel processing industries equipped with BF-BOF processing route. The likely sources of iron emissions at both Cringila and Whyalla sites are: (i) emissions from blast furnace and other iron processing equipment, (ii) fugitive dust from stockpiles of iron ores stored on site, (iii) fugitive emissions from material handling, and (iv) short and long range transport particles based on atmospheric conditions during the sampling campaign. The Fe(III) form appears significant, may be due to the prevailing hematite minerals in the atmospheric particles, shown in Chapter 6.

Mixture of both Fe(II) and Fe(III) forms in atmospheric particles was found at the MQ site, which could be categorised as a typical urban environment. The iron concentration in atmospheric particles at the urban background MQ site was also found significantly lower compared with industrial CR, RT and WH sites (Figure 7.3). In the absence of any major industrial source, the iron containing atmospheric particles at MQ site can be originated from both soil dust, and long range transport particles.

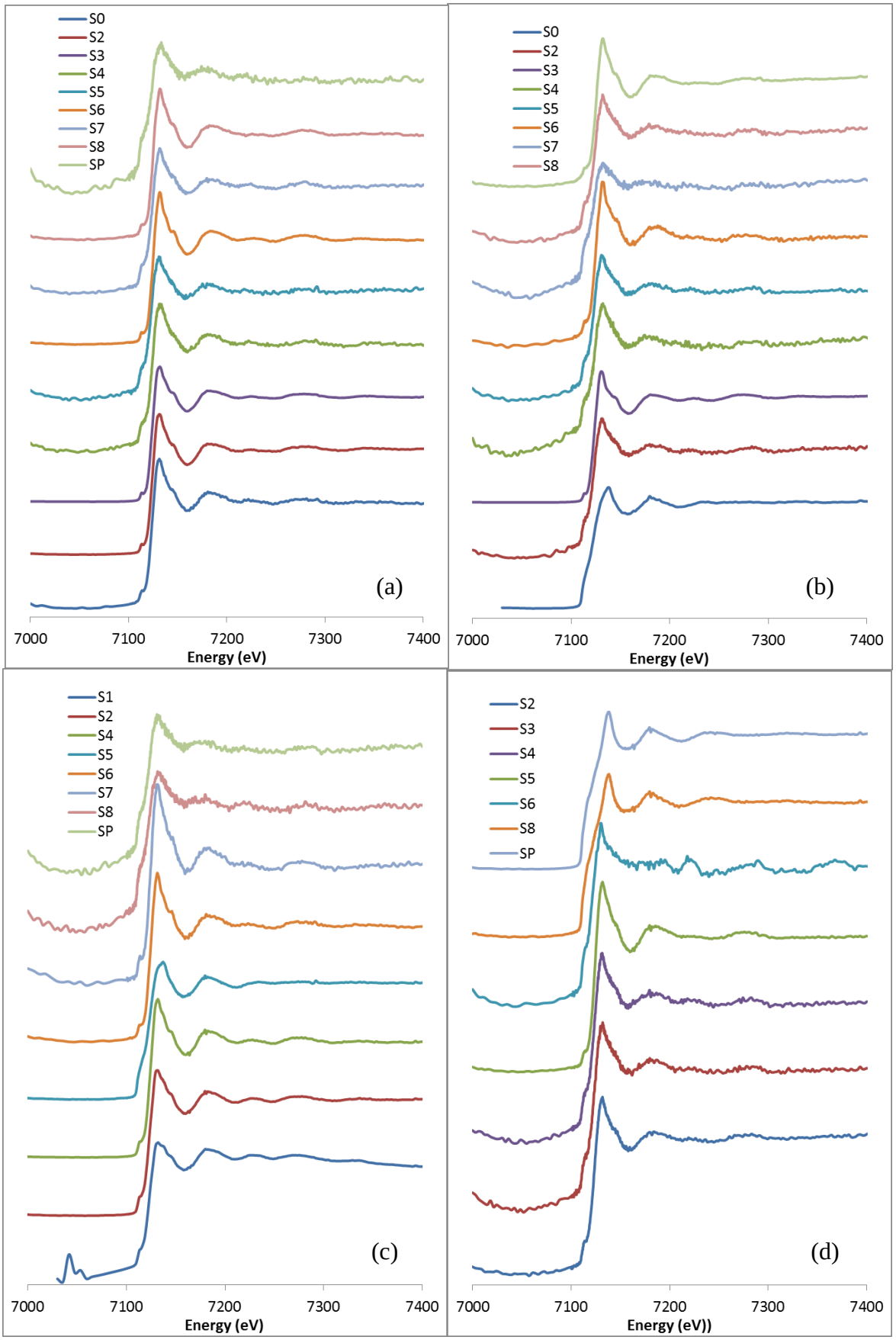

Figure 7.6 Fe K-edge XANES spectra for samples located at sites: (a).Cringila (CR); (b) Rooty Hill (RT); (c) Whyalla (WH); and (d) Macquarie Park (MQ)

Table 7.2 Qualitative speciation of XANES data

Sample Location	Sample stage	Particle size range, μm	E_0 value from XANES data	Qualitative Fe speciation		
				Fe(II)	Fe(III)	Note
CR	S2	5.6-10	7124	✓	✓	
	S3	3.2-5.6	7126		✓	
	S4	1.8-3.2	7124		✓	
	S5	1-1.8	7120	✓	✓	
	S6	0.56-1	7125		✓	
	S7	0.32-0.56	7124	✓	✓	
	S8	0.18-0.32	7125		✓	
	SP	<0.18	7110	NA	NA	Poor S/N
RT	S2	5.6-10	7124		✓	
	S3	3.2-5.6	7127		✓	
	S4	1.8-3.2	7124		✓	
	S5	1-1.8	7125		✓	
	S6	0.56-1	7126		✓	
	S7	0.32-0.56	7111	NA	NA	Poor S/N
	S8	0.18-0.32	7125		✓	
	SP	<0.18	7126		✓	
WH	S1	10-18	7122	✓	✓	
	S2	5.6-10	7123	✓	✓	
	S4	1.8-3.2	7127		✓	
	S5	1-1.8	7125	✓	✓	
	S6	0.56-1	7126		✓	
	S7	0.32-0.56	7126		✓	
	S8	0.18-0.32	7111	NA	NA	Poor S/N
	SP	<0.18	7111	NA	NA	Poor S/N
MQ	S2	5.6-10	7123	✓	✓	
	S3	3.2-5.6	7124	✓	✓	
	S4	1.8-3.2	7127		✓	
	S6	0.56-1	7125		✓	
	S8	0.18-0.32	7110	NA	NA	Poor S/N
	SP	<0.18	7110	NA	NA	Poor S/N

S/N = signal to noise ratio

7.3.5 *Dispersion of particles from steelmaking industries*

Figure 7.7 shows the average concentration, average deposition, and position with cross-section of iron containing particles at WH site using the particle dispersion HYSPLIT model. The atmospheric condition was found as strong influencing parameter for particle dispersion, concentration, deposition, long range transport behaviour, and the ultimate fate of particles generated from iron and steelmaking industries. The 'hotspots' (maximum concentration in particles in respect to the mass of toxic metals) of particles can be formed, moved and shifted depending on the meteorological conditions during the sampling campaign. In this model, the iron bearing particles from Whyalla steelworks were dispersed mostly in the SE direction and could travel thousand kilometres within couple of days. The particles can

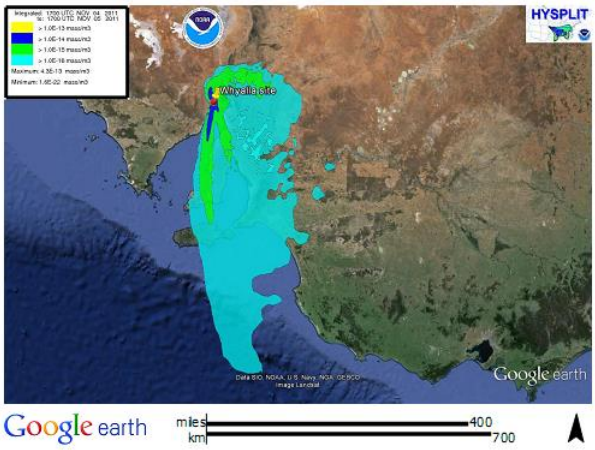

(a) Average Particle concentration, mass/m²

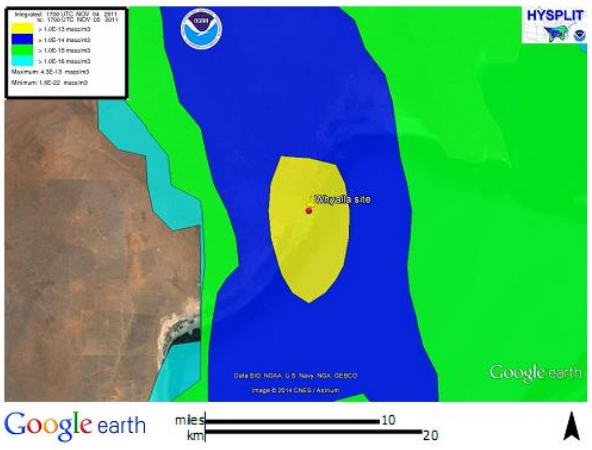

(b) 'Hotspot' of iron containing particles

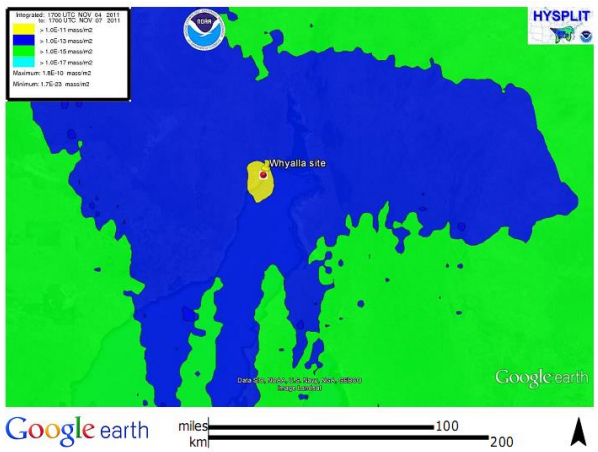

(c) Particle deposition concentraion, mass/m²

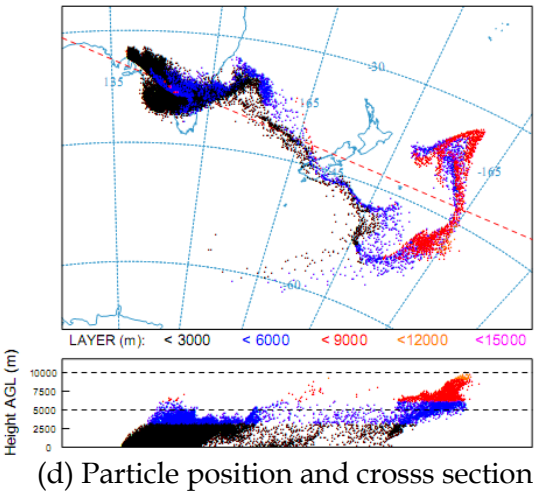

(d) Particle position and crosss section

Figure 7.7 Dispersion and concentration of iron containing particles releasing from Whyalla steelworks during sampling campaign starting on 4 Nov 11, considering single point source and 1 unit mass of iron containing particles

reach up to 10,000 m levels and travel over to New Zealand, however the impact of particles around 5 km region of the WH sampling site is significantly higher as the 'hotspots' (Figure 7.7b,c: yellow coloured zone) occurred in this region considering the maximum concentration and deposition of iron containing particles. In case of Cringila and Rooty Hill sampling sites the hotspots were also found nearby the iron and steelmaking industries, shown in respective appendices.

This study concludes with strong focus on the 'hotspots' of particles in the vicinity of iron and steelmaking industries as the exposure of iron and other toxic metals is significantly higher, (Mohiuddin et al., 2014a; Mohiuddin et al., 2014b) in the 'hotspots' compared to other urban areas such as MQ site. There is no existing separate regulatory measures for these 'hotspots' of particles nearby iron and steelmaking industries, resulting in none/inadequate monitoring of toxic metals, and none/inadequate information sharing to the residents in real-time about the particle exposure and toxicity risks. It is worth mentioning that currently the residents of NSW are informed in real-time (updated hourly) about the air quality in NSW using the air quality index (AQI) method. However, this AQI of atmospheric particles in NSW is calculated only based on particle mass, and excludes the importance of particle chemistry.

7.4 Conclusions

The iron speciation study was performed on size resolved atmospheric particles collected in the vicinity of three Australian iron and steel processing industries and at one background urban site. The iron concentration in these particles was found decreasing with size, for the particles collected near ironmaking sites operated with BF-BOF processing plant, while for the electric arc furnace operated site the iron was also present in the submicron particles at substantial quantities.

The iron in the particles collected nearby the steelmaking site equipped with electric arc furnace (RT site) indicated dominant Fe(III) oxide iron phases in all particle size fractions. The atmospheric particles collected near two integrated iron and steelmaking facilities (CR and WH sites) operated by the blast furnace route, had similar iron phase speciation with presence of both Fe(II) and Fe(III) iron phases in the coarse and fine particle size ranges, while for the ultrafine size range of particles, Fe(III) was the dominant form of iron. Comparing to Fe(II), Fe(III) has slightly higher toxicological effects with lower LD_{50} value, and is non-flammable form of iron (TOXNET, 2013). The morphology of iron

containing particles indicates the association of toxic metals with iron. These particles can form local hotspots within 5 km distance from the iron and steelmaking industries, which indicates research priorities to identify all hotspots, assess the risk, and take necessary measures to protect the air quality, human health, and environment.

7.5 References

Andjelkovich, D. A., Mathew, R. M., Rong, C. Y., Richardson, R. B. & Levine, R. J. 1992. Mortality of iron foundry workers: II. Analysis by work area. *Journal of Occupational and Environmental Medicine,* 34**,** 391-401.

Banks, D. E., Shah, A. A., Lopez, M. & Wang, M.-L. 1999. Chest illnesses and the decline of FEV1 in steelworkers. *Journal of occupational and environmental medicine,* 41**,** 1085-1090.

Chen, P.-C., Doyle, P. E. & Wang, J.-D. 2006. Respirable dust exposure and respiratory health in male Taiwanese steelworkers. *Industrial health,* 44**,** 190-199.

Chen, B., Stein, A. F., Maldonado, P. G., Sanchez De La Campa, A. M., Gonzalez-Castanedo, Y., Castell, N. & De La Rosa, J. D. 2013. Size distribution and concentrations of heavy metals in atmospheric aerosols originating from industrial emissions as predicted by the HYSPLIT model. *Atmospheric Environment,* 71**,** 234-244.

Cohen, D. D. 1993. Applications of simultaneous IBA techniques to aerosol analysis. *Nuclear Instruments and Methods in Physics Research Section B: Beam Interactions with Materials and Atoms,* 79**,** 385-388.

Connan, O., Smith, K., Organo, C., Solier, L., Maro, D. & Hébert, D. 2013. Comparison of RIMPUFF, HYSPLIT, ADMS atmospheric dispersion model outputs, using emergency response procedures, with ^{85}Kr measurements made in the vicinity of nuclear reprocessing plant. *Journal of environmental radioactivity,* 124**,** 266-277.

Draxler, R. R. & Hess, G. 1998. An overview of the HYSPLIT_4 modelling system for trajectories. *Australian Meteorological Magazine,* 47.

Draxler, R. R. & Rolph, G. D. 2013. *HYSPLIT (HYbrid Single-Particle Lagrangian Integrated Trajectory) Model access via NOAA ARL READY Website* [Online]. NOAA Air Resources Laboratory, College Park, MD. Available: (http://www.arl.noaa.gov/HYSPLIT.php) [Accessed 22 May 2014.

Driscoll, T., Nelson, D. I., Steenland, K., Leigh, J., Concha-Barrientos, M., Fingerhut, M. & Prüss-Üstün, A. 2005. The global burden of non-malignant respiratory disease due to occupational airborne exposures. *American journal of industrial medicine,* 48**,** 432-445.

Garimella, S. & Deo, R. N. 2008. Characterization of aerosols generated in a steel processing factory. *The South Pacific Journal of Natural and Applied Sciences,* 25**,** 78-82.

Johansson, S. A. & Johansson, T. B. 1976. Analytical application of particle induced X-ray emission. *Nuclear Instruments and Methods,* 137**,** 473-516.

Lewis, P. R., Hensley, M. J., Wlodarczyk, J., Toneguzzi, R. C., Westley-Wise, V. J., Dunn, T. & Calvert, D. 1998. Outdoor air pollution and children's respiratory symptoms in the steel cities of New South Wales. *Medical Journal of Australia,* 169**,** 459-463.

Marple, V. A., Rubow, K. L. & Behm, S. M. 1991. A microorifice uniform deposit impactor (MOUDI): Description, calibration, and use. *Aerosol Science and Technology,* 14**,** 434-446.

Mcgowan, H. & Clark, A. 2008. Identification of dust transport pathways from Lake Eyre, Australia using HYSPLIT. *Atmospheric Environment,* 42**,** 6915-6925.

Mohiuddin, K., Strezov, V., Nelson, P. & Stelcer, E. 2014a. Characterisation of trace metals in atmospheric particles in the vicinity of iron and steelmaking industries in Australia. *Atmospheric Environment,* 83**,** 72-79.

Mohiuddin, K., Strezov, V., Nelson, P. F., Stelcer, E. & Evans, T. 2014b. Mass and elemental distributions of atmospheric particles nearby blast furnace and electric arc furnace operated industrial areas in Australia. *Science of The Total Environment,* 487**,** 323-334.

Morgan, G., Corbett, S. & Wlodarczyk, J. 1998a. Air pollution and hospital admissions in Sydney, Australia, 1990 to 1994. *American journal of public health,* 88**,** 1761-1766.

Morgan, G., Corbett, S., Wlodarczyk, J. & Lewis, P. 1998b. Air pollution and daily mortality in Sydney, Australia, 1989 through 1993. *American journal of public health,* 88**,** 759-764.

Oakes, M., Weber, R., Lai, B., Russell, A. & Ingall, E. 2012. Characterization of iron speciation in urban and rural single particles using XANES spectroscopy and micro X-ray fluorescence measurements: investigating the relationship between speciation and fractional iron solubility. *Atmospheric Chemistry and Physics,* 12**,** 745-756.

Querol, X., Alastuey, A., Viana, M., Rodriguez, S., Artiñano, B., Salvador, P., Garcia Do Santos, S., Fernandez Patier, R., Ruiz, C. & De La Rosa, J. 2004. Speciation and origin of PM10 and PM2. 5 in Spain. *Journal of Aerosol Science,* 35**,** 1151-1172.

Querol, X., Viana, M., Alastuey, A., Amato, F., Moreno, T., Castillo, S., Pey, J., De La Rosa, J., Sánchez De La Campa, A. & Artinano, B. 2007. Source origin of trace elements in PM from regional background, urban and industrial sites of Spain. *Atmospheric environment,* 41**,** 7219-7231.

Rolph, G. D. 2013. *Real-time Environmental Applications and Display sYstem (READY)* [Online]. NOAA Air Resources Laboratory, College Park, MD. Available: (http://www.ready.noaa.gov) [Accessed 20 May 2014.

Toxnet. 2013. Toxicology Data Network, United States National Library of Medicine Available: http://toxnet.nlm.nih.gov/ [Accessed 22 March 2013].

Wang, J., Hiscox, A. L., Miller, D. R., Meyer, T. H. & Sammis, T. W. 2009a. A comparison of Lagrangian model estimates to light detection and ranging (LIDAR) measurements of dust plumes from field tilling. *Journal of the Air & Waste Management Association,* 59**,** 1370-1378.

Wang, J., Sammis, T. W., Miller, D. R., Hiscox, A. L., Granucci, D., Holmén, B., Kasumba, J., Shukla, M. K., Dennis, S. O. & Zhang, X. 2009b. Simulate Regional PM10 Dispersion from Agricultural Tilling Operations Using HYSPLIT4. *Journal of the Air & Waste Management Association,* 59.

Wang, Y., Stein, A. F., Draxler, R. R., De La Rosa, J. D. & Zhang, X. 2011. Global sand and dust storms in 2008: Observation and HYSPLIT model verification. *Atmospheric Environment,* 45**,** 6368-6381.

Xu, X., Christiani, D. C., Dockery, D. W. & Wang, L. 1992. Exposure—Response relationships between occupational exposures and chronic respiratory illness: a community-based study. *American Review of Respiratory Disease,* 146**,** 413-418.

Chapter 8

Conclusions and recommendations

Preface

This chapter summerises the conclusions from all chapters, and provides the recommendations for future studies. The practical implications are also presented along with research objectives and their findings.

8.1 Summary of the conclusions

This research sampled size resolved atmospheric particles in the vicinity of three Australian iron and steelmaking industries and one urban background site using MOUDI sampler, and analysed the sampled particles using PIXE, FTIR, XRD, SEM-EDS, and XANES techniques. The windrose, back trajectory and dispersion modelling were also performed during sampling campaign. This comprehensive assessment on characterisation of size resolved atmospheric particles reveals that:

- The literature assessment on iron ore and their processing revealed that the ironmaking industries can achieve industrial and environmental sustainability by increasing process efficiency while decreasing pollutants emission. The historical pollutants emission (per ton of iron) from iron ore processing industries in Australia is significantly reduced, while the productivity of blast furnace during ironmaking is increased. The process efficiency can be enhanced by optimising the consumption of raw materials and reduce the pollution load using improved pollutants recycling and recovery activities. The productivity and energy efficiency of DRI process, an alternative to reduce the pollutant burden from coke oven, sinter or pellet plant, can be increased by improved understanding of flow kinetics and effect of operational variables on reduction rates.

- The historical emission data analysis from iron and steel processing industries shows that steel industries in Australia exhibit reducing trends in PM_{10} and heavy metals emission by adopting energy efficient technologies, although more

emission reduction of these pollutants still remains a priority in order to reduce the negative impacts on air quality, human health and environment from local to global scale. It is worth mentioning that the iron and steelmaking industries are not reporting the emission of iron to the atmosphere, according to the National Pollutants Inventory (NPI) reporting protocol, however iron in the form of inhalable particles can cause significant risk to human health, although iron (non-particle form) is essential to our human body.

- The mass concentration analysis reveals that the dominant mass concentration was found in the particle size range between 3.2 and 5.6 μm for the coarse particles and between 0.18 to 0.32 μm for the fine particles at all sampling sites. The $PM_{2.5}$ fractions in the PM_{10} particles at all sites were found in the range from 35 to 62%. Similarly, PM_1 to the total PM_{10} at all sites varied from 20 to 46% contributing significantly to the PM_{10} mass loading. The largest number of particles and surface area concentration were detected for the particle size of 0.1 μm, most likely originating from high temperature thermal activities.

- The elemental analysis concluded that the trace metals Co, Cr, Cu, Fe, Mn, Ni, Ti, V and Zn had significantly higher concentrations in the atmospheric particles collected nearby the iron and steelmaking industries compared to the background site. Iron (0.20-12.2%) and zinc (0.05-2.0%) were found the leading contributors in the total PM_{10}, $PM_{2.5}$ and PM_1 concentrations.

- The average metal enrichment of the atmospheric particles in the vicinity of iron and steel industries was found to be about 3.4 to 14 times higher compared to the background site. This finding shows that the chemical composition of particles, which is currently not regulated, may be as important as the particle mass concentration, in order to provide comprehensive risk assessment of atmospheric particles.

- The metal correlation results showed that Fe and Co have very strong correlation in coarse particles at all three industrial sites, most likely generated from iron and steel processing industries, whereas the background site had no significant metal correlation except for the Ti-Fe correlation, possibly due to the contribution from natural source (soil dust).

- The modality types of atmospheric particles are found highly variable between the particle mass and elements detected in the particles; and among elements in the particles collected from urban and industrial areas. Both unimodal and bimodal particle distribution was observed for the dominant metals Mn, Fe and Zn in all industrial sampling sites which are most likely influenced by particles generated from the nearby steelworks, which is significant in exposure and risk assessment modelling of atmospheric particles.

- Fe was found as the dominant metal in the three industrial ironmaking sites for each particle size fraction. The industrial fraction of Fe at the submicron and ultrafine size particles at the three industrial sites were estimated to range up to 95%, which is most likely a result of emissions from high temperature thermal activities.

- Bonding structure analysis revealed that the –OH, -CH, -NH, and –CO bonding dominated in the organic compounds in atmospheric particles at all sampling sites, indicating the H-bonded alcohol, n-alkane, 2^0 amines, and conjugated ketone classes, respectively, occurred in organic compounds in atmospheric particles.

- The functional groups distribution were found variable between mass and bonding groups, among bonding groups, and among urban and industrial areas. These functional groups in organic compounds at all industrial sites can originate from iron and steelmaking industries and motor vehicle exhaust, whereas strong influence of organic functional groups at the urban background site can be assigned to the local biogenic emissions.

- Mineral analysis of atmospheric particles revealed that the hematite mineral was found predominant in the vicinity of iron and steelmaking industries, which likely originates from the raw materials handling, and high temperature combustion processes, whereas the background minerals quartz, calcite and halite, were found predominantly at the urban background site.

- The iron speciation study on atmospheric particles unveiled that the iron in the particles collected nearby the steelmaking site equipped with electric arc furnace indicated dominant Fe(III) oxide iron phases in all particle size fractions. The

atmospheric particles collected near two integrated iron and steelmaking facilities operated by the blast furnace route, had similar iron phase speciation with presence of both Fe(II) and Fe(III) iron phases in the coarse and fine particle size ranges, while for the ultrafine size range of particles, Fe(III) was the dominant form of iron.

- Backward air-mass trajectories showed that the long range transport particles can contribute to the particle loading from desert, ocean, urban and regional areas in Australia within 1000 km range from the sampling site. The morphology of iron containing particles indicates the iron association with other toxic metals. The particle dispersion model suggests that these particles can form local hotspots within 5 km distance from the iron and steelmaking industries, which indicates research priorities to identify all hotspots, assess the risk, and take necessary measures to ensure safe air quality, human health, and environment.

- The air quality index (AQI) of atmospheric particles in NSW is calculated only based on particle mass, which may contain significant amount of toxic metals in the industrial areas (Chapter 4-7), and assigned the 'safe label' named 'good' or 'very good', despite having no 'safety threshold' for particles. The outcome of this research on atmospheric particles using advanced technologies, such as PIXE, FTIR, SEM-EDS, XRD, and synchrotron-based XANES techniques, indicates the need to consider the particle chemistry in the AQI calculation method.

8.2 Recommendations for future studies

Based on the research objectives, methods, results and discussion, and above mentioned conclusions, the following recommendations could be further implied for future studies:

- Assessment of the importance of particle chemistry in air quality reporting, monitoring and particle standards, as this research showed significant variations in elemental compositions nearby industrial areas compared with one background urban areas for the same particle concentration level.
- Study on ultrafine particles (less than 180 nm) in urban and industrial areas, as the particle number and surface area are higher in the ultrafine particle range. The fine resolution of particle size range will provide dominant nanoparticle size fraction and the same for surface area.

- Study the atmospheric particles using single particle analyser, as the single particle size, mass and elemental composition can provide better understanding of particle behavior within single particles and bulk particles like $PM_{0.1}$.
- Study the atmospheric particles for long period of time for seasonal variation, as the varying atmospheric conditions in seasons which could provide better understanding of particle behavior.
- Study the iron isotopes in size resolved air particles, as iron isotopes could provide the fingerprint of the particle source.
- Study the speciation of toxic metals, such as nickel, chromium which are associated with iron containing particles in the vicinity of iron and steel processing industries, as the toxicity depends on the amount and oxidation states of these toxic metals.
- Study the exposure and risk assessment of size resolved air particles in the vicinity of iron and steelmaking industries, as the risk could be higher especially for the vulnerable groups of very young and elderly when they exposed atmospheric particles containing toxic metals for long duration.
- Study the implementation of risk based licensing and policy, considering particle chemistry, elemental modality and speciation of toxic metals.

Appendix A: Declaration of authorship contribution

J1. **Mohiuddin, K.**, Strezov, V., Nelson, P. & Stelcer, E. 2014. Characterisation of trace metals in atmospheric particles in the vicinity of iron and steelmaking industries in Australia. *Atmospheric Environment,* 83**,** 72-79.

Contribution of PhD Candidate (Kazi Mohiuddin): 88%

Kazi Mohiuddin was collected the atmospheric particles from Cringila, Rooty Hill, Whyalla and Macquarie Park in Australia, and performed the laboratory analysis at ANSTO, Sydney for the mass and elemental compositions of atmospheric particles with the assistance of Ed Stelcer. Kazi was analysed the data generated from the PIXE technique and prepared the initial draft manuscript. Kazi was revised the draft and prepared the final manuscript by incorporating the changes and comments from Strezov, Nelson, and Stelcer.

J2. **Mohiuddin, K.,** Strezov, V., Nelson, P. F., Stelcer, E. & Evans, T. 2014. Mass and elemental distributions of atmospheric particles nearby blast furnace and electric arc furnace operated industrial areas in Australia. *Science of The Total Environment,* 487**,** 323-334.

Contribution of PhD Candidate (Kazi Mohiuddin): 90%

Kazi Mohiuddin was sampled and analysed the atmospheric particles in the vicinity of iron and steelmaking industries in Australia. Kazi was further analysed the data generated from the PIXE technique and prepared the draft manuscript. Kazi was revised the draft and prepared the final manuscript by incorporating the changes and comments from Vladimir Strezov, Peter Nelson, Ed Stelcer, and Tim Evans.

P1. **Mohiuddin, K.**, Strezov, V., Nelson, P. & Evans, T. 2014. Bonding structure and mineral analysis of size resolved atmospheric particles near Australian steelmaking sites. *Journal of Aerosol Science (to be submitted)*.

Contribution of PhD Candidate (Kazi Mohiuddin): 92%

Kazi Mohiuddin was sampled the atmospheric particles. Kazi was performed the laboratory testing using Fourier Transform Infra-Red (FTIR) technique for bonding structure analysis, and X-Ray Diffraction (XRD) technique for mineral analysis. Kazi was analysed the data generated from the FTIR and XRD techniques and prepared the draft manuscript. Kazi was revised the

draft and prepared the final chapter by incorporating the changes and comments.

P2. **Mohiuddin, K.**, Strezov, V., Nelson, P. & Evans, T. 2014. Speciation of size resolved iron containing particles in proximity of Australian steelmaking industries. *Aerosol Science and Technology (to be submitted).*

Contribution of PhD Candidate (Kazi Mohiuddin): 92%

Kazi Mohiuddin was sampled and analysed the elemental compositions of atmospheric particles. Kazi was performed the laboratory testing using Scanning Electron Microscope coupled with Energy Dispersive Spectrometer (SEM-EDS) for particle morphology, and X-ray emission near edge structure (XANES) technique for iron speciation. Kazi was also performed the back trajectories and dispersion modelling using ARL online laboratory. Kazi was analysed the data generated from the SEM-EDS, XANES, and dispersion modelling, and prepared the draft manuscript. Kazi was revised the draft and prepared the final chapter by incorporating the changes and comments.

B1. **K Mohiuddin**, V Strezov and P Nelson 2010, "Industrial and Environmental Sustainability of Ironmaking Technologies", Book Chapter 5, Advances in Environmental Research, Volume 12, Nova Science Publishers Inc, ISBN 978-1-61122-540-2.

Contribution of PhD Candidate (Kazi Mohiuddin): 95%

Kazi Mohiuddin was reviewed and assessed the literature on iron ore, their origin, transportation, processing, trade, global production and iron ore production and processing in Australian perspective. Kazi was prepared the draft chapter. Kazi was also revised the draft and prepared the final chaper by incorporating the changes and comments from Vladimir Strezov, Tim Evans, and Peter Nelson.

C1. **K Mohiuddin**, V Strezov, T Evans and P Nelson (2010), "Assessment of CO_2, PM_{10} and heavy metal emissions from iron and steel industries in Australia", Chemeca 2010: The 40th Australasian Chemical Engineering Conference, paper # 443 (10 pages). ISBN: 978-085-825-9713.

Contribution of PhD Candidate (Kazi Mohiuddin): 95%

Kazi Mohiuddin was reviewed and assessed the literature on major pollutant emission from seventeen Australian iron and steel processing industries, including their process type and particle reduction practices. Kazi was prepared the draft paper. Kazi was also revised the draft and prepared the final paper by incorporating the changes and comments from Vladimir Strezov, Tim Evans, and Peter Nelson.

C2. **Mohiuddin, K.,** Strezov, V., Stelcer, E. & Nelson, P. F. 2013, "Chemistry of air particles collected near Australian Industrial sites", 21st International Clean Air & Environment Conference: CASANZ 2013 Conference, paper# 179 (5 pages). ISBN: 978-0-9874553-2-1.

Contribution of PhD Candidate (Kazi Mohiuddin): 88%

Kazi Mohiuddin was collected the atmospheric particles and performed the laboratory analysis at ANSTO, Sydney for the mass and elemental compositions of atmospheric particles with the assistance of Ed Stelcer. Kazi was analysed the data generated from the PIXE technique and prepared the draft paper. Kazi was revised the draft and prepared the final paper by incorporating the changes and comments from Vladimir Strezov, Ed Stelcer, and Peter Nelson.

C3. **K. Mohiuddin**, V Strezov, E Stelcer, A Morrison and P Nelson (2012) "Characterization of size resolved air particulates in the vicinity of electric arc furnace steelmaking facility", Poster presentation in the sixth international conference on environmental science and technology held on June 25-29, 2012 at Houston, Texas, USA.

Contribution of PhD Candidate (Kazi Mohiuddin): 88%

Kazi Mohiuddin was collected the atmospheric particles and performed PIXE analysis for elemental compositions of atmospheric particles with the assistance of Ed Stelcer. Kazi was analysed the data generated from the PIXE technique and prepared the poster. Kazi was revised and prepared the final

poster by incorporating the changes and comments from Vladimir Strezov, Ed Stelcer, Anthony Morrison, and Peter Nelson.

C4. **K Mohiuddin**, V Strezov, E Stelcer, A Morrison and P Nelson (2011) "Iron containing aerosol in Sydney airshed", poster presentation in the 17th AINSE conference of nuclear and complimentary techniques of analysis held on 5-7 December 2011 at Canberra, Australia.

Contribution of PhD Candidate (Kazi Mohiuddin): 92%

Kazi Mohiuddin was sampled and analysed the atmospheric particles using PIXE technique. Kazi was analysed the data generated from the PIXE technique and prepared the poster. Kazi was revised and prepared the final poster by incorporating the changes and comments from Vladimir Strezov, Ed Stelcer, Anthony Morrison, and Peter Nelson.

Appendix B: Supplementary data for dispersion model

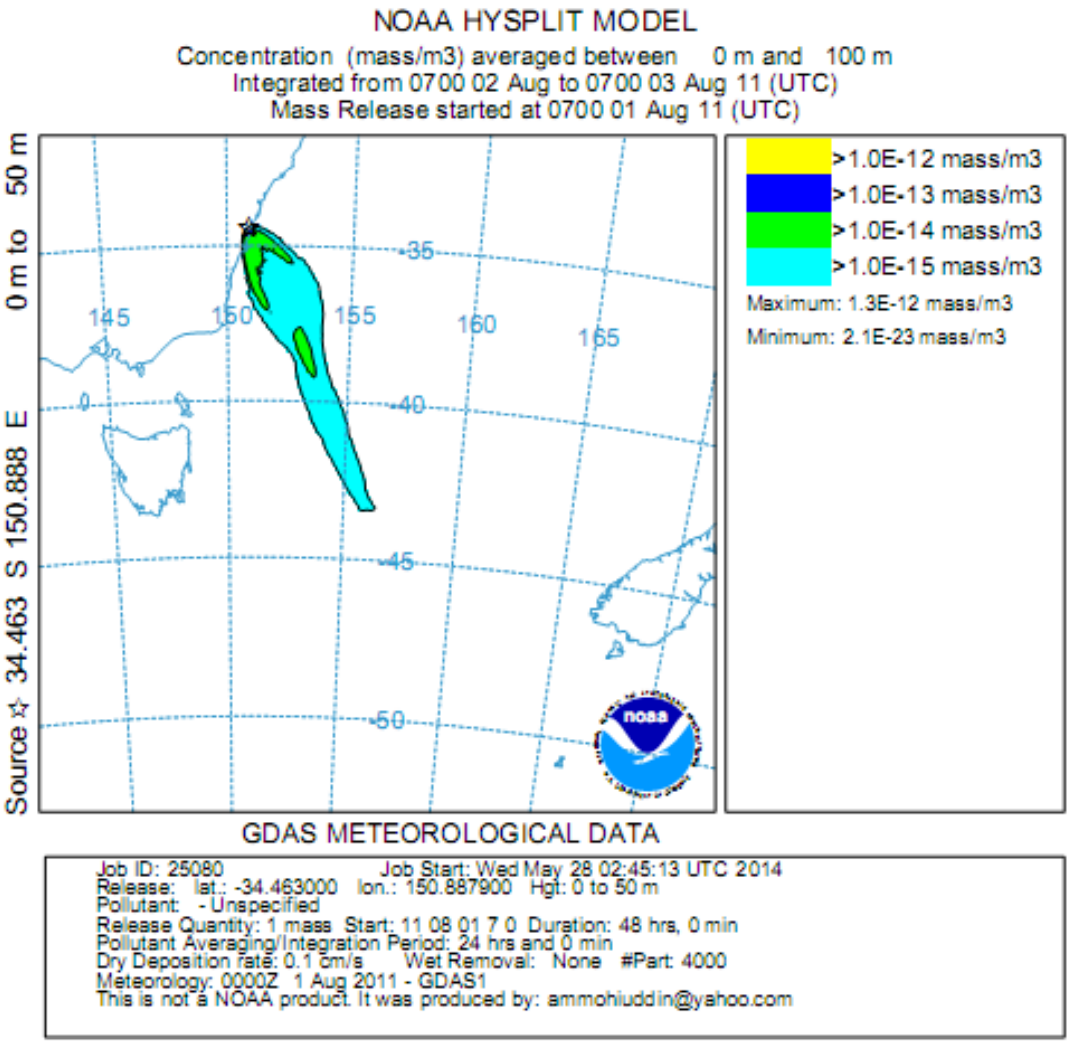

Figure B1. Concentration of particles emitted from Wollongong steelworks

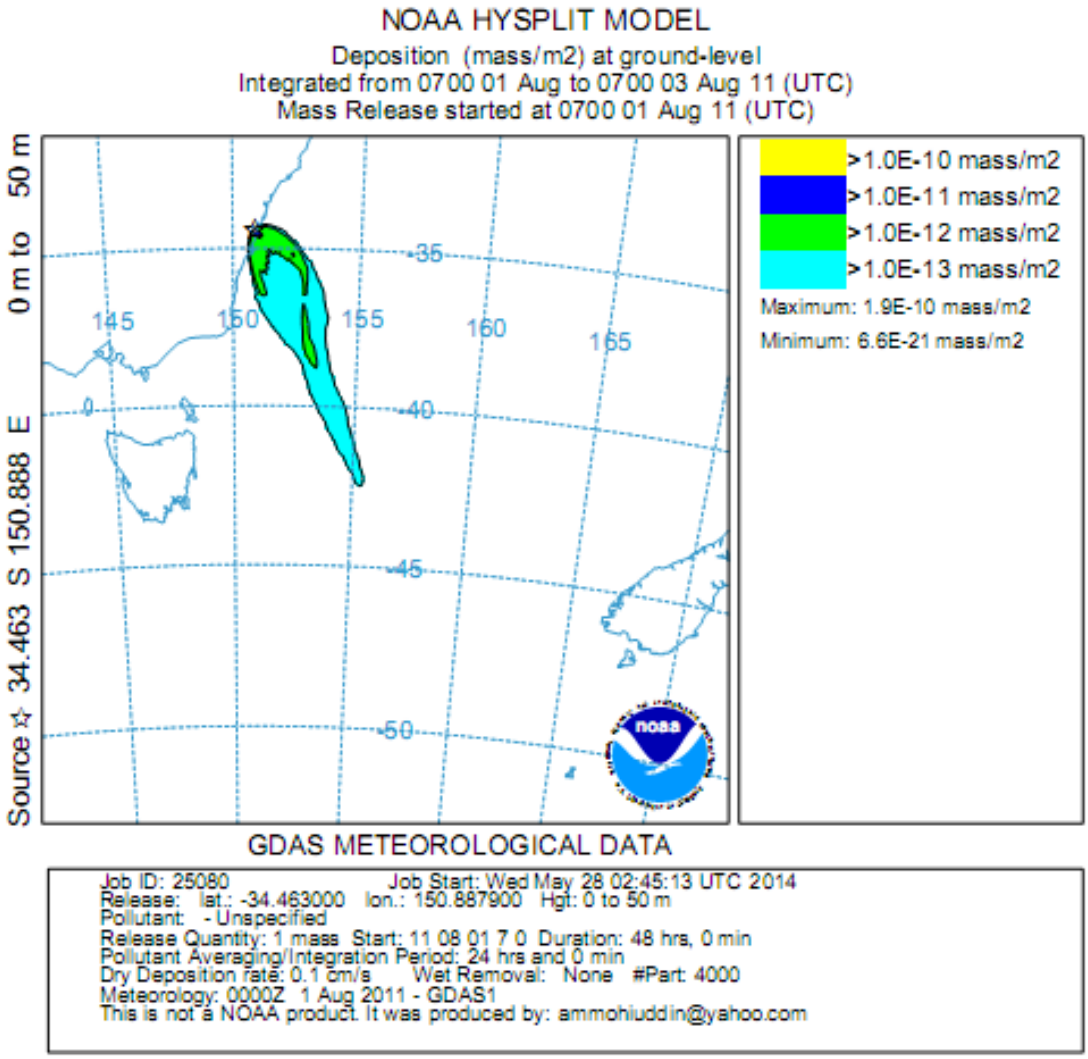

Figure B2. Deposition of particles emitted from Wollongong steelworks

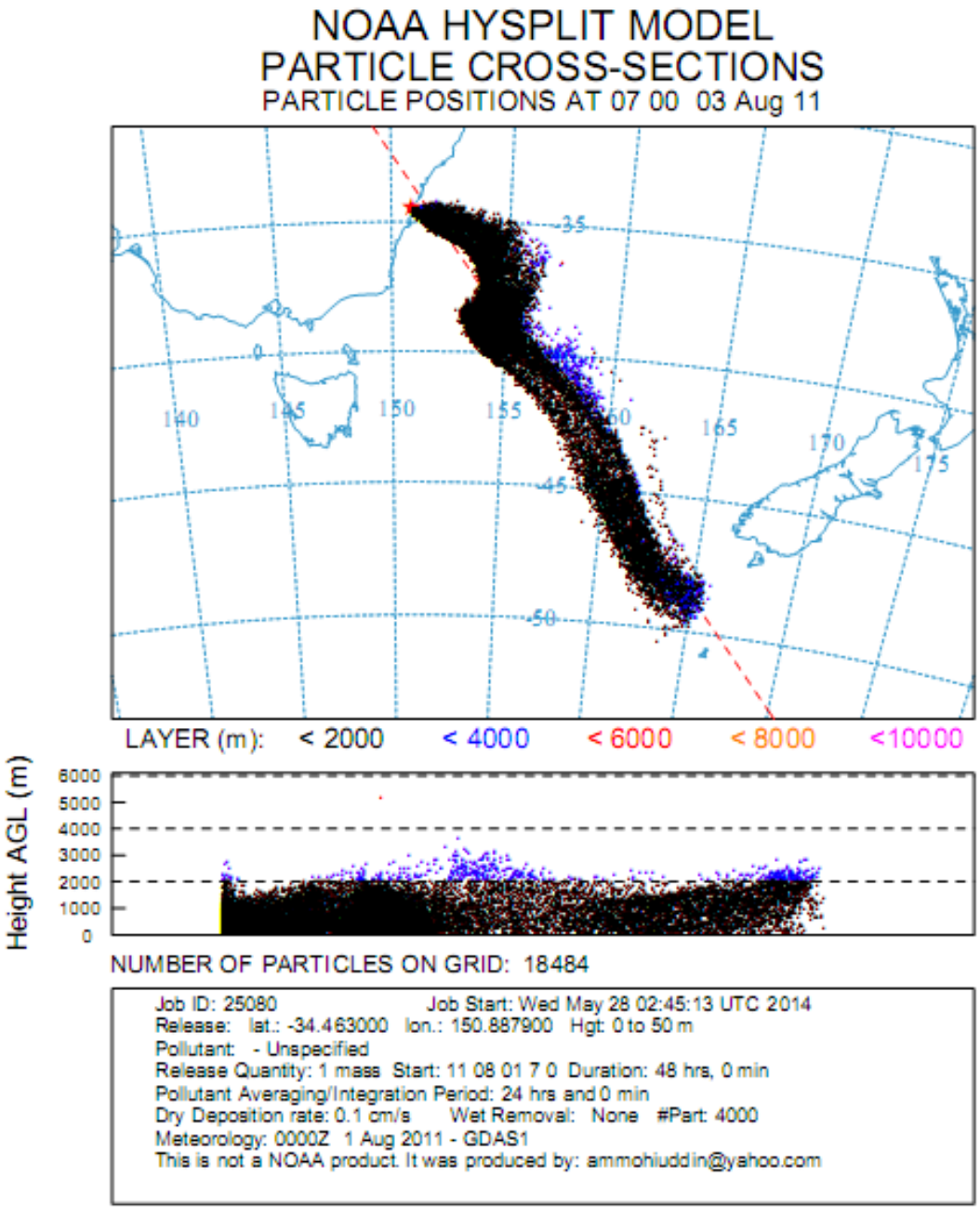

Figure B3. Particle position with cross section emitted from Wollongong steelworks

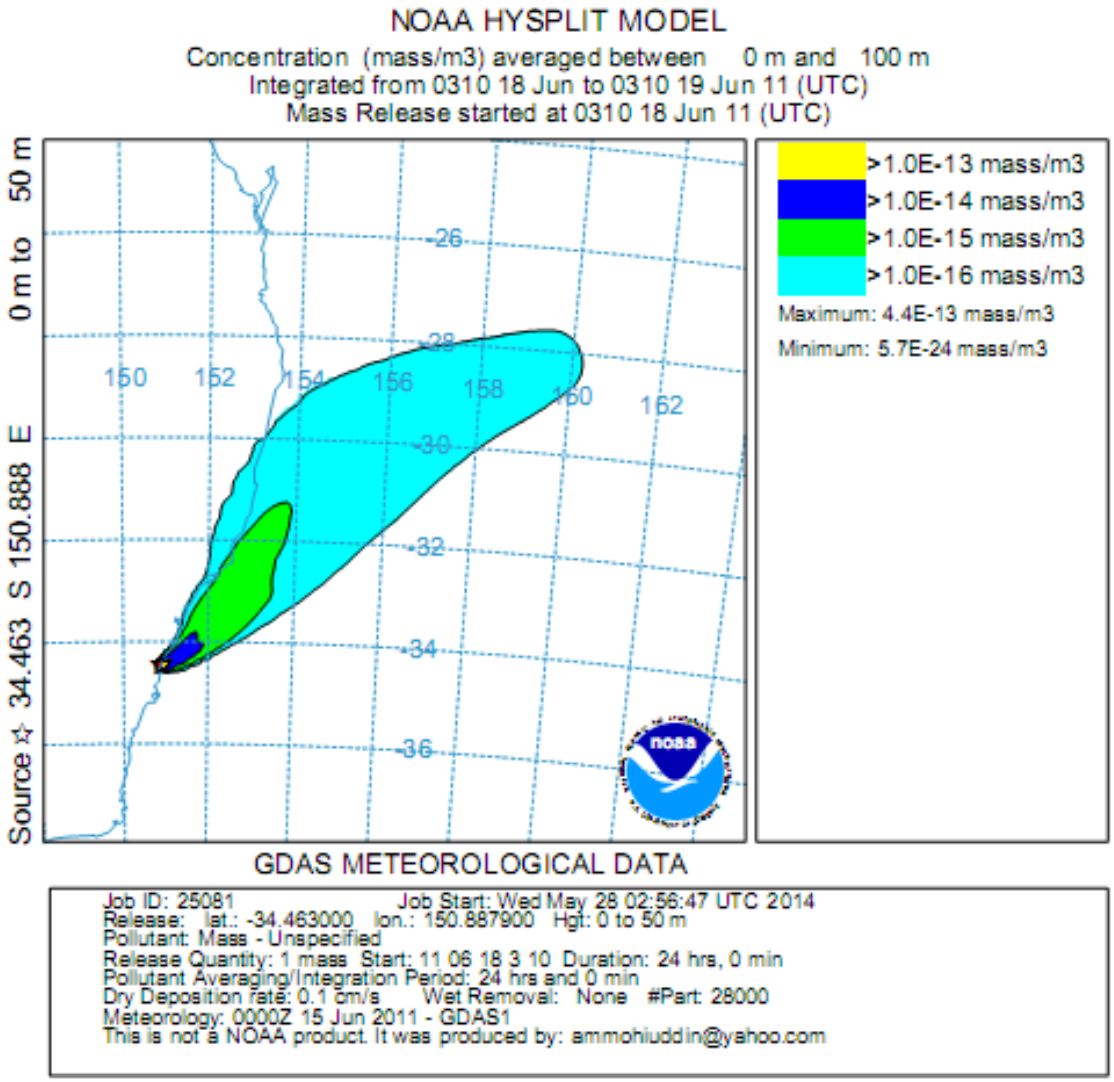

Figure B4. Concentration of particles emitted from Rooty Hill steelworks

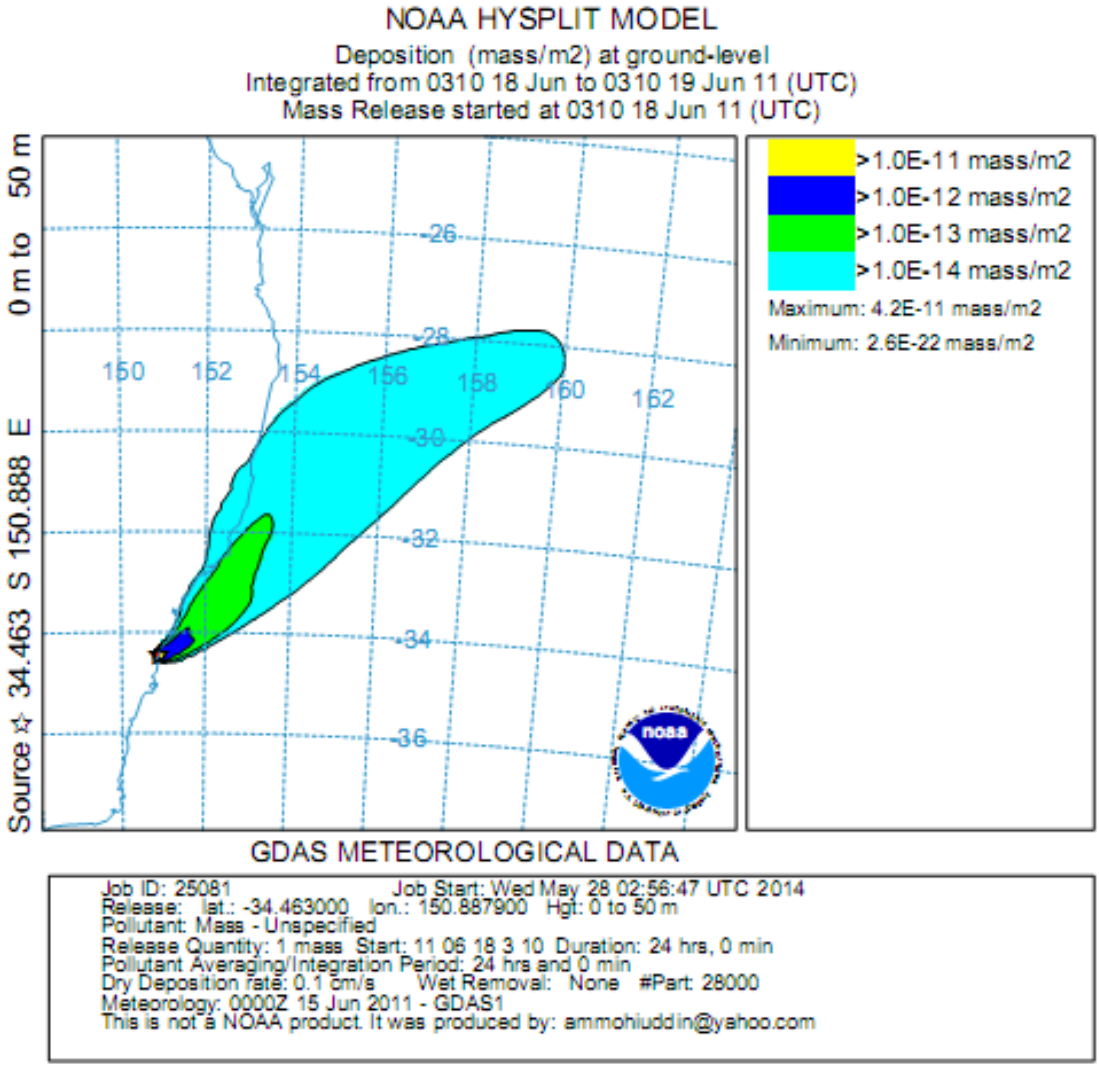

Figure B5. Deposition of particles emitted from Rooty Hill steelworks

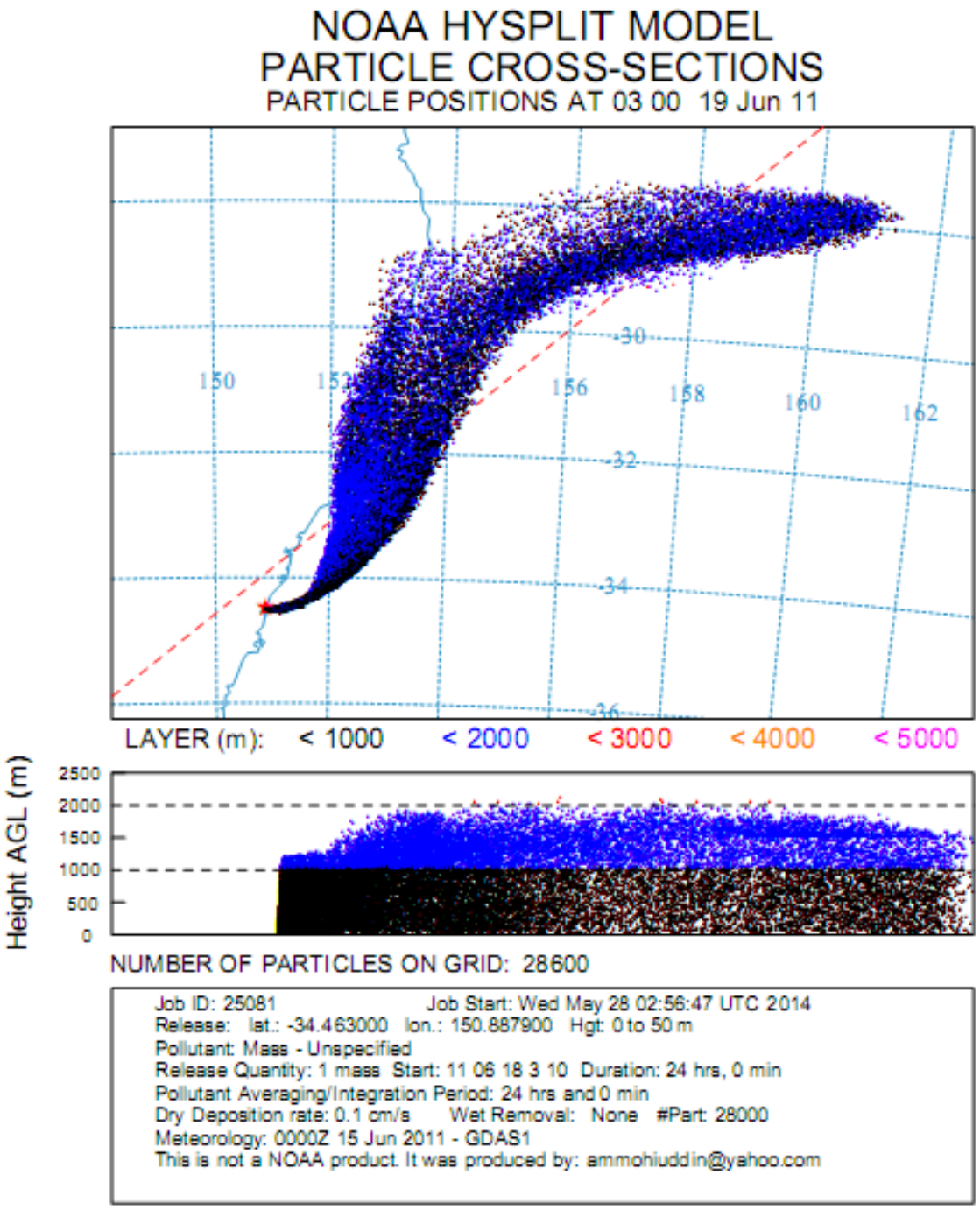

Figure B6. Particle position with cross section emitted from Rooty Hill steelworks